INFORMATION TO USERS

This manuscript has been reproduced from the microfilm master. UMI films the text directly from the original or copy submitted. Thus, some thesis and dissertation copies are in typewriter face, while others may be from any type of computer printer.

The quality of this reproduction is dependent upon the quality of the copy submitted. Broken or indistinct print, colored or poor quality illustrations and photographs, print bleedthrough, substandard margins, and improper alignment can adversely affect reproduction.

In the unlikely event that the author did not send UMI a complete manuscript and there are missing pages, these will be noted. Also, if unauthorized copyright material had to be removed, a note will indicate the deletion.

Oversize materials (e.g., maps, drawings, charts) are reproduced by sectioning the original, beginning at the upper left-hand corner and continuing from left to right in equal sections with small overlaps.

Photographs included in the original manuscript have been reproduced xerographically in this copy. Higher quality 6" x 9" black and white photographic prints are available for any photographs or illustrations appearing in this copy for an additional charge. Contact UMI directly to order.

Bell & Howell Information and Learning
300 North Zeeb Road, Ann Arbor, MI 48106-1346 USA
800-521-0600

MODELING AND PERFORMANCE ANALYSIS OF ABS SYSTEMS WITH NONLINEAR CONTROL

Tianku Fu

A Thesis

in

The Department

of

Mechanical Engineering

Presented in Partial Fulfillment of the Requirements
for the Degree of Master of Applied Science at
Concordia University
Montreal, Quebec,
Canada

September 2000

ABSTRACT

MODELING AND PERFORMANCE ANALYSIS OF ABS SYSTEMS WITH NONLINEAR CONTROL

Tianku Fu

ABS antilock braking systems are closed-loop control devices implemented in ground vehicles that prevent wheel lock-up during braking. The existing ABS controls have the ability to regulate the level of pressure to optimally maintain the wheel slip within the vehicle stability range. However, the ABS exhibits strong nonlinear characteristics. The vehicles equipped with the existing controllers can still have a tendency to oversteer and become unstable. In this study, a new integrated Nonlinear Tracking Control (NTC) is developed that includes the dynamic analysis of the hydraulic braking systems. In the developed algorithm, the desired set points for the slip values are iterated from a nonlinear tire model based on the Magic Formula. Simulations of hard braking and steering maneuvers are conducted using the nonlinear Yaw-plane Four-wheel steering vehicle model with Limited Roll motion (YFLR) incorporating the nonlinear Magic Formula tire model (MF). Similar maneuvers are applied to the same vehicle model that is equipped with the conventional PID controller. Braking and vehicle stability performances are compared for the two implemented control systems to verify the reliability of the proposed control. In this study, Four-wheel Steering Control (4WSC) and Variable Slip-ratio Control (VSC) are also developed along with the NTC in the YFLR model to assess the cornering characteristics of the vehicle during braking and turning. Three controllers are independent but are coupled through the states of the longitudinal and lateral tire forces. Considering the tire friction ellipse, the control systems are designed using model matching control method to impose the vehicle braking performances following a desired dynamic model even during large decelerations or lateral accelerations. This study indicates that the action of the three controllers implemented in the YFLR model is able to provide the directional control and stability and can reduce the tendencies of oversteer in extreme emergency situations for the specific road conditions. Simulations of the integrated controllers and ABS systems for different conditions demonstrate significant improving in braking and vehicle stability performances.

ACKNOWLEDGEMENTS

The author wishes to thank sincerely his thesis supervisors, Dr. I. Stiharu and Dr. C. Y. Su for their guidance and efforts during the course of this investigation.

Thanks are due to the faculty members, staff, and other graduate students of CONCAVE Research Centre, and the Department of Mechanical Engineering for their help and contributions during the course of this study.

Finally, the author would like to express a deep appreciation to his parents, wife and the other family members for their continuous concerns, encouragement and supports.

TABLE OF CONTENTS

LIST OF FIGURES

LIST OF TABLES

NOMENCLATURE

A_f	Frontal area of vehicle
A_1	Piston diaphragm area in master cylinder
A_2	Piston diaphragm area in booster chamber
a_x	Longitudinal acceleration
a_y	Lateral acceleration
B	Magic Formula stiffness factor
B_f	Fluid force friction coefficient
C	Magic Formula shape factor
C_d	Vehicle drag coefficient
$C_{\alpha f}$	Front per axle cornering stiffness
$C_{\alpha f}$	Rear per axle cornering stiffness
C_φ	Roll damping
C_{YM}	Yaw moment drag coefficient
C_s	Side force coefficient
C_l	Longitudinal drag coefficient
c_i	Valve orifice coefficients
D	Magic Formula peak factor
D_x	Longitudinal stop distance
D_y	Lateral stop distance
E	Magic Formula curvature factor
e	Position error

e_c	Distance from the roll center to the sprung mass center
e^{-TS}	Time axis actuator caused by the actuator "dead-time"
F	Piston force
F_{ax}	Longitudinal aerodynamic force
F_{ay}	Lateral aerodynamic force
F_d	Desired force
F_{d1}	Hydraulic force on master cylinder
F_{d2}	Hydraulic force on booster chamber
F_L	Longitudinal weight transfer load
F_t	Road tractive force
F_r	Tire rolling resistance force.
F_x	Total force in longitudinal direction
F_y	Total force in lateral direction
F_{s1}	Spring force on first chamber of master cylinder
F_{s2}	Spring force on second chamber of master cylinder
F_{s3}	Spring force booster chamber
F_{zf}	Normal load on front wheels
F_{zr}	Normal load on rear wheels
F_{xi}	Tire force components along x-axis
F_{yi}	Tire force components along y-axis
F_{xwi}	Longitudinal tire force along wheel axis
F_{ywi}	Lateral tire force along wheel axis
$g(\dot{x})$	Coulomb friction forces

$\hat{g}(\dot{x})$	Estimate of the friction forces
h_c	Center of gravity height of the vehicle
J_w	Wheel moment of inertia about the axle
J_z	Yaw moment of inertia of the vehicle
J_x	Roll moment of inertia
K_f	Fluid stiffness coefficient
K_m	Scaling constant
K_φ	Roll stiffness
k	Spring constant
k_l	Function constant
k_f	Positive force error gain
$K(\alpha)$	Variable Slip-ratio gain
L	Wheel base length of vehicle
$L(x,t)$	Lyapunov like function
l_f	Longitudinal distance from vehicle cg to front axile
l_r	Lateral distance from vehicle cg to rear axile
M	Optimizer reference signal switching strength
M_{az}	Yawing moment by aerodynamic
M_P	Mass of the prime mover
M_{zi}	Yaw moment about the c.g of the vehicle
M_z	Self aligning torque
m	Pushrod and piston mass in booster chamber
m_b	Vehicle sprung mass

m_c	Vehicle mass
m_e	Vehicle effective mass
m_{tire}	Tire mass
m_m	Piston mass in master cylinder
m_t	Total mass of the quarter vehicle
P_r	Atmospheric pressure
p_o	Initial pressure for open check valve
p_s	Supply pressure
p_{fs}	Pressure of front calipers
p_{rs}	Pressure of rear calipers
p_r	Reservoir pressure
p_1	Pressure on master cylinder
p_2	Pressure on booster chamber
q_1	Master cylinder fluid flow
q_2	Booster chamber fluid flow
q_{11}	Fluid flow to the first chamber of master cylinder
q_{12}	Fluid flow to the second chamber of master cylinder
R_w	Wheel radius
r	Yaw rate
S_x	Magic Formula horizontal shift
S_v	Magic Formula vertical shift
s	Laplacian operator
s_{fo}	Optimal slip of front wheels
s_f	Front wheel slip

s_{ro}	Optimal slip of rear wheels
s_r	Rear wheel slip
T_b	Braking torque
T_{fb}	Braking torque on front wheels
T_{rb}	Braking torque on rear wheels
T_r	Air temperature in degrees Fahrenheit
t_0	Dead time
t_1	Distance between front wheels
t_2	Distance between rear wheels
u	Control applied to the spool valve
u_0	Optimizer independent variable gain
V_x	Longitudinal velocity of vehicle
V_y	Lateral velocity of vehicle
V_{wf}	Velocity along front axle
V_{wr}	Velocity along rear axle
$V_{w1,2}$	Estimated magnitudes of front axle velocities
$V_{w3,4}$	Estimated magnitudes of rear axle velocities
V_s	Slip speed vector
V_{11}	Total fluid volume in the first chamber of master cylinder
V_{12}	Total fluid volume in second chamber of master cylinder
V_1	Total fluid volume in master cylinder
V_2	Total fluid volume in booster chamber
V_{10}	Initial fluid volume in the master cylinder
V_{20}	Initial fluid volume in the booster chamber

X	Represent the slip angle or longitudinal slip
x	Piston position in booster chamber
x_c	Actuator displacement
x_d	Commanded displacement
x_f	Piston position for front wheels
x_r	Piston position for rear wheels
x_I	Piston position in master cylinder
Y	Stands for either forces or moment
z	Nonzero control quantity
α	Side slip angle
α_w	Relative wind angle
α_f	Front wheel slip angle
α_r	Rear wheel slip angle
β	Fluid bulk modulus
δ	Optimizer error interval width
δ_f	Front wheel steering angle
δ_r	Rear wheel steering angle.
Δ	Optimizer hysteresis width
$\Delta(g)$	Friction disturbance.
ε	Defines the tracking error
θ	Design parameter.
ω_i	Angular velocity of wheel i
φ	Roll angle

$\dot{\varphi}$ Roll rate

ψ Yaw angle

ρ Mass density of the air

ν Auxiliary signal can be obtained by a three positional relay.

$\mu(s)$ Road adhesion coefficient

CHAPTER 1
INTRODUCTION

1.1 GENERAL

Many modern vehicles use electronically controlled braking systems to give the driver more steering control and shorter stopping distances on some surfaces during severe braking conditions. The base braking system is shown in Figure 1.1.

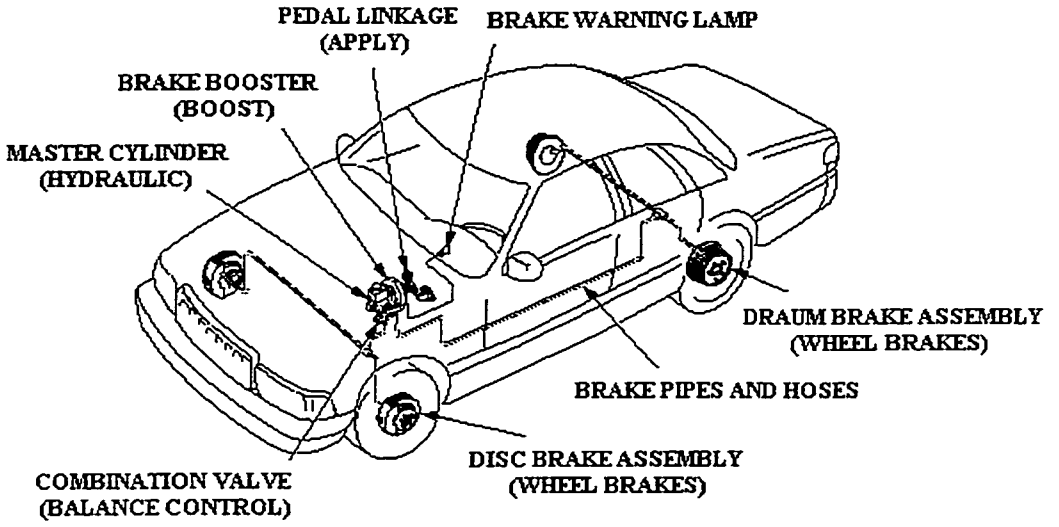

Fig. 1.1 Base Brake System Components
(Modified from www.ACDelco.com)

To improve the braking performance and to maintain the directional stability and maneuverability of road vehicles, anti-lock braking systems have been used since 1970's. The trend in improving performances of braking systems yield to the development of a large number of braking system models, vehicle models and control strategies.

A modern ABS antilock braking system is an electronic feedback control system, which greatly increases the ability of driver and vehicle to avoid accidents on slippery

roads and during hard braking circumstances. An ABS system consists of a standard braking system incremented with an electronic control unit (ECU), an electronic brake control modulator (EBCM), and a wheel magnetic pickup speed sensor (Figure 1.2).

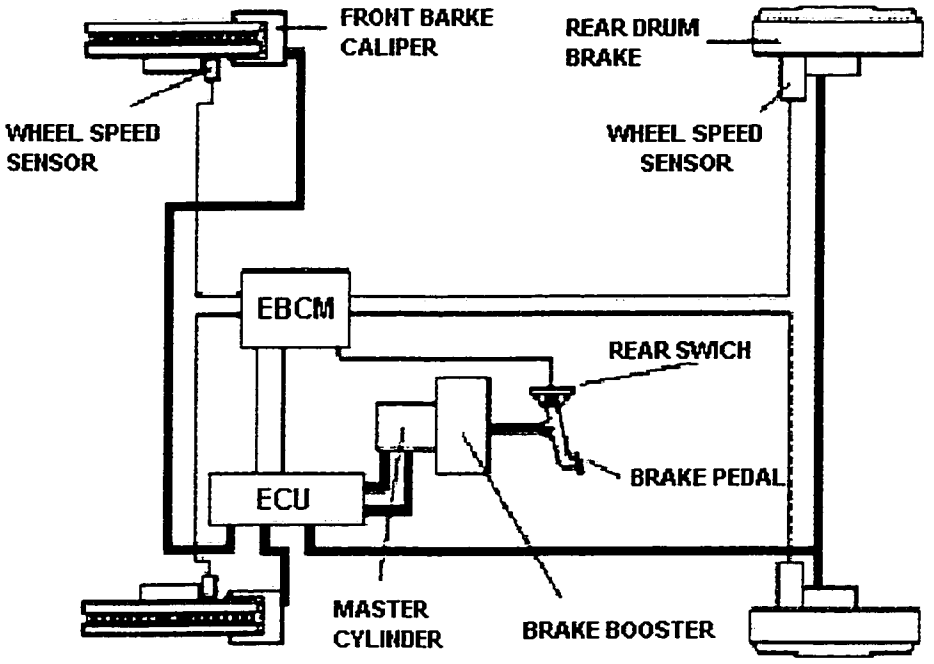

Fig. 1.2 Typical Antilock Braking System
(Modified from www.ACDelco.com)

The conventional design of an ABS system begins with a complete understanding of the tire-road friction characteristics. The braking in terms of minimum stopping distance would be optimized if the slip of the tire on which the brake is applied could always be kept at values corresponding to peak friction levels. The objective of ABS is to maximize the tire traction by preventing the wheels from being locked during braking while to help maintaining adequate vehicle stability and steerability. In practice, it is difficult to determine the tire skid accurately, primarily due to the lack of a practical and cost-effective means to directly measure the nonlinear speed of the tire center during

braking. Therefore, the control strategy of an ABS is usually formulated based on some easily measurable parameters, such as the angular speed and angular deceleration or acceleration of the tire and linear deceleration of the vehicle. When wheel lock is detected, the pressure in one or more of the braking cylinders is reduced until the wheel speed exceeds a predetermined value, at which time the pressure is again increased.

With the development of electronics circuits and vehicle sensors [1, 2], ABS system enables the controller to maintain a specified value of longitudinal slip [3] by measuring the relative velocity of the tire with respect to the road. The sensors measure the speed of wheels and supply feedback signals to the electronic controller. On the basis of the individual wheel speeds, the electronic controller detects any tendency of wheel lock-up and controls the solenoid valves of hydraulic control element, which is located between the master brake cylinder and the wheel brake cylinder. The three most common approaches and their combination developed for the ABS nonlinear systems are: *i*) variable structure control (sliding mode control) [4-11], *(ii)* fuzzy logic control [12-17], and *iii*) adaptive control [18-24].

While controlling a practical system, the designer rarely knows its parameters accurately. The characteristics of the process can change with time due to a variety of factors. There may also be unforeseen change in the statistics of the external inputs and disturbances that may be considered as changes in the environment in which the system operates. The tools of conventional control theory, even when used efficiently in the design of controllers for such systems may be inadequate to achieve satisfactory performance in the entire range over which the characteristics of the system may vary. The adaptation is defined as "an advantageous conformation of an organism to changes in

its environment". Inspired by the definition, adaptive system in control theory refers to the control systems that monitor their own performance and adjust their parameters in the direction of better performance [25]. In general, the adaptive approach is applicable to a wider range of uncertainties, but variable structure controls are simpler to implement and no time is required to tune the controller to the plant variations. Variable structure control is a dynamical system control with discontinuous state feedback controllers consisting of a set of continuous subsystems with a proper switching logic. It rests on the concept of changing the structure of the controller in response to the changing states of the system to obtain a desired response. During the past several years, fuzzy control has emerged as one of the most active and fruitful areas for research in the realm of industrial processes, which do not lend themselves to control by conventional methods because of a lack of quantitative data regarding the input-output relations. Fuzzy control is based on fuzzy logical system that is much closer in human thinking and natural language than traditional logical systems.

Most of the adaptive controllers recently developed use a linearized model for the ABS system, hence provide only local stability. These systems have the ability to cope with changing system parameters, but the lack of a global stability proof is often a major disadvantage of the linearized adaptive controllers. Fuzzy control, on the other hand, based upon the logic description between slip ratio and braking pressure to detect wheel seizure and avoid excessive slipping. However, because the ABS systems not only dependent on the control logic, they also account to the braking system and vehicle dynamics, many unknown parameters often affect the control logic and make the fuzzy control unreliable. The variable structure controls have been used to maintain the value of

slip within the desired range. However, the drawback in using this approach is that the controller requires states measurements of the slip ratio and road adhesion, which are, in the case of ground vehicles very difficult and expensive to measure.

An ABS system that can determine on-line the optimal wheel slip region without expensive road surface sensors would be much desired. In this study, a new integrated Nonlinear Tracking control based upon the dynamic analysis of the hydraulic braking system is proposed. The realization of ABS systems relies on the control of hydraulic braking system as well as other vehicle systems. Modeling of the hydraulic braking system is essential to design of ABS dynamic systems. The control law uses Lyapunov's stability theorem for the development of the braking control algorithm, where the longitudinal slip trend is calculated and re-evaluated based upon the steering wheel angle. The developed scheme uses a Lyapunov function candidate to synthesize both the control law and the adaptation law, necessary to estimate the unknown parameters of the system. The desired set points for the slip values are calculated within the control algorithm to aid the controller in maintaining vehicle stability during emergency maneuvers consisting of combined hard braking and severe steering. Simulations of hard braking and steering maneuvers were conducted using a nonlinear vehicle model together with a nonlinear tire model. The nonlinear Yaw-plane Four-wheel steering vehicle model [26-29] with Limited Roll Motion [30-31] [YFLR] incorporating the nonlinear Magic Formula tire model (MF) [32-35] is used in the analysis. This model has eight degrees of freedom: longitudinal and lateral velocities, yaw rate, roll angle and rotational velocity for each wheel. The response characteristics derived from the proposed model are compared with the conventional PID control system to demonstrate its validity. Four-wheel Steering

Control (4WSC) [36] and Variable Slip-ratio Control (VSC) [31] are applied together for the cornering characteristics. The two controllers are independent but are coupled through the states of the longitudinal and lateral tire forces. Four-wheel control by steering the rear wheels out-of-phase with the front wheels to reduce the turn radius, thus improving maneuverability and cornering stability, and also yield a quicker response with better damping of the yaw oscillation that occurs with initiation of turn. Variable slip-ratio control is an optimal way to balance the longitudinal and lateral forces. While more longitudinal traction force is desired during driving straight, more lateral force is desired during turning in order to be able to turn without lateral slippage, and thus to increase the vehicle stability. Considering the tire friction ellipse, the control system is designed using model matching control method to make the vehicle braking performances follow a desired dynamic model even during large decelerations or lateral accelerations.

1.2 LITERATURE REVIEW

The concept of ABS dates back to the 1930's [37], but has only become truly practical with the implementation of the electronics on the modern vehicles. The systems were initially deployed in the early 1970s [37] on trucks with air brakes, and have evolved into advanced hydraulic braking systems in passenger vehicles. All manufacturers producing ABS systems in the early 1970s used state-of-the-art components including vacuum as energy source and analog electronics. The basic shortcomings of the early ABS brakes revolved around the low reliability of system electronics, and to some extent slow cycle rates due to limitations associated with the vacuum source. In 1978, BOSCH was the first supplier on the market to offer full-function antilock braking systems. In the past

couple of decades or so, antilock brake systems have made their debut in several types of vehicles (Oakley et al., 1973 [38]; Klein, 1974 [39]; O'keefe, 1977 [40]; Satoh, 1982 [41]; Leiber, 1983 [42]; Bleckmann, 1986 [43]; Jonner, 1986 [44]). A discussion of customary ABS systems is found in the Bosch Automotive Handbook [45]. There are two major advantages of an ABS over conventional brakes: *i)* ABS can provide shorter stopping distances on most road surfaces, and *(ii)* ABS can enhance steering control during hard braking maneuvers. Since 1986, the traction wheel slip control or anti-wheel spin regulator has been theoretically developed in numerous publications (Gerstenmeier, 1986 [46]; Maisch, 1987 [47]; Petersen, 1990 [48]). In 1993, BOSCH delivered the first Traction Control System (TCS) for passenger cars, 1993 [49]; in the meantime, a considerable amount of experience has been gained through ongoing development and testing. TCS is used to maximize the longitudinal friction coefficient by maintaining an appropriate slip ratio. If the TCS detects too much slippage in one or more driving wheels, it reduces engine torque and, if necessary, brakes the slipping wheel. This makes it possible to accelerate on icy roads and increases tracking stability. For many situations, a quick throttle valve intervention is enough for the TCS of front-wheel-driven passenger vehicles. Many different types of TCS are developed by TOYOTA, GM, BMW, BOSCH, etc.[50-53]. The acquired experience in the field enables to define the requirements for directional stability, optimum control strategy, maximum usage of the entire spectrum of drive torque intervention possibilities, and optimized hydraulics for automatic brake intervention. Besides traction control, especially Electronic Stability Control (ESC) of the vehicle is the most sophisticated directional and stability control systems currently under development [54]. Using a network of sensors, a particularly powerful electronic system

analyzes steering activity, wheel slippage levels, lateral acceleration and the vehicle's yawing behavior. Through ongoing comparison among these data, the ESC is able to detect whether the actual course of the automobile corresponds to the desired direction of travel. The Electronic Stability Program (ESP) has been developed by TEVES [55].

1.2.1 Basic Control Strategies and Methods

The control laws of exiting ABS were mostly developed through iterative laboratory experiments and engineering tests. There are some theoretical and systematic study reports about conventional ABS. Guntur (1972 [21]) and Ouwerkerk (1973 [56]) listed and studied several criteria used in ABS; some for predicting the occurrence of the lock-up of wheels and others for reapplying brakes while the danger of lock-up is averted. On the other hand, frequency domain methods such as the describing function method by Flin and Fenton (1981 [57]) and a classical feedback control approach by Zellner (1984 [58]) were used to analyze and design ABS. The ABS dynamics, however, exhibits strongly nonlinear characteristics. Frequency domain provides limited information regarding the dynamic performance of the braking. Most of the control laws that have been developed for the nonlinear ABS systems are based on the three most common approaches - adaptive control, variable structure control and fuzzy logic control.

Adaptive control strategies as one of robust control methods have been used for ABS control system [18-24]. At present, there are no affordable sensors available that can accurately identify the road surface and make this information available to the ABS controller. However, the road surface conditions can be inferred from the vehicle's braking pressure, wheel slip measurements, and deceleration rate comparison. A self-

tuning adaptive velocity control has been developed by Huang and Wang, 1995 [19]. A digital adaptive controller concept based on least squares optimization was developed by Landau, 1986 [20]. An adaptive sliding mode traction control algorithm for a vehicle, which included the weighted least squares estimation, the adjustment algorithm and the sliding mode, was identified by Tan and Tomizuka 1990 [22]. Masugi and Karl presented another adaptive sliding mode control 1999 [23], which can handle nonlinear tire forces. They tried to adapt unknown parameters of road friction in a known structure of braking system. Although this brings an improvement over previous controller designs, the adaptive method must sample a sufficient set of new data points after each change of plant parameters. This requirement introduces a significant additional delay each time a new control law is computed.

Fuzzy controllers, on the other hand, have an inherently parallel structure, which allows the controller to respond immediately once a new situation has been identified. Since ABS systems are nonlinear and dynamic in nature they are prime candidates for fuzzy logic control. Mauer (1994 [12]) presented a fuzzy logic controller and a decision logic network by identifying the current road condition based upon current and past readings of the slip ratio and braking pressure. The controller could detect wheel seizure immediately and avoid excessive slipping. A fuzzy logic surface identification scheme incorporating braking pressure, slip measurements, and vehicle deceleration rate comparisons is given in Mauer (1995 [13]). Layne, Passino, and Yurkovich (1993 [14]) proposed a fuzzy learning ABS controller, which used a learning mechanism to regulate wheel slip to a given target slip value. Cheok et al. (1996 [15]) described a fuzzy logic approach to design, implement, and tune an expert knowledge based traction control

system for a four-wheel drive vehicle. Wu, Lee, and Shih (1998 [16]) developed a neuro-fuzzy controller design for different road surface conditions. Conventional ABS control algorithms must account for non-linearity in braking torque due to temperature variation and dynamics of brake fluid viscosity. However, due to the nature of fuzzy logic, influential dynamic factors are accounted for in a rule-based description of ABS. This type of "intelligent" control (1999, [17]) allows for faster development of system codes.

Furthermore, variable structure control strategies are also employed for the ABS system. Lin, Dobner, and Fruechte (1993 [6]) proposed a linear feedback controller in their ABS system based on sliding mode control law. In this type of system, braking pressure mainly dependent on the wheel acceleration/deceleration during braking and the braking pressure is controlled to increase, decrease or hold according to each specific braking condition. An ABS algorithm for finding the optimal slip, using a friction force observer, is described by Drakunov et al. (1995 [7]). Sliding mode feedback control was described by Unsal and Kachroo (1999 [8]) who used a nonlinear feedback controller. The sliding observer is found promising while the extended Kalman filter is unsatisfactory due to unpredictable changes in the road conditions. Will, Hui, and Zak (1998 [9]) presented a nonlinear control system that combines a sliding mode-based optimizer and a proportional-plus-integral-plus-derivative (PID) controller for the antilock braking system. This controller can be implemented to compute the optimal slip rate on line using data obtained from commonly available longitudinal accelerometers and wheel speed sensors.

1.2.2 Vehicle Models

The mathematical models of vehicle dynamics are largely available and have been described in detail in the papers [59, 60]. The quality of a vehicle dynamic model, in general, relies upon the modeling methodology, characterization of properties of the vehicle and its components, and the validation of the model. The basic methodologies of modeling a vehicle include both analytical and experimental tasks. The analytical approach usually establishes the equations of motion of the vehicle and its components, which are considered valid under certain assumed conditions, while the experimental approach generally involves evaluations of the vehicle system or subsystem and vehicle parameters estimation.

Most of vehicle subsystems are frequently designed and developed independently of each other. The dynamics of these subsystems, however, often interact. The dynamic coupling between the braking and steering systems has considerable effect on the stability, controllability and stopping distance of the vehicle [61, 62]. For example, the maximum available longitudinal and lateral forces at the tire are strongly coupled. More longitudinal traction force is desired during straight line braking and more lateral force is desired during turning and braking. In combined cornering and braking/acceleration maneuvers, the vehicle's transition dynamics can not be governed by some equilibrium conditions as in a constant speed turning, when understeer or oversteer, to yield the stability conditions. However, by neglecting the effects of the change in vehicle speed in short periods of time, a quasi-steady-state condition can be assumed. The equilibrium equations of the vehicle motion with constant lateral and longitudinal accelerations then

can be developed and solved. The characteristic description of the vehicle turning behavior in acceleration or in braking can be also derived [63, 64].

Vehicle characteristics can be described in a single diagram over a large range of motions, including the nonlinear dynamics and transient states. The analysis of the performances of the vehicle is based upon the sideslip angle when no yaw and lateral motions at the center of gravity of the vehicle is assumed [26]. The dynamic response characteristics of yaw and lateral directional have been extensively investigated for different vehicle combinations through development and analysis of simplified yaw-plane models. Bernad et al. [65] examined the yaw stability of a vehicles with four-wheel steering through analysis of a linear yaw plane model. Xia and Law [66] investigated analytically both the steady state and transient response characteristics of a linearized yaw-plane model. While majority of the reported yaw-plane models assumes linear cornering characteristics of the tires, some studies have incorporated nonlinear cornering properties of tires based upon regression functions and "Magic Formula" [32-35]. Nonlinear yaw plane four-wheel models for vehicle braking system were developed by many authors in the literature (Kazunori [67], Huei [68], His-Fu [69]). The yaw-plane models provide effective assessment of rearward amplification, dynamic off-tracking, yaw and lateral stability limits of vehicle combinations, while the contributions due to pitch and roll motions and suspension dynamics can not be evaluated. Such simplified models offer considerable advantages in which relatively fewer number of parameters are required to evaluate the directional performance with reasonably good accuracy.

The static roll stability limit of a vehicle is frequently characterized by its rollover threshold, defined as the maximum lateral acceleration to which the vehicle can

withstand without rolling over in a steady turning maneuver. The roll instability is attained whenever the overturning moment, generated by the centrifugal forces, exceeds the net stabilizing moment. The location of the roll center of a vehicle in a unique point gives a certain restrictions to the models. The distribution effect of the roll moment could yield more accurate estimate of the rollover threshold. Nonlinear vehicle models were developed by Williams and Haddad [30] to incorporate the effect of roll moment distribution. Other nonlinear eight DOF four-wheel model used slip control for the braking system [70] while the longitudinal, and lateral weight transfer, tire force generation lag, roll steer, and steering compliance were used to assess the rollover threshold. The directional dynamics of heavy vehicles under simultaneous applications of braking and steering have been investigated through development of variable speed three-dimensional models. The Phase IV program perhaps represents the most comprehensive vehicle dynamics model for analysis of yaw, roll and lateral stability of heavy vehicles subject to braking and steering [61]. The model integrates the properties of braking and anti-lock braking system, nonlinear cornering properties of tires under braking and steering using lookup tables, nonlinear force-deflection properties of suspension springs, static properties of the articulation mechanism, and the combination of steering (open-loop and closed-loop), and driving/braking torque. The vehicle model is developed to analyze different vehicle combinations comprising up to three units and ten axles, with a maximum of 71-DOF. The Phase IV model is thus considered as a complex model, which requires extensive knowledge of the vehicle parameters. The study concluded that more sophisticated simulation models, such as the Phase IV model, do not necessarily yield more accurate predictions in quantitative terms than the simpler models, such as the

nonlinear yaw plane model. A comparison of the simulation results with the measured data further revealed that the more sophisticated, Phase IV also does not necessarily yield more accurate transient response than the simpler nonlinear yaw plane model.

In conclusion, a large number of vehicle models have been proposed in the open literature with varying degrees of complexities. While comprehensive three-dimensional models permit analyses under wide range of operating conditions, they require more tedious characterization of a large number of vehicle parameters. Simplified nonlinear yaw-plane models, on the other hand, yield lateral and yawing directional response with a reasonably accurate manner, assuming negligible contributions due to roll dynamics of the vehicle. For the development of vehicle braking model and identification of vehicle design, it is desirable to use a simpler, yet credible vehicle model.

1.2.3 Tire Models

Over the years, many braking and steering control systems were developed. The performances of such systems were assumed by using linear or linearized tire models. However, the linear tire model is only adequate for evaluating the lateral force of a tire with small slip and camber angles. The development of a more comprehensive braking system, especially for adverse road conditions, requires nonlinear tire models. Numbers of tire friction models have been developed for specific purposes and have limited applications. Several researchers have investigated the lateral and longitudinal dynamics of tires [71-73]. Usually a "relaxation length" or similar metric is used to characterize a first order lag in lateral shear force buildup; traditional kinematic relationships relating wheel spin to longitudinal slip, and longitudinal slip to shear forces at the tire road interface provide an adequate model for most simulation purposes. Van Zanten [74]

presented an experimental result with "unexpected" oscillations in wheel spin just after rapid application of braking torque. It was hypothesized that these oscillations would likely influence the performance of antilock brake systems. An insightful overview by Segel [75] on tire and vehicle modeling, calls for further elaboration of the tire shear forces and moments that are generated under time varying lateral and longitudinal slip. The friction potential between tire and road is a function of many parameters, related to the tire (such as compound, tread type, tread depth, inflation pressure, temperature), to the road (such as type of surface, texture, drainage capacity, temperature, lubricant such as water or snow), and to the vehicle state (such as speed, slip). Most of these parameters, especially the tire and road related parameters, are uncontrollable from the driver's point of view; furthermore, the parameters influence each other's effects on the frictional process. Over the last ten years, much research effort has been spent to estimate and predict the friction coefficient between tire and road, either by monitoring effects of the frictional process itself on the vehicle or the tire, or by monitoring some parameters influencing the frictional process [76-78]. Relatively recently, an empirical model-known as Magic Formula tire model, which is partly based on physical insight into tire force generating properties, has been developed [32-35]. The Magic Formula tire model gives a good representation of measured tire characteristics and certain coefficients of the model retain a physical significance, and therefor be expected to react to road surface variations in a meaningful manner. Van and Parsons [79] described a method using the Magic Formula tire model to correct laboratory data of tires to the road data. They used two additional coefficients to the Magic Formula tire model and the different road surfaces on the tire test results in order to achieve a high degree of correlation between instrumented

test and simulation results. It was indicated that this new method is very powerful to correct lateral force data for a specific road surface. High degree of correlation is often desired to validate vehicle dynamic models under specific transient maneuvers.

1.2.4 Braking and Steering Combined Maneuver

The basic purpose of a conventional ABS system is to prevent any wheel from locking and to keep the longitudinal slip in an operational range by cycling the braking pressure. This permits the vehicle to achieve a shorter stopping distance with good directional control and stability during moderate maneuver [60]. However, during severe braking and cornering maneuvers, the control logic of ABS may still yield limited levels of lateral force that poses serious problems to the stability and controllability of the vehicle. The handling performance of a vehicle is strongly dependent on both steering and traction.

With the progress in the application of electronic control in vehicle design, integrated electronic control systems for improved vehicle performance are now possible [80]. Nakazato, et al. [81] have presented a system to independently control the braking force between the inner and outer tires to reduce the yaw motion of the vehicle when driving in a turn. To obtain better stability and maneuverability, Matsumoto and Tomizuka [82] proposed a lateral velocity and yaw rate control law which used front differential force, rear differential force, and rear steering angle as extra control inputs. Their study indicates that the independent front and rear steering system allow wider variation of the lateral velocity and yaw rate in steady state conditions. By using a robust servomechanism control design methodology [83] and a linearized vehicle dynamic model, Salman [84] designed a command augmentation system for coordinated control of

the braking force and steering angle. The system, while taking into consideration the coupling between the braking and steering systems, adjusts the driver braking and steering inputs to improve vehicle path tracking and thus its directional stability. This command augmentation system was extended later by Salmon et al. [85] where the four braking torque and the rear steering angles are coordinated such that the deceleration and the yaw rate commands can be reached. Taheri and Law [86] introduced a slip control braking system, which can maintain the longitudinal wheel slip at pre-specified slip values during combined hard braking and severe steering. The desired longitudinal slip is modified as a function of the front wheel steering angle to make sure that sufficient levels of lateral force are available to maintain the vehicle lateral stability. Margolis et al. [87] have developed an integrated torque and steering controller using neutral handling as the desired target performance. The input-output linearization technique and slide mode control law was used by Yu and Moskwa [88] to develop a control algorithm to enhance the stability and performance of a vehicle in combined steering and braking actions by modifying driver's steering and braking commands. The simulation results show that vehicle maneuverability and stability can be improved by coordinating both steering and braking commands.

The dynamic coupling between the steering and braking negatively affects the dynamic performances of the vehicle in a combined braking and steering maneuver. However, it has been shown that an additional steering angle of the rear wheels, which is called active rear wheel or four-wheel control, may improve vehicle maneuverability and stability [36]. Active rear wheel braking and steering systems have extensively been investigated and developed over the past two decades to improve handling and stability

characteristics of the vehicle [89]. Four-wheel Steering Control (4WSC) techniques are being widely studied in this regard. The capabilities of 4WSC for improved directional response were extensively investigated. Sato et al. (1983 [90]) proposed a 4WSC system that used yaw rate feedback to equalizes front and rear centripetal accelerations. Sano et al. (1986 [91]) developed a relationship for the ratio of the rear to the front steering angle that results in a minimum sideslip angle in a steady-state turn. This relationship depends only on the vehicle speed alone and yields the following characterization: at low speeds the ratio is negative (out of phase steering) which results in a shorter turning radius thereby improved maneuverability. At high speeds the ratio is positive (in phase steering) and the delay in the lateral acceleration response is reduced. However, the rate of change of turning radius at high speeds is fairly high reflecting a decrease in lateral acceleration gain. Shibahata et al. (1986 [92]) suggested the use of an active four-wheel steering system that keeps the sideslip angle at minimum while maintaining a constant lateral acceleration gain over the entire speed range. Takiguchi et al. (1986 [93]) developed another four-wheel steering system that again varied the steering ratio as a function of the vehicle speed. However, instead of determining the ratio based on minimum sideslip criterion, the ratio was chosen so as to equalize the phase lags of the yaw rate and lateral acceleration. Acceptable lateral acceleration gain was maintained at high speeds. Whitehead (1988 [94]) proposed a linear control law that utilizes the yaw rate and the front steering angle to determine the rear steering angle. The gains in the control law were selected to be dependent on vehicle speed under the condition of minimum sideslip angle during general transient maneuvers. Xia and Law (1990 [95]) implemented this control law to improve performance in a collision avoidance maneuver. Lee [96]

designed a stability augmentation system to enhance stability of a 4WSC vehicle during high-speed straight-line motion under crosswind disturbance. The driver's steering command to the front wheels is improved while the steer at the rear wheels is controlled based on the yaw rate, lateral acceleration and side slip angle.

In addition to active rear wheel control system, direct yaw moment control systems using driving and braking forces have been investigated and developed to improve handling and stability of the vehicle [97]. These direct yaw moment control systems have been expected to suppress the deterioration of the steering control effects in nonlinear or large lateral acceleration ranges. Masao et al. [29] also developed an integrated control system for active rear wheel steering and moment control using braking forces. The performances of the controller are analyzed to verify its robustness in severe driving conditions. These control system is a model matching controller that makes the vehicle follow the desired dynamic model by using state feedback of both the yawing rate and the side slip angle. A new technique, Intelligent Sliding Surface Control (ISSC) which makes use of an adaptive sliding mode controller, has recently been used by Masugi and J. Karl [23], to prevent the instability induced by saturated functions of the control system. The simulation results show that the adaptive sliding mode controller can achieve robust performance with a smaller discontinuity gain than the traditional sliding mode controller.

1.2.5 Test and Simulation Techniques

Evaluating and comparison in the performance of various braking systems is usually carried out through test and laboratory measurements. Srinivasa et al. [98], presented the test results of two commercially available antilock devices to illustrate the necessity of

the test facilities. From the results shown, it appears that the laboratory testing should be used to compare and to evaluate the slip performance and braking effectiveness of various antilock devices. Results obtained could provide the vehicle and the brake designers with guidance to optimize the performance of antilock devices. The test comparison of vehicle equipped with standard brakes and the vehicle equipped with ABS have been described in many papers. Oppenheimer [99] investigated the parameters that influence the stopping distance potential of passenger cars equipped with or not with ABS. Essers [100] compared the performance of commercial vehicle equipped or not with ABS while cornering. Since 1970's, the 4WSC system have become available, many Japanese companies [101-103] provided the simulation test model for their vehicles. 4WSC system was able to improve vehicle maneuverability and cornering stability. Since 1986, the Traction Control System (TCS) had been theoretically proposed. Numerous publications presented various implementations of the TCS on vehicle. Test models and simulations were developed for this system. Peterson [104] described a modular system configuration including the components and some new features and control modes. Eubanks [105] presented a compilation of data from a series of skid tests comparing some of the control strategies and braking equipment. These tests were performed with an assortment of vehicles each equipped with or monitored by selection of device designed/applied to quantify some combination of time, distance and velocity. The implementation of ABS on different vehicles changes the longitudinal dynamics of the vehicle; one could assess the dynamic performance of the vehicle though significant investigations on the skid marks. An examination [106] was conducted by Strickland and Dagg with 19 different vehicles traveling at known speeds while being brought to a

straight line stop or through evasive and lane change steering maneuvers while applying full braking. The study established the friction coefficient exhibited by a number of different vehicles in the above described situation while standard braking systems were used.

Computer simulations of mechanical systems have been explored widely in many engineering areas. Vehicle dynamics widely employs simulations to evaluate the performances of newly designed vehicles. One of the simulation codes used in the ABS is the dynamic analysis proposed by Olson and Milacic [107]. This simulation code allows one to study the dynamic performances of a vehicle under various accelerations and braking conditions. Bowman and Law [108] described the simulation and evaluation of a slip control braking system using a comprehensive nonlinear, four-wheel vehicle model. A method and the corresponding FORTRAN code was proposed to evaluate the performances of the vehicle under slip controls that collect signals from the available sensors. Michaels [109] proposed the use of graphical modeling environment for real-time hardware-in-the-loop (HIL) simulation of automotive ABS systems. The prevalence of microprocessor-based controllers in automotive systems has greatly increased the need for software and hardware tools, which can be used to validate and test the performances of the control systems over an extended range of operation. Suh [110] developed the real time simulator of an ABS system and the methodology based on HIL simulation using a personal computer. The simulator can be implemented to develop more advanced control systems, such as traction control system, vehicle dynamic control system, etc. F. Svaricek [111] described a new software tool called Black Box Test that supports the ABS controller design process and that can be used for the detection of software and hardware

failures and further enhancement of the controller performance. Schneider [112] provided an example examination of a simplified ABS logic element that is representative of an ABS control strategy. For the development of control algorithms a special test stand was built by Maron [113]. This consists of the seat capsule, the actuator and the PC-based electronic control unit. As the electronic unit simulates a real time vehicle, the actuator is merged within a complete HIL system. Recently, M. W. Sayers [114] proposed a simulation code that was generated with the AutoSim multibody dynamic software that was linked with C code functions that enables communicate with braking hardware to create a real-time simulation with HIL. The model was also integrated with SIMULINK environment to provide a design tool for control engineers.

1.3 MOTIVATION AND SCOPE OF THE THESIS

From the review of literature studies, ABS can enhance vehicle dynamic performances during combined moderate braking and steering emergency maneuvers. The conventional design of an ABS system begins with a complete understanding of the tire-road friction characteristics. The braking in terms of minimum stopping distance would be optimized if the slip of the tire on which the brake is applied could always be kept at values corresponding to peak friction levels. The objective of ABS is to maximize the tire traction by preventing the wheels from being locked during braking whiie help maintain adequate vehicle stability and steerability. Although maximum traction force is desirable in straight-line motion, during cornering, when combined hard braking and severe steering maneuvers are performed, a trade off between stability and stopping distance

may be necessary. Under such type of maneuvers vehicles, even those equipped with conventional ABS control, could become oversteer and spin out.

1.3.1 Objective of the Thesis

The objective of this investigation is to develop a new comprehensive control system to overcome the tendency of oversteering and unstable situations during emergence braking, and to further improve the braking and vehicle stability performances. The trend in improving braking performances and stability of the vehicle yield to the development of a large number of braking system models, vehicle models and control strategies. Hence, the specific objectives of the study include the following:

- Develop a comprehensive hydraulic braking system model to represent strong nonlinear characteristics of the braking actuator systems;
- Based on the hydraulic and dynamic analysis of the actuator systems, investigate a new controller to minimize the tracking control errors;
- Develop an effective directional dynamic model of four-wheel steering vehicle to study the effects of yaw and roll, hence, to increase the vehicle stability;
- Develop a Four-wheel Steering Control (4WSC) and a Variable Slip-ratio Control (VSC) for the cornering characteristics to further improve the vehicle stability and maneuverability;
- Improve a Magic Formula (MF) tire model to respond within the performance characteristics of the ABS system under all foreseeable operating and road conditions;

- Compare a sliding mode optimizer with Magic Formula (MF) optimization to determine the optimal slip ratio with maximum friction forces;
- Determine the most desirable vehicle and braking system parameters, such that the ABS system can be ideally adapted to the different operating conditions.

The coefficient of friction between the tire and road surface plays the most important role. When operating on road surfaces with changing coefficient of friction or split friction, a vehicle may exhibit an unexpected dynamic behavior such as skidding or unbalance yaw motion. Thus, it is necessary to study the dynamic behavior of the vehicle and develop more comprehensive control system to improve the dynamics of the vehicle under the assumption that the friction coefficient between tire-road does not remain constant under the different road conditions.

The actuator braking system dynamics also plays an important role in ABS performances. The ABS must have the ability to change the system parameters depending on the actuator systems and a comprehensive control system must be developed based upon the analysis of the actuator system dynamics. Unfortunately, the dynamic characteristics of these systems are highly nonlinear and thus relatively difficult to control. The choice of the control force is strongly related to the fluid force and spring force in the master cylinder. The total force on the piston needs to include friction because friction in the hydraulic cylinder has a significant effect on the controller's performance, as predicted by simulations. Therefore, modeling of the hydraulic actuator as a dynamic system is essential when design an ABS.

1.3.2 Organization of the Thesis

In Chapter 2, a basic ABS control system is developed using the sliding mode based optimizer and PID controller. This system is trimmed based on the prediction of slip, detection of the road states, which are compared to the optimal slip to provide the best braking torque control. A simplified model of a vehicle undergoing a braking maneuver is used to evaluate the performance of the proposed ABS control system. The sliding mode optimizer performs an on-line search for the optimal wheel slip that corresponds to the vehicle maximum deceleration. According to the typical nonlinear tire characteristics, the optimal slip can be evaluated such that the greatest friction force between the tire and the road surface is provided. The PID controller and the sliding mode optimizer are coupled to regulate the vehicle braking torque and to control the wheel slip such that the optimal slip value is achieved. The information that the controller requires could be obtained from a longitudinal accelerometer and a wheel speed sensor, which are readily available and inexpensive. The performances of the proposed control schemes are illustrated with simulation examples. Simulation results from the implementation of the PID controller can be further used to compare with and derive the new nonlinear tracking control system, which are described and discussed in Chapter 3 and Chapter 4, in order to get the best braking performances and improve the stability of the vehicle.

In Chapter 3, the Magic Formula tire model (MF) is employed to develop a more comprehensive Nonlinear Tracking Control system (NTC), which would better face the adverse road driving conditions. The Magic Formula tire model was employed because it gives a good representation of measured tire characteristics and since certain coefficients of the model retain a physical significance, and is therefore expected to represent road

surface variations in a meaningful manner. The sensitivity of the MF on different road conditions is investigated for a selected tire. The MF tire model derived for different road conditions, are compared for validation with the available measured data. Examples of simulation were presented to illustrate the influence of the different road conditions, the brake-force distribution and the antilock control on the stop capability for the straight line braking. It is indicated that the optimum distribution of the friction and braking forces is necessary to achieve more robust vehicle directional stability, controllability and braking performance. Based on such optimal distribution and applying a nonlinear MF tire model, a new integrated NTC is developed for the nonlinear characteristics of the braking system. In the further approach, the actuator dynamics is included as a subsystem in a new integrated NTC, which is developed for the hydraulic braking system. This approach uses a candidate Lyapunov function to synthesize both the control law and the adaptation law necessary to estimate the unknown parameters of the system. The response characteristics of the resulting controller from the proposed model are compared with the available measured data presented in literature and the results are yielded in Chapter 2, to demonstrate its reliability for different road and operating conditions during straight line braking.

In Chapter 4, a nonlinear Yaw-plane Four-wheel steering control model with Limited Roll motion (YFLM), incorporating nonlinear cornering characteristics of the tires and compliance of the braking system accounting for the effect of weight transfer, is thus initially developed to study the braking responses of the vehicle. The new integrated NTC is applied for the hydraulic braking system, and Four-wheel Steering Control (4WSC) and Variable Slip-ratio Control (VSC) are developed for the cornering

characteristics. Three controllers are independent but coupled through the states of the longitudinal and lateral tire forces. 4WSC algorithm is developed with the objective of improving the stability and maneuverability of the vehicle. The driver's steering and braking inputs are interpreted to yield commanded vehicle states during a combined braking and steering maneuver. The braking forces are coordinated to equalize and hence minimize the force ratios at inner and outer wheels while ensuring that they provide a net zero yaw moment. The VSC algorithm gives a good balance between maximum longitudinal force and maximum lateral force, therefore, it can increase the vehicle stability and shorter the stopping distance. The desired set points for the slip values are calculated within the control algorithm to aid the controller in maintaining vehicle stability during emergency maneuvers consisting of combined hard braking and severe steering. The response characteristics derived from the proposed model are compared with the available measured data and the results from PID control system to demonstrate its validity. Simulations of the integrated controllers and ABS systems, for each system model, demonstrate the reliability and stability of the system. The system could overcome the tendency of oversteering during emergence braking or when braking during turning.

General conclusions concerning the dissertation research, major analysis and conclusions are finally presented in Chapter 5. Possible extension of the results to more specific problems and recommendations for future work are also included in this Chapter.

1.4 SYSTEM SIMULATION DESCRIPTION

The proposed simulation test stand was presented in the literature [16] by M.C.Wu, et al., who used hardware-in-the-loop (HIL). However, the mentioned paper described the

system incorporated with a vacuum booster system. Another particularity of the proposed system is that the braking pressure is considered to develop through a hydraulic booster unit instead of the vacuum booster system for the active brake control as described in the above paper. The hydraulic brake booster could produce a higher braking boost ratio and faster braking pressure response than the vacuum booster system. The hydraulic brake actuator is composed of a hydraulic brake booster unit, a master cylinder, the power supply unit and the control valve units. The hydraulic brake booster unit generates a hydraulic assisted force according to the brake pedal force applied by the driver. The basic schematic construction is shown in Figure1.3.

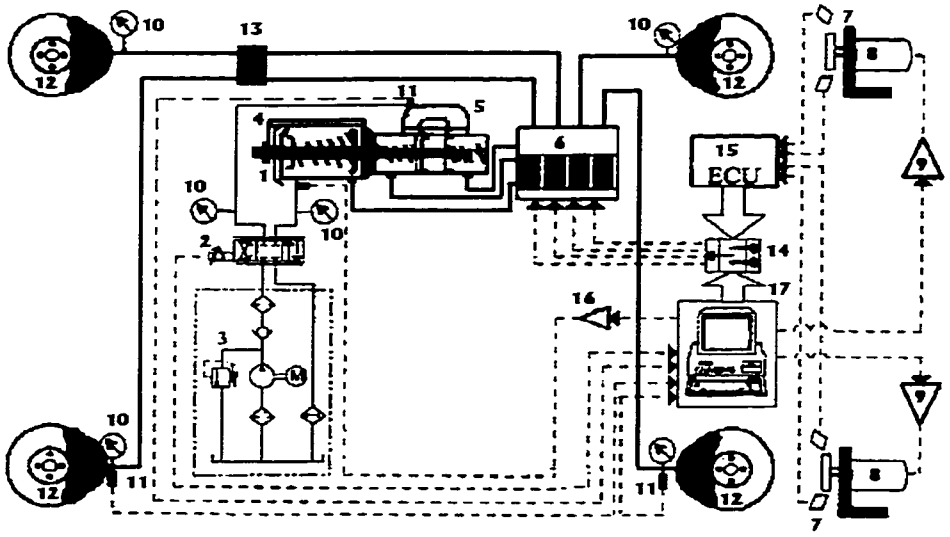

1. **hydraulic brake booster**
2. **servo valve**
3. **power source**
4. **LVDT**
5. **master cylinder**
6. **ABS modulator**
7. **wheel speed sensor**
8. **DC servo motor**
9. **motor driver**
10. **pressure gage**
11. **pressure sensor**
12. **brake disk**
13. **proportioning valve**
14. **swich**
15. **ECU**
16. **amplification circuit**
17. **computer hardware**

Fig. 1.3 Schematic Diagram of ABS Test Stand (modified from [16])

The system consists of an electric servomotor, driver and sensors, response time of which is considerably higher than that of the hydraulic elements. Thus, the main focus of

the analysis will be directed toward the performance of the hydraulic system. The power supply and control valve units are used to actuate the brake booster unit and master cylinder. The power braking assembly that is connected to booster chamber can amplify the input force from the pedal and push the rod of the master cylinder. High-pressured brake fluid flows from master cylinder though the ABS hydraulic modulator into each of the four cylinders. The hydraulic modulator is composed of four solenoid valves, one brake oil pump and two lower pressured tanks. The rotating tires are modeled as DC servomotors charged with the tractive braking load. The pressure at the calipers, the vehicle velocity and the rotating speeds of the tires are calculated by the computer. Either the electric brake control unit (ECU) or the computer could be used as controllers to regulate the brake fluid pressure.

The hydraulic brake boosters present the following advantages when compared with the conventional vacuum boosters:

- Higher braking boost ratio and faster braking pressure response since it utilizes high accumulator pressure;
- Braking effectiveness can be actively controlled by managing the hydraulic pressure since the braking disc deforms according to the reaction in the pressure chamber and the contact area;
- Suitable for adaptive brake characteristics since it considers a variable brake booster ratio and boost mechanism;
- Minimized small size and light weight actuator with the brake booster unit, master cylinder and regulator placed along the same axes;

- Easily applied to vehicle control systems since it uses the same power supply unit for brake booster and master cylinder.

The hydraulic brake booster generates a hydraulic assist force in relation with the brake pedal force applied by the driver. Fig 1.4 and Fig. 1.5 [116] show the qualitative characteristics and braking pressure responses of the hydraulic booster, respectively, compared with the conventional vacuum booster. It can be seen that the hydraulic brake booster exhibits higher brake boost ratio and faster pressure response than the conventional vacuum brake booster system.

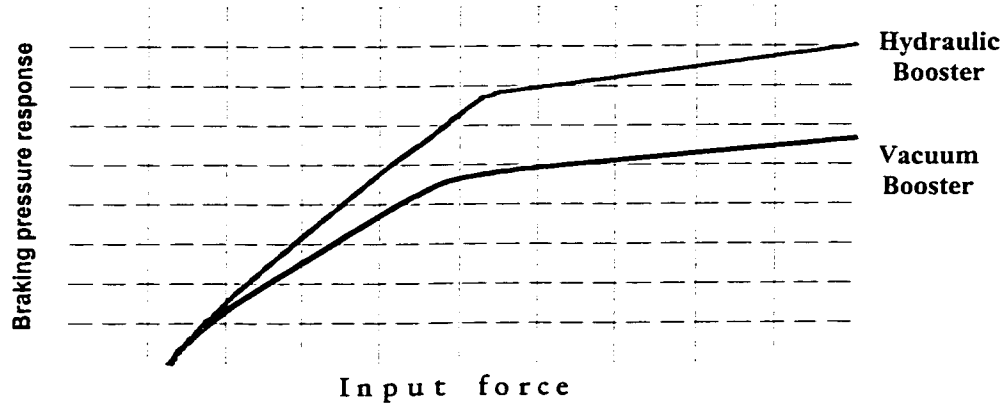

Fig. 1.4 Brake Booster Characteristics [116]

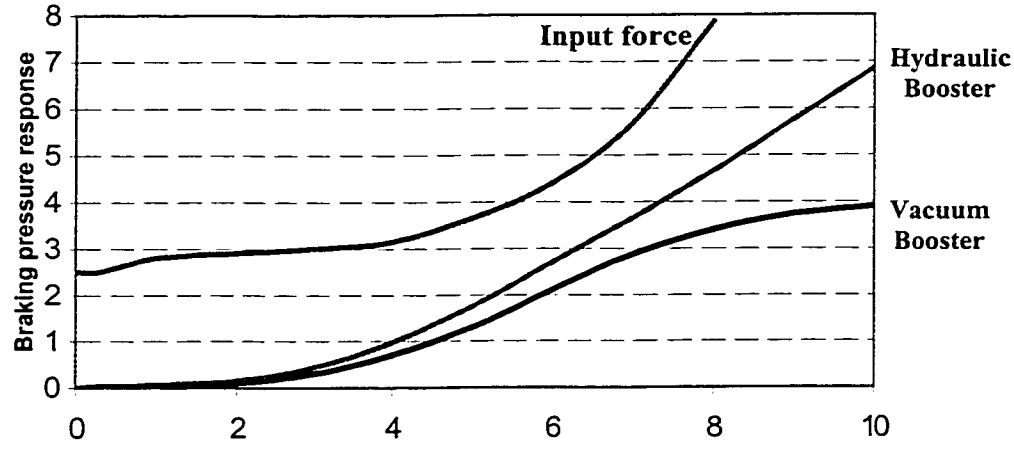

Fig. 1.5 Braking Pressure Response [116]

The basic simulation flowchart further considered in this study is shown in Figure 1.6. The system include: vehicle and wheel dynamics block, prediction of slip and detection of road state block, brake control logic block, hydraulic braking system dynamics block, which includes the developed hydraulic braking torque. The brake control logic is based on NTC for the hydraulic braking system, and optimum 4WSC and VSC for the vehicle system. The vehicle and tire model cooperates for the different road conditions. The wheel speed sensor would be able to detect the angular speed and angular deceleration of the wheels. When the wheel lock is detected, the pressure in one or more of the braking cylinders is reduced until the wheel speed exceeds a predetermined value.

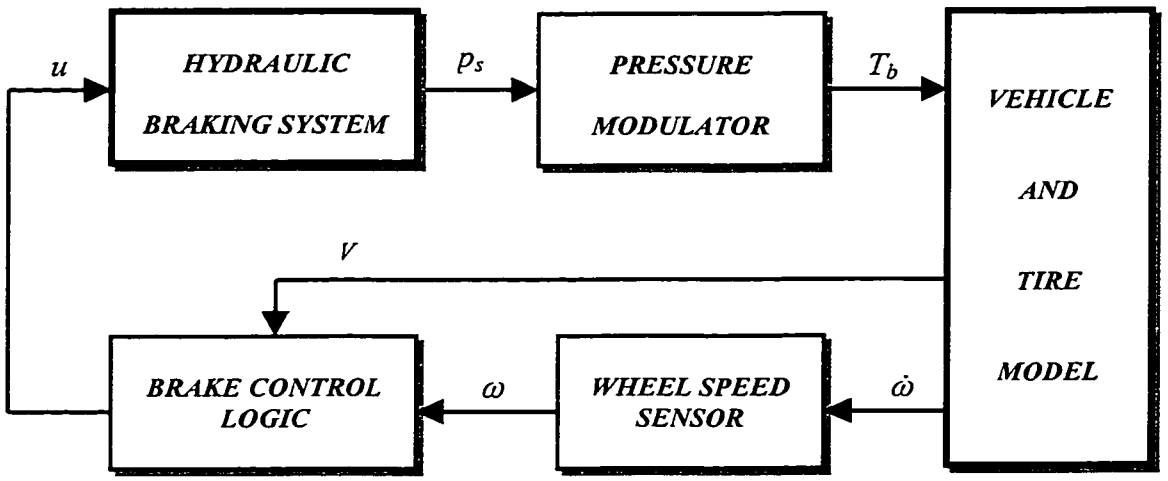

where T_b – *braking torque;* p_s – *braking pressure;* u – *slip control signal;* ω – *wheel speed;* V – *vehicle speed.*

Fig. 1.6 Basic Simulation Chart of ABS Control

CHAPTER 2

BASIC ABS CONTROL SYSTEM AND SYSTEM OPTIMIZATION

2.1 GENERAL

In 1978, Bosch came on the market with the first full-function antilock braking system (ABS). In 1993, Bosch delivered the first Traction Control System (TCS) for passenger cars. In the meantime, a considerable amount of experience has been gained through ongoing development and testing carried out all over the world. This experience further enabled to better define the requirements for directional stability, optimum control strategy, maximum usage of the entire spectrum of drive and optimized hydraulics for antilock brake intervention.

The typical schematic of an ABS system is shown in Figure 1.2. The large majority of ABS are integrated systems. They combine the master cylinder, hydraulic booster, and ABS hydraulic circuitry into a single hydraulic assembly. A wheel speed sensor transmits a signal of impending wheel lockup to the logic control which, in turn, provides a signals to a modulator to reduce brake line pressure that causes the wheel to be released and rotational speed to increase again.

The performance of an antilock braking system relies upon a proper identification of the road surface type. At present, there are no available affordable sensors that can accurately identify the road surface and make this information available to the ABS controller. However, the road surface type and conditions can be inferred from the vehicle's braking pressure, wheel slip measurements, and deceleration rate comparisons. One of the objectives of the ABS is to regulate the wheel slip so that the road adhesion

coefficient is maximized. In turn, this strategy leads to the minimization of the vehicle stopping distance. However, the desired slip range is strongly road surface dependent. The existing ABS systems attempt to regulate the wheel slip to a range close to the maximum.

It is known that a locked-up wheel generates a reduced braking force, smaller than the peak value of the available adhesion between tires and road. A locked-up wheel will also lose most of its capability to sustain any lateral force. This may result in the loss of vehicle stability and controllability. The basic purpose of a conventional ABS system is thus to prevent any wheel from locking and to keep the longitudinal slip in an operational range by cycling the braking pressure. This permits the vehicle to achieve a shorter stopping distance with good directional control and stability during moderate maneuvers.

The basic ABS brake control logic designed for this study include: *i)* prediction of slip; *ii)* detection of road state; *iii)* the scanning of optimal slip; and *iv)* actuator PID controller. The simulation model includes the control logic that has been illustrated in Figure 2.1. The function of the slip predictor is to estimate the slip, while the road surface state is judged through the deceleration of the vehicle and the angular deceleration of the wheels in conjunction with the pressure applied to the brake. According to the nonlinear tire model, the optimal slip can be identified within the point in which the greatest friction force between the tire and the road surface occurs. This optimal slip is used as the reference input to the actuator PID controller. The PID controller controls the slip to trace the reference input and try to maintain the greatest friction force under different braking conditions.

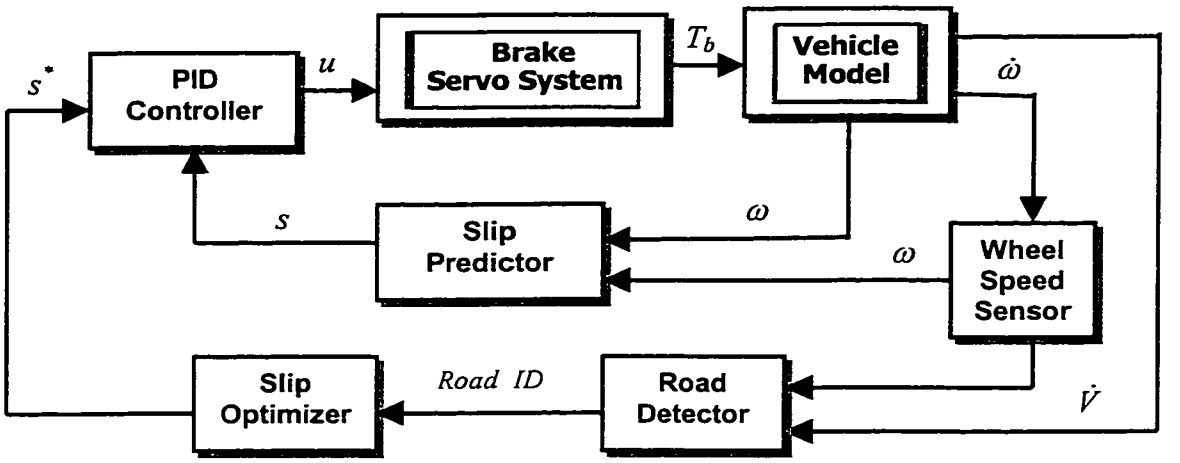

where T_b – *braking torque;* u – *slip control signal;* s^* – *optimal slip;*
s – *wheel slip;* ω – *wheel speed;* V – *vehicle speed.*

Fig. 2.1 Simulation Model of the Basic ABS Control

2.2 ABS SYSTEM OPERATION PRINCIPLES

When the driver quickly and firmly applies the brakes and maintains the pressures to the pedal, the brakes of a vehicle which is not quipped with ABS will almost immediately lock the wheels. Good drivers have always pumped the braking pedal mostly on bad road conditions during panic stops, to avoid wheel lockup and the loss of steering control. During such time, it is difficult for the driver to keep the vehicle along the desired path, which is known likely that the vehicle will skid, out of control. The locking of the wheels is the main cause of the skidding and lack of control. If the driver would be able to release the brake pedal just before the wheels locked up then reapply the brakes, the skidding would be avoided. This release and reapply of the brake pedal is exactly what an ABS does. When the brake pedal is pumped or pulsed, pressure is quickly applied and released at the wheels. Pressure modulation works to prevent wheel locking. By

modulating the pressure to the brakes, friction between the tires and the road is maintained and the vehicle is able to come to a controllable stop.

The structure and function of the ABS hydraulic unit was illustrated before. TEVES was one of the first companies to introduce a compact integrated ABS system in 1985 on some Ford passenger vehicles (Figure 2.2-Figure 2.5)[117]. The four-wheel ABS system uses hydraulic brake fluid for the braking function of the wheel pads and the hydraulic booster. Major system components are master cylinder, hydraulic booster, electric pump, accumulator, electronic controller, reservoir, relays, wheel speed sensor, and warning lights. The brake booster is located behind the master cylinder in basic conventional arrangement. The booster control valve is located in a parallel bore above the master cylinder and operated by a lever mechanism connected to the pushrod of the brake pedal (Figures 2.3-2.5). Advantages include compact design requiring reduced space; moreover, the performance characteristics of the booster can be selected and easily optimized for the particular application. Unlike conventional brake boosters, the brake master cylinder pistons are decoupled from the brake pedal. This makes possible to dimension the diameters of the master cylinder pistons such that, in the event of a pressure supply failure, higher brake line pressures and, hence, greater decelerations can be achieved with normal pedal forces. If a brake circuit fails, the counter-pressure at the brake pedal remains stable as s result of the decoupling process. With conventional brake boosters, a brake line failure may cause sagging of the brake pedal due to the absence of any resistance force against the brake pedal.

From Figure 2.2, when a wheel speed sensor signals the ABS control module that a high rate of deceleration is taking place at its wheel and the wheel is likely to lock and

skid, the controller will initially impose the hydraulic unit to keep the hydraulic pressure constant at the wheel. If the wheel continues to decelerate, the controller will signal the solenoid valve to reduce hydraulic pressure to the affected wheel. This procedure reduces braking at the wheel, reducing the risk of lockup. The wheel continues to spin as a result of the reduced braking pressure. Once a specific limit of spin has been reached, the controller registers that the wheel is not being sufficiently braked. Thus, the wheel is again decelerated by increasing the pressure on the braking pad, which was initially reduced. The control cycles may be executed many times in a second depending upon the road conditions.

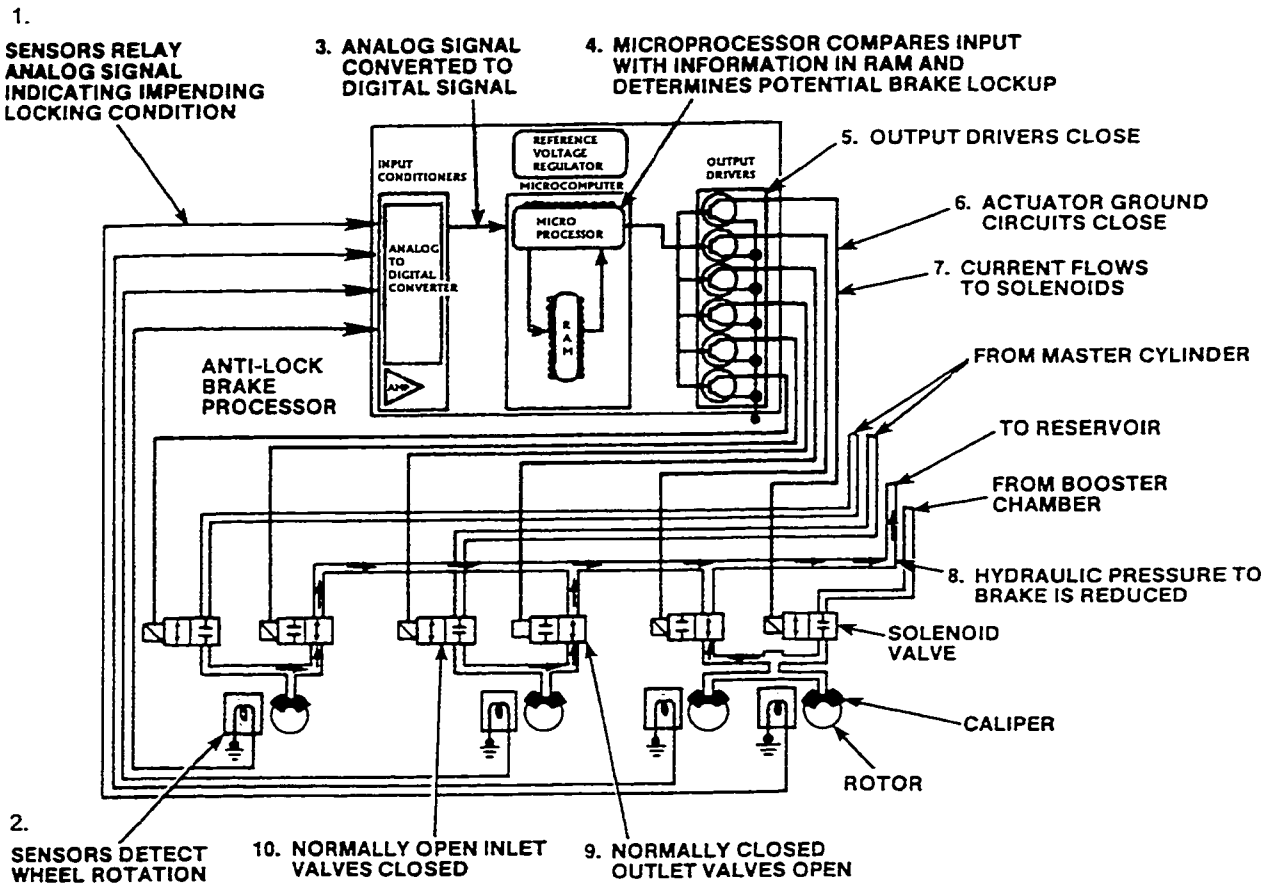

Fig. 2.2 ABS Operation – Potential Brake Lock Condition ([117] TEVES)

A typical ABS system operates in three different modes, according to the braking levels and the vehicle dynamics: *i)* no braking applied (Figure 2.3); *ii)* normal braking – ABS not activated (Figure 2.4); *iii)* anti-lock mode - ABS in operation (Figure 2.5).

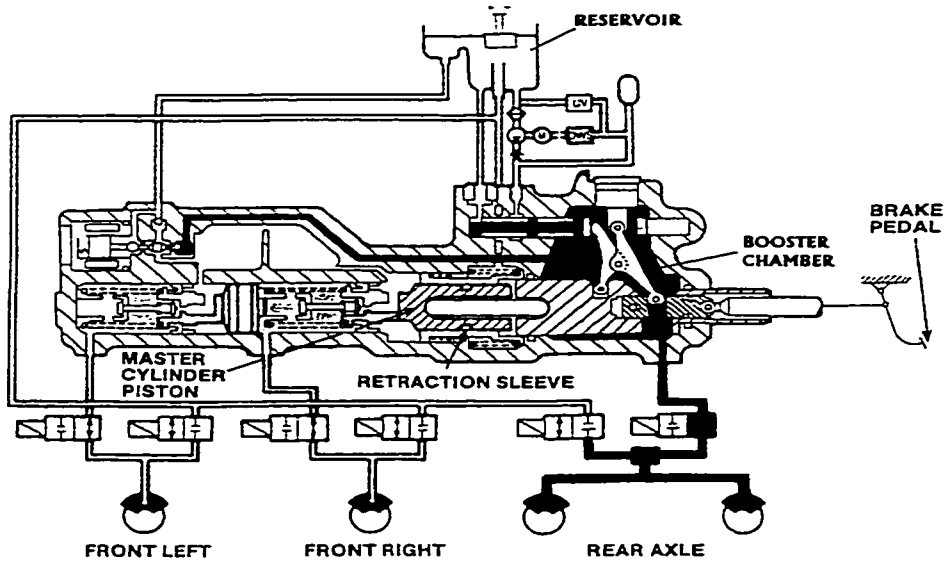

Fig. 2.3 No Braking Applied ([117] TEVES)

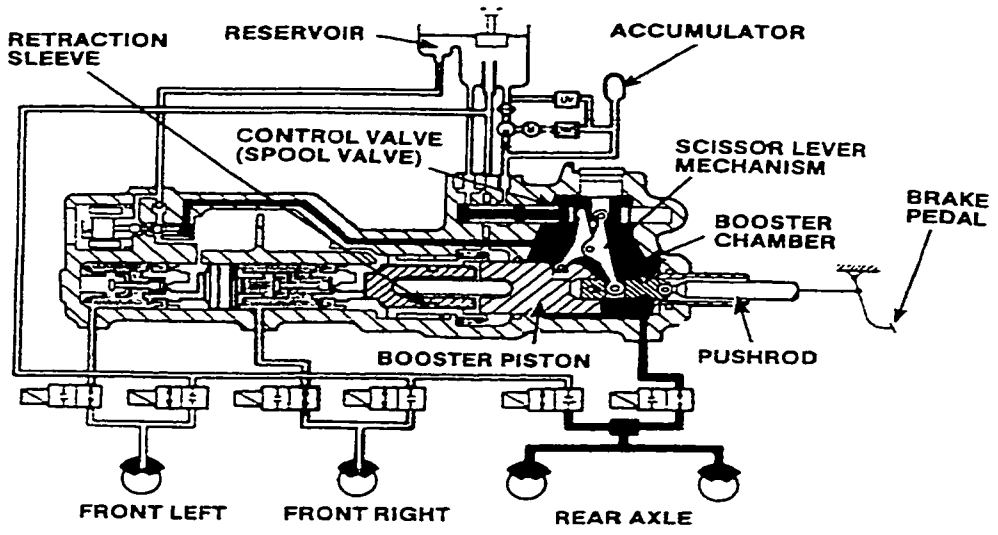

Fig. 2.4 Normal Braking – ABS Not Activated ([117] TEVES)

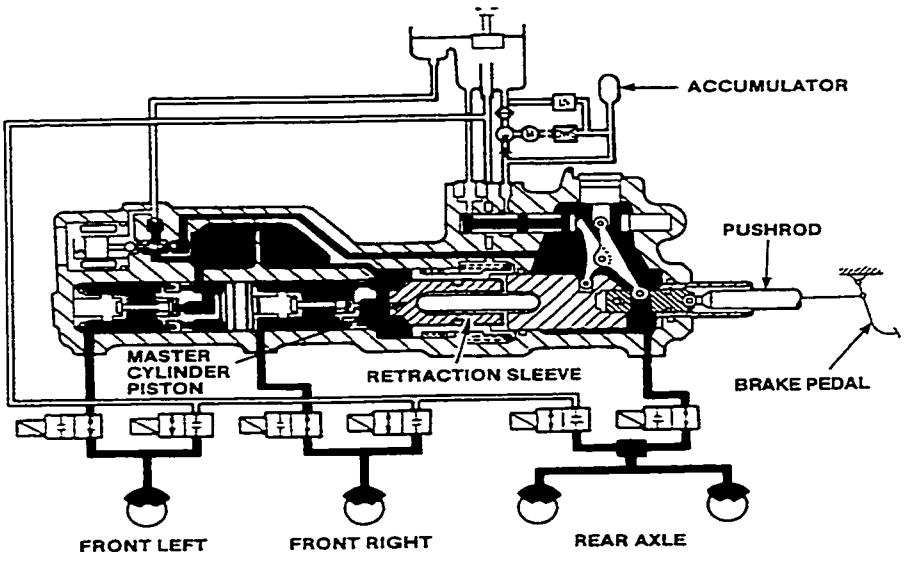

Fig. 2.5 ABS in Operation ([117] TEVES)

i). From Figure 2.3, when the brakes are not applied, or when the brakes are released, the piston in the master cylinder is retracted. The booster chamber is vented to the reservoir, and the fluid in the chamber is kept at the same low pressure as in the reservoir.

ii). In normal braking, when the brakes are applied under normal conditions, the brake pedal actuates a pushrod (Figure 2.4). This operates a scissors lever, which moves a spool valve. When the spool valve moves, it closes the port from the booster chamber to the reservoir and partially opens the orifice from the accumulator, which is opening proportional to the pressure on the brake pedal. This allows hydraulic fluid under pressure from the accumulator to enter the booster chamber. As hydraulic pressure enters, it pushes the booster piston forward, providing hydraulic assist to the mechanical thrust from the pushrod.

iii). In ABS operation, the ABS is activated when the controller determines that the wheels are about to lock up based on rotation speed and deceleration rate. The controller commands to open the valve that supplies the chamber between the two master cylinder pistons and the chamber between the retraction sleeve and the first master cylinder piston (Figure 2.5). The hydraulic pressure on the retraction sleeve activates the pushrod to move back the brake pedal. In effect, the hydraulic pressure to the front wheels is now supplied by the accumulator but not by the brake pedal action. The controller also opens and closes the solenoid valves to cycle the brakes on the wheels that have been locking up. When the solenoid valves are open, the master cylinder pistons supply hydraulic fluid to the front brakes while the boost pressure chamber provides hydraulic pressure to the rear. When the solenoid valves are closed, the hydraulic fluid from both the master cylinder pistons and booster pressure chamber is cut off. The hydraulic fluid is returned from the brakes to the reservoir. The solenoid controlling the isolation/inlet valve in the hydraulic circuit is activated, which prevents the fluid flow from the master cylinder and hydraulic booster, and also prevents the hydraulic pressure from reaching wheels.

The electronic circuitry monitors the electromechanical components of the system according to the strategy established by the controller. Malfunction of the ABS causes the electronic controller to shut off or inhibit the system. However, normal power-assisted braking remains. Malfunctions are indicated by the warning lights inside the vehicle. Loss of hydraulic fluid or power booster pressure disables the antilock braking system. In most malfunctions of the antilock braking system, the check antilock braking or braking

light is illuminated. The sequences of illumination of these warning lights combined with the problem symptoms determine the appropriate diagnostic tests to perform.

2.3 SIMPLIFIED VEHICLE MODEL

In this Chapter, a simplified model of a vehicle undergoing a braking maneuver, which is used to evaluate the performance of the basic ABS control system, is developed. The quarter vehicle as a simplified model is firstly considered in this section as shown in Figure 2.6. The rolling resistance force is small due to braking, which can be neglected. More complicated Nonlinear Yaw-plan Four-wheel steering system with Limited Roll Motion will be further presented and discussed in Chapter 4.

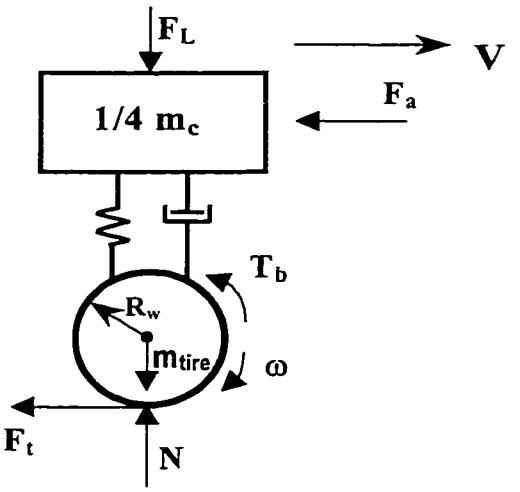

Fig. 2.6 Free Body Quarter Vehicle Model

2.3.1 Vehicle Dynamics

According to Newton's second law, the equation of motion of the simplified vehicle can be expressed by

$$m_t \dot{V} = -F_t - F_a \tag{2.1}$$

where V = *vehicle velocity*
F_t = *road friction force*
F_a = *aerodynamic force acting on the vehicle*
m_t = *total mass of the quarter vehicle.*

The road friction force is given by Coulomb law

$$F_t = \mu N \tag{2.2}$$

where N = *total normal load*
μ = *road adhesion coefficient.*

The total mass of the quarter vehicle can be written as

$$m_t = m_{tire} + \frac{1}{4} m_c \tag{2.3}$$

where m_c = *vehicle mass*
m_{tire} = *tire mass.*

Thus, the total normal load can be expressed by

$$N = m_t g - F_L \tag{2.4}$$

where $F_L = \frac{m_c h_c}{2L} \dot{V}$ *is the longitudinal weight transfer load due to braking*
h_c = *center of gravity height*
L = *wheel base.*

The aerodynamic force acting on the vehicle is proportional to the square of the speed of the vehicle with respect to the air and depends on the vehicle shape and size [118] and [119]. Thus,

$$F_a = \frac{1}{4}\left(\frac{\rho}{2} C_d A_f V^2\right) \tag{2.5}$$

where ρ = *mass density of the air*
C_d = *vehicle drag coefficient*
A_f = *vehicle frontal area.*

The aerodynamic forces are generated through two different mechanisms: one is the airflow over the exterior of the vehicle body, and the other is the flow through the engine radiator system and the interior of the vehicle for cooling, heating, and ventilation. The former is accounts for more than 90% of the total aerodynamic force of a passenger car. The skin friction may become more significant, however, for a long vehicle, such as a bus or a tractor-semitrailer.

The air density is variable depending on temperature, pressure, and humidity conditions, which can be estimated by the relationship [119]

$$\rho = 1.23\left(\frac{P_r}{101.32}\right)\left(\frac{519}{460+T_r}\right) \tag{2.6}$$

where P_r = *atmospheric pressure in kPa*
T_r = *air temperature in degrees Fahrenheit.*

For standard atmospheric conditions, the mass density of the air can be taken as 1.23 kg/m^3, which is used in this study.

For passenger cars, the relationship between the frontal area and the vehicle mass may be approximately expressed by [119]

$$A_f = 1.6 + 0.00056(m_c - 765) \tag{2.7}$$

where A_f = *frontal area in* m^2;
m_c = *vehicle mass in kg.*

The vehicle drag coefficient C_d varies over a broad range from 0.4 - 0.7 with the shape [118], [119]. In addition to the shape of the vehicle body, the attitude of the vehicle defined by the angle of attack, ground clearance, loading conditions, and other operational factors, such as radiator open or blanked, and window open or closed, also affect the aerodynamic drag coefficient.

2.3.2 Wheel Dynamics

During braking, a stoppage torque is applied to the wheel, the wheel speed decreases and the vehicle speed also decreases as shown in Figure 2.6. The rolling resistance force is much smaller than the friction force and is neglected. According to Newton's second law, the equation of motion at wheel level for the rotational DOF is given by

$$J_w\dot{\omega} = -T_b + F_t R_w \tag{2.8}$$

where J_w = *wheel moment of inertia*
ω = *wheel speed*
R_w = *wheel radius*
T_b = *braking torque*
F_t = *road friction force.*

2.3.3 Braking Dynamics of the System

From the above analysis, the governing equations of the vehicle model resulting from (2.1) to (2.8) can be expressed as

$$\begin{aligned}(m_t - \mu(s)m_e)\dot{V} &= -\mu(s)m_t g - (\rho/2)C_d A_f V^2/4 \\ J_w\dot{\omega} &= -T_b + \mu(s)(m_t g - m_e\dot{V})R_w\end{aligned} \tag{2.9}$$

where $m_e = m_c h_c/(2L)$, *which is effective mass.*

Letting $x_1 = x$, $x_2 = V$, $x_3 = \omega$, the vehicle model in state-space format is

$$\begin{bmatrix}\dot{x}_1\\ \dot{x}_2\\ \dot{x}_3\end{bmatrix} = \begin{bmatrix}1 & 0 & 0\\ 0 & 1 & 0\\ 0 & -\dfrac{R_w}{J_w}(\mu(s)m_e) & 1\end{bmatrix}\begin{bmatrix}x_2\\ \dfrac{1}{m_t - \mu(S)m_e}\left(-\mu(s)m_t g - \dfrac{\rho}{2}\dfrac{C_d A_f x_2^2}{4}\right)\\ \dfrac{m_t R_w}{J_w}(\mu(s)g)\end{bmatrix} + \begin{bmatrix}0\\ 0\\ -\dfrac{1}{J_w}\end{bmatrix}T_b \tag{2.10}$$

2.4 ANTILOCK BRAKING SYSTEM OPTIMIZATION

In this section, a simple hybrid wheel slip controller that contains a sliding mode module coupled to a PID control module is proposed. Further, its operation is illustrated with simulation examples. This controller can be implemented on-line to compute the optimal slip rate using data obtained from commonly available longitudinal accelerometers and wheel speed sensors. In Chapter 3, the above PID control system will be used as reference to compare its performance with the proposed nonlinear tracking control system.

2.4.1 Wheel Slip and Road Adhesion

The present ABS is controlled by the slip ratio and the wheel acceleration. When the braking action is initiated, a slippage between the tire and the contacted road surface will occur, which make the speed of the vehicle to be different from that of the tire. It is known that tire forces are nonlinear functions of the slip angle and the slip ratio. They are also dependent on the vertical load (which may vary due to the longitudinal and lateral load transfer) and also the coefficient of friction on the tire-road contact patch. The top view schematic of a tire during combined braking and cornering at the wheel centre on contact patch is shown in Figure 2.7. Note that for straight line driving vehicle, the wheel slip ratio α will be zero.

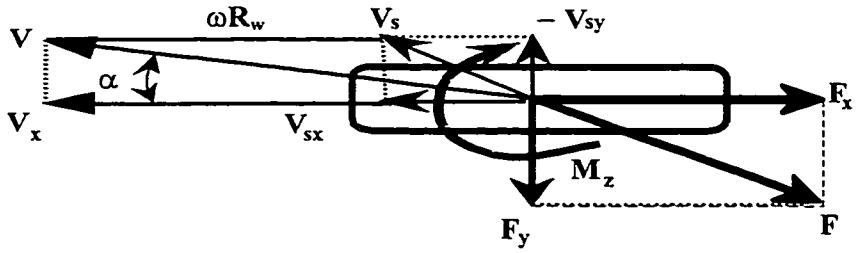

Fig. 2.7 Velocity and Force Vector Diagrams of Tire

where F_x = *total force in longitudinal direction*

F_y = *total force in lateral direction*

M_z = *self aligning torque*

V = *vehicle speed in travel direction*

V_s = *slip speed vector*

ω = *wheel angular velocity*

R_w = *wheel radius*

α = *sideslip angle.*

The longitudinal slip is defined as

$$s_a = \frac{V\cos\alpha - \omega R_w}{V\cos\alpha} \tag{2.11}$$

The side slip angle is

$$\alpha = \tan^{-1}\left(\frac{V_{sy}}{V_x}\right) \tag{2.12}$$

As the equation indicates, braking slip occurs as soon as the wheel decelerates to a rotational speed below that which would normally correspond to a given vehicle velocity. However, this is the only state in which braking forces can be generated. The road adhesion coefficient (coefficients of friction) is frequently expressed as a function of braking slip. The significant physical relationships of ABS control for straight line braking is illustrated in Figure 2.8, and for braking while turning is shown in Figure 2.9 [37]. These typical experimental test results are used mostly by many automotive industries. The suitable slip-range is about 5% ~ 20% on normal roads and changes with different road conditions.

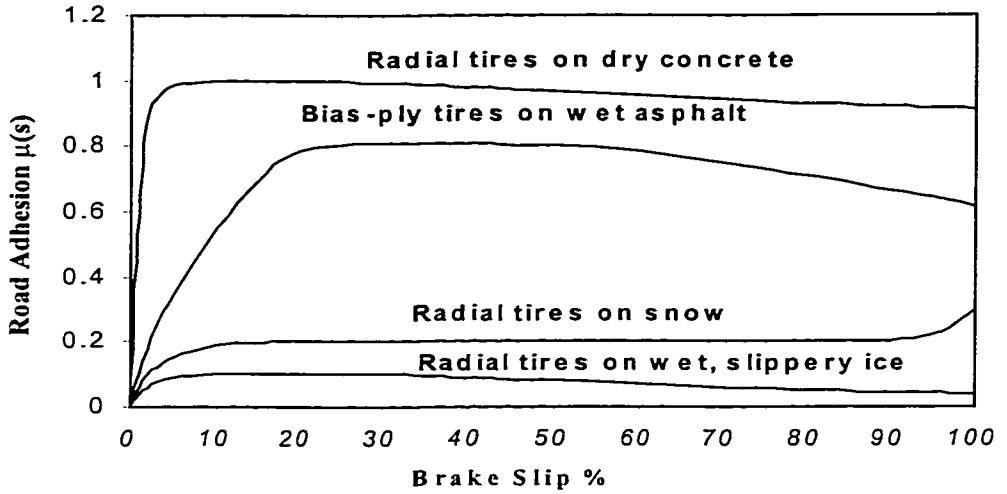

Fig. 2.8 Road Adhesion vs. Wheel Slip for Straight Line Braking ([37] Bosch)

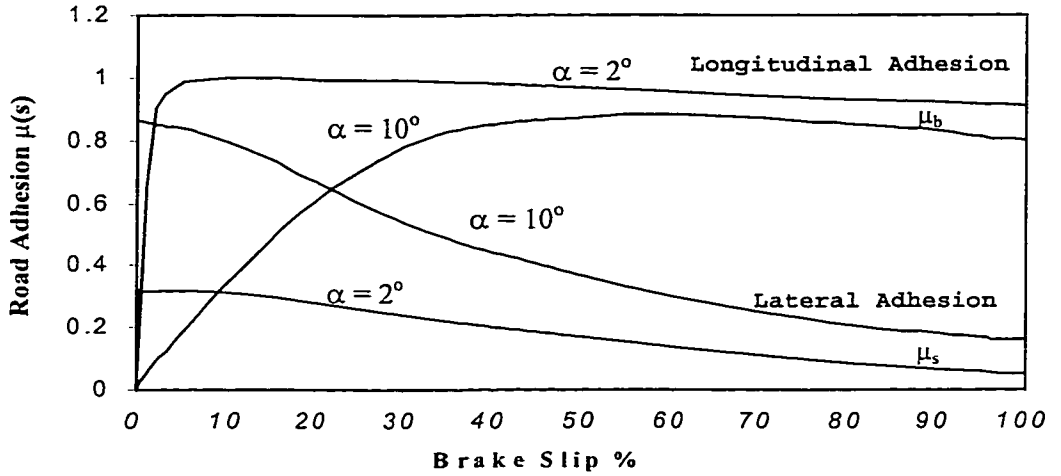

Fig. 2.9 Road Adhesion vs. Wheel Slip and Slip Angle for Braking while Turning ([37] Bosch)

Both the vehicle's steady-state handling, as well as its response characteristics during directional transitions is significant factors in evaluating the brake performances of the vehicle. These characteristics are relevant, for instance, when the driver of a vehicle traveling in a straight line must suddenly initiate evasive maneuvers. When braking on snow, the snow wedge forming under the locked tire causes an additional

retarding effect [37]. Figure 2.8 gives the surface adhesion coefficient curve against the wheel slip, which usually consists of two regions: one region with a positive slope, the other with a negative slope. In normal braking, the brake operates in the region with positive slope, the negative slope in braking being related to the vehicle directional instability. When excessive wheel slip occurs, the brake operates in the region of negative slope. Therefore, to avoid the directional instability, the ABS control is needed.

Of all the maneuvers encountered in everyday driving, one of the most critical and most significant for vehicle design is braking during turning. The significant physical relationship for braking while turning is shown in Figure 2.9. The inspections of the two curves associated with low (at 2- degree slip angle) and high (at 10-degree slip angle) lateral acceleration indicates that the ABS control range must cover a wide performance spectrum. During severe braking and turn, the ABS system should intervene early with initially low deceleration values while the lateral acceleration remains still near its maximum value permitted by the tire road friction coefficient. As speed decreases and lateral acceleration drops, the ABS system produces increasing levels of braking slip. For optimally designed ABS, the stopping distance while turning is only slightly longer than that associated with a straight stopping. The cornering braking control system will further be discussed detail in Chapters 3 and 4.

2.4.2 Sliding Mode Optimization

The braking control system that makes use of the slip as the feedback signal to control the ABS is proved to shorten the braking distance effectively, and to improve the controlling and stability of the vehicle while the brake is applied.

From Equations (2.1) and (2.9), the equilibrium of forces on the vehicle can be written as

$$F_t + F_a = \mu(s)\frac{m_t g}{m_t - \mu(s)m_e} + \frac{(\rho/2)C_d A_f V^2/4}{m_t - \mu(s)m_e} \tag{2.13}$$

In the above equation, the road adhesion coefficient μ is a unimodal function of the wheel slip s. Thus, the function μ(s) has only one minimizer. One assumes that $m_t - \mu(s)m_e > 0$, note that the second term of the right hand helps to increase the friction force which in turn reduces the stopping distance. Hence, maximization of the friction force leads to the maximization of the first term in Equation (2.13) which is denoted by

$$F = \mu(s)\frac{m_t g}{m_t - \mu(s)m_e} \tag{2.14}$$

First, F_t has only one critical point that coincides with the maximizer of μ. The greatest friction force will occur at the desired slip s^*, therefore it can be found from

$$\left.\frac{dF}{ds}\right|_{S=S^*} = 0 \tag{2.15}$$

Hence $\left.\frac{dF}{ds}\right|_{S=S^*} = \frac{m_t^2 g}{(m_t - \mu(s)m_e)^2}\frac{d\mu(s)}{ds} = 0$ if and only if $\frac{d\mu}{ds} = 0$, which means that F has only one critical point that coincides with the maximizer of μ.

Second, s^* is the maximizer of F. Applying the second derivative test, one has

$$\left.\frac{d^2F}{ds^2}\right|_{S=S^*} < 0 \tag{2.16}$$

Hence $\left.\frac{dF}{ds}\right|_{S=S^*} = \left(\frac{2m_e m_t^2 g}{(m_t - \mu(s)m_e)^3} + \frac{m_t^2 g}{(m_t - \mu(s)m_e)^2}\right)\frac{d\mu^2(s)}{ds^2} < 0$ if and only if $\frac{d^2\mu}{ds^2} < 0$.

This means that s^* is indeed the maximizer of F.

The sliding mode optimizing algorithm method was first proposed by Korovin and Utkin [10], and further developed by Utkin [11]. Under the proposed optimizing strategy, the unidimensional plant is described by the equation

$$y = f(s) \tag{2.17}$$

During the optimization run, the objective function $f(s)$ will be decreasing and leader minimum at a certain unknown value of the input variable s^*, which is the only minimizer, in the interior of the interval [a, b], and

$$dy/ds \neq 0 \text{ at } s \neq s^* \tag{2.18}$$

The requirement is to initiate a search process that will yield minimized plant output. Then, the objective function, $y = f(s)$, should be decreasing in time tracking a monotonically decreasing function

$$g(t) = -\theta (t - t_0) \tag{2.19}$$

where t_0 = *initial time*
θ = *design parameter.*

A block diagram of this optimizer has been described in detail by General Motors NAO Electric Centre [9] and the literatures [10, 11] as shown in Fig. 2.10.

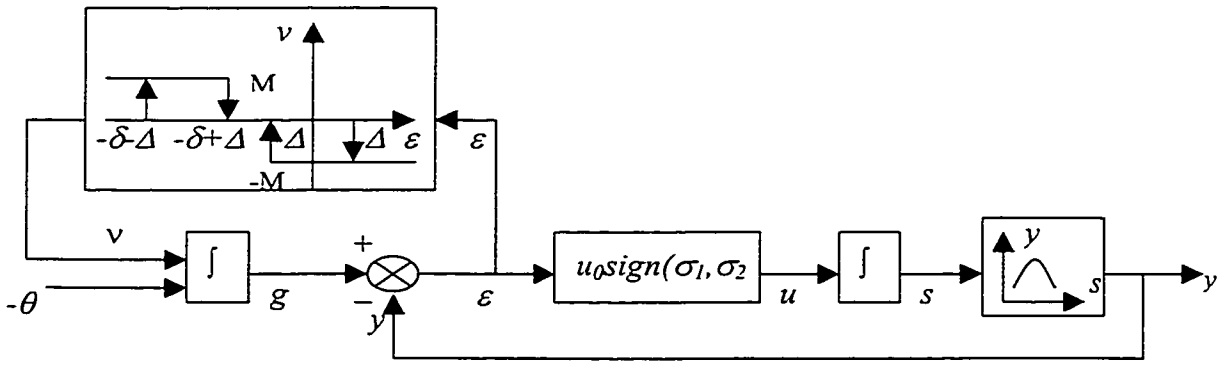

Fig. 2.10 Sliding Mode Based Optimizer

The control system is described by the set of equations [9] as

$$\begin{aligned} y &= f(s) \\ \dot{s} &= u \\ u &= u_0 sign(\sigma_1, \sigma_2) \\ \sigma_1 &= \varepsilon \\ \sigma_2 &= \varepsilon + \delta \\ \varepsilon(t) &= g(t) - y(s) \\ \dot{g} &= -\theta + Mv(\sigma_1, \sigma_2) \end{aligned} \tag{2.20}$$

where u_0 = *optimizer independent variable gain*
M = *optimizer reference signal switching strength*
δ = *optimizer error interval width*
Δ = *optimizer hysteresis width*
ε = *defines the tracking error*
$v(\sigma_1, \sigma_2)$ = *auxiliary signal can be obtained by a three positional relay.*

The auxiliary signal parameter M is chosen to satisfy

$$M > u_0 \left| \frac{dy}{ds} \right| + \theta \tag{2.21}$$

It is clear that the control input u controls the independent variable of the trajectory $s(t)$ and the objective function $y(s)$.

When the magnitude of the initial tracking error ε is large, an auxiliary function $v(\varepsilon)$ is generated by the relay force as error into the region where:

$$(\sigma_1 + \Delta)(\sigma_2 - \Delta) < 0 \tag{2.22}$$

The design parameter $\Delta < 0$ is chosen to satisfy the inequality

$$2\Delta < \delta \tag{2.23}$$

Inside the region where $(\sigma_1 + \Delta)(\sigma_2 - \Delta) < 0$, the tracking error satisfies

$$\dot{\varepsilon} = -\theta - \frac{dy}{ds}\dot{s} = -\theta + u_0 \frac{dy}{ds} \tag{2.24}$$

Hence, the trajectory *s(t)* will reach the uncertainty region around the minimizer and will stay within this region thereafter. The uncertainty region is described by

$$\frac{dy}{ds} \leq \frac{\theta}{u_0} \tag{2.25}$$

Therefore, at a certain instant of time the system will be under the condition $(\sigma_1-\Delta)(\sigma_2+\Delta) < 0$ and v become zero. The parameters u_0 and θ control the width of the uncertainty interval, and there are sufficient conditions for the sliding mode optimization.

Assuming

$$\left|\frac{dy}{ds}\right| \leq \frac{\theta}{u_0} = \eta \tag{2.26}$$

Then the trajectory *s(t)* is in the desired uncertainty region around the minimizer and will stay in this region thereafter. Thus, the trajectory *s(t)* moves towards the minimizer and will reach the uncertainty region in finite time by properly selecting the design parameters.

Further, let assume

$$\frac{dy}{ds} > \frac{\theta}{u_0} \tag{2.27}$$

This condition describes the situation corresponding with the position to the right of the uncertainty region,

$$\dot{s} = u = -u_0 \tag{2.28}$$

Hence the trajectory, *s(t)*, will be evolving toward the minimizer s^*, and there is a sufficient condition for a sliding mode if $\sigma_1 = 0$ holds,

$$\varepsilon\dot{\varepsilon} = \sigma_1\dot{\sigma}_2 < 0 \tag{2.29}$$

This is a sufficient condition for a sliding mode to commence on $\sigma_1 = \varepsilon = g - f = 0$.

Finally, let assume

$$\frac{dy}{ds} < -\frac{\theta}{u_0} \tag{2.30}$$

This condition describes the situation corresponding with the position to the left of the uncertainty region, and there also is a sufficient condition for a sliding mode if $\sigma_2 = 0$,

$$\varepsilon\dot{\varepsilon} = \sigma_2\dot{\sigma}_2 < 0 \tag{2.31}$$

This is a sufficient condition for a sliding mode to commence on $\sigma_2 = \varepsilon = g - f = 0$.

From the above analysis, one can see that the use of the variable structure sliding mode optimizing algorithm can yield the optimal slip rate, which is associated with the maximum friction force. The proposed sliding mode based optimizer can be used on the ABS control system as shown in Fig.2.11.

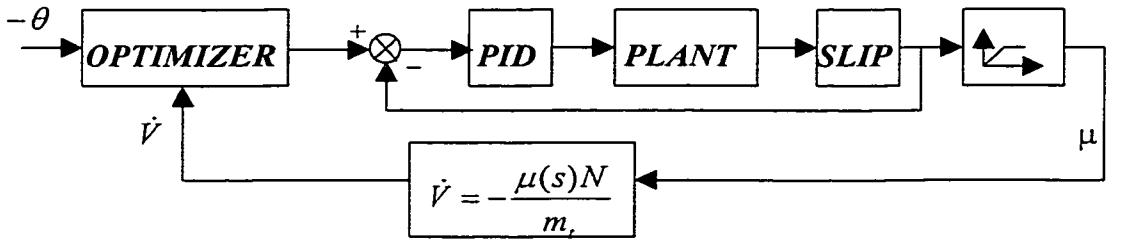

Fig. 2.11 PID Sliding Mode ABS Controller

2.5 BASIC SIMULATION SYSTEM

The basic simulation model is illustrated in Figure 2.1. More details are presented below. The block diagram of the simulation system is shown in Figure 2.12.

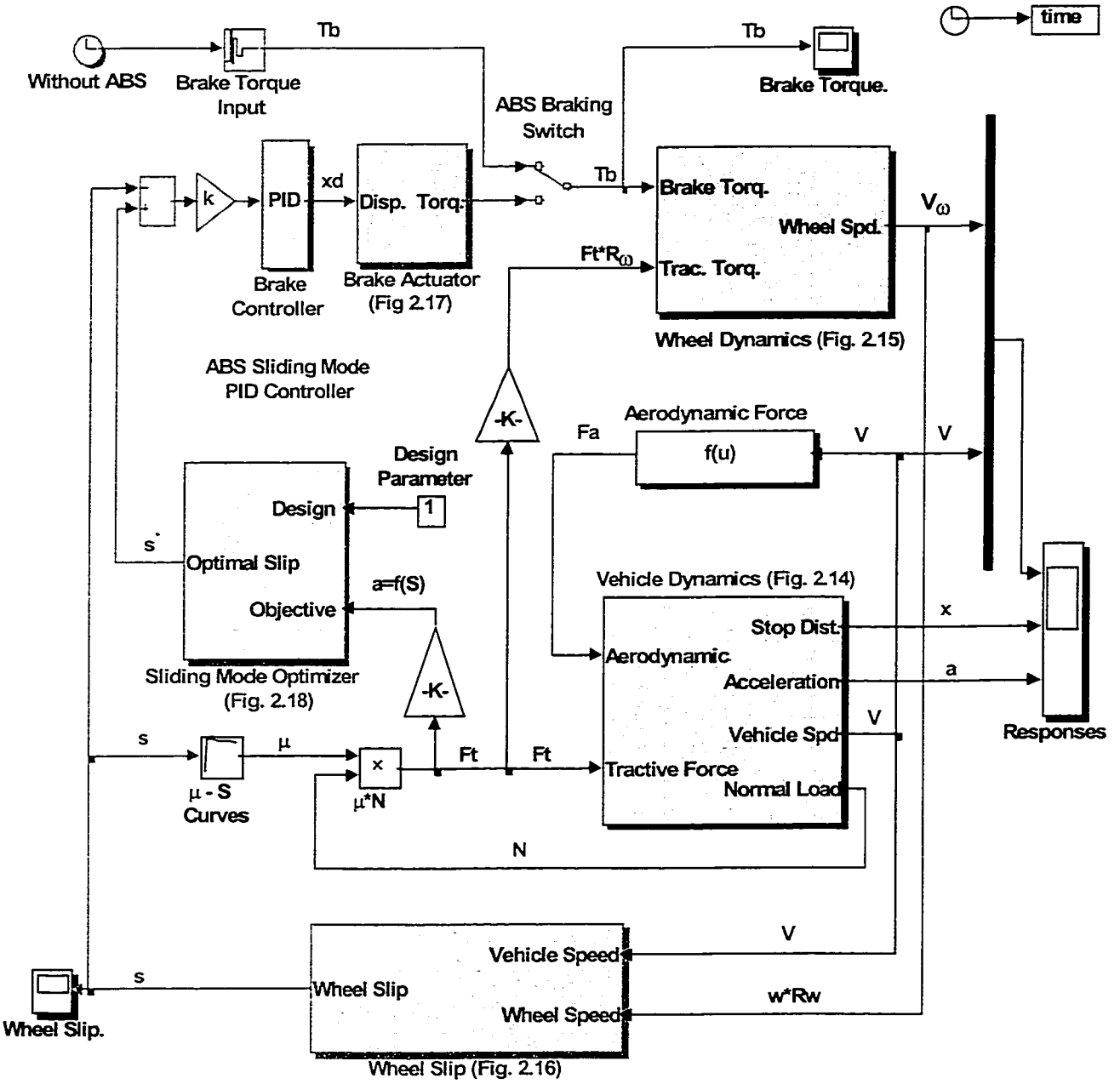

where T_b – *braking torque;* x_c – *commanded displacement;* x_d – *desired position;* s – *wheel slip;* s^* – *optimal slip;* μ – *road adhesion;* F_a – *aerodynamic force;* R_ω – *wheel radius;* F_t – *friction force;* N – *normal load;* V – *vehicle speed;* V_ω – *wheel speed;* D – *stopping distance;* a – *vehicle acceleration.*

Fig. 2.12 Block Diagram of Basic ABS System

2.5.1 Brake Actuator Simplified Model

In this basic ABS system, the simplified hydraulic brake actuator model is represented by a transfer function [9]. A more complex hydraulic braking system and details will be discussed in Chapter 3.

This system consists of three main components as shown in Fig. 2.13. The first component is the hydraulic brake actuator that controls the fluid flow to the brake caliper and regulate braking pressure. The other two components are the brake calipers and the brake pads. The brake caliper is a mechanical device that enables the application of the pressure to the brake pad to deliver a specific torque though the brake pads to the wheel disks.

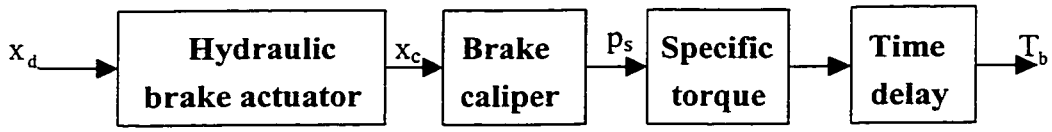

Fig. 2.13 Basic Hydraulic Brake System

The equation of motion for the hydraulic servo motor was obtained as described in detail in [9] by

$$M_p\ddot{x} + B_f\dot{x} + K_f(x_c - x_d) = 0 \tag{2.32}$$

where M_P = *mass of the prime mover*
B_f = *fluid force friction coefficient*
K_f = *fluid stiffness coefficient*
x_c = *actuator displacement*
x_d = *commanded displacement.*

Thus, the transfer function for the actuator system can be expressed by

$$\frac{x_c}{x_d} = \frac{K_f}{M_p s^2 + B_f s + K_f} \tag{2.33}$$

and

$$\frac{T_b}{p_s - p_0} = K_t e^{-t_0 s} \tag{2.34}$$

where T_b = *braking torque*
p_s = *caliper pressure*
p_o = *initial pressure for the open check valve*
K_t = *specific torque constant*
s = *Laplacian operator*
$e^{-t_s s}$ = *time axis actuator caused by the actuator "dead-time"*
t_0 = *dead time.*

To be noted that [9] the brake caliper pressure can be modeled as a nonlinear function of displacement of the brake fluid and that the specific torque constant is the ratio of braking torque to caliper pressure. The transport delay, shown as a time delay in Figure 2.13, represents the brake actuator time delay. The initial response time defines the delay between application of force to the control mechanism and the onset of the effective force.

2.5.2 System Simulation Input

The implementation of the proposed PID sliding mode controller and brake actuator was performed on vehicle dynamic parameters. It is assumed that the braking maneuver occurs on a dry concrete surface whose road adhesion coefficient versus wheel slip characteristic is shown in Figure 2.8. The system parameters can be taken from the results of General Motors NAO Electric Centre [9] as below.

a). Actuator system parameters

The model parameters of the actuator system are shown in Table 2.1.

Table 2.1 Actuator system parameters

SYM.	*VALUE*	*NAME*	*SYM.*	*VALUE*	*NAME*
M_{pm}	*0.1kg*	*servo motor prime mover mass*	K_t	*1.7*	*specific torque constant*
B_{ft}	$30N/ms^{-1}$	*fluid viscous friction coefficient*	p_0	$6.5N/m^2$	*initial braking pressure*
K_{ft}	*50000N/m*	*fluid stiffness coefficient*			

b). Vehicle system parameters

The model parameters of the vehicle are also taken from the GM NAO Centre [9] as shown in Table 2.2.

Table 2.2 Vehicle system parameters

SYM.	*VALUE*	*NAME*	*SYM.*	*VALUE*	*NAME*
g	$9.81 m/s^2$	*gravitational acceleration*	f_0	*0.01*	*basic coefficient*
l	*2.5m*	*wheel base*	f_s	*0.005*	*speed effect coefficient*
h_c	*0.5m*	*centre of gravity height*	K_m	*2.237*	*scaling constant of speed*
m_{tyre}	*40kg*	*tire mass*	A_f	$2.04m^2$	*vehicle frontal area*
$m_c/4$	*375kg*	*quarter vehicle mass*	V_0	*30m/s*	*initial velocity*
J_w	$1.7kgm^2$	*wheel inertia*	ρ	$1.23kg/m^3$	*mass density of the air*
R_w	*0.326m*	*wheel radius*	C_d	*0.539*	*vehicle drag coefficient*

c). PID sliding mode controller

Based on the dynamics of the vehicle and actuator, the sliding mode component can generate an optimum wheel slip value if the controller gains are selected properly. This optimum slip value sets as the control input to the PID controller and the PID controller forces the wheel to track the optimum wheel slip. Hence, the PID sliding mode gains can be obtained as Table 2.3 using the MATLAB nonlinear control toolbox, which uses a sequential quadratic optimization method.

Table 2.3 PID sliding mode gains

SYM.	*VALUE*	*NAME*	*SYM.*	*VALUE*	*NAME*
K_p	*0.2431*	*PID controller proportional gain*	M	*300*	*optimizer switching strength*
K_I	*0.5329*	*PID controller integral gain*	δ	*0.4*	*optimizer error interval width*
K_d	*0.0023*	*PID controller derivative gain*	Δ	*0.025*	*optimizer hysteresis width*
u_0	*30*	*optimizer variable gain*			

2.5.3 Block Diagrams of the Simulation System

The implementation of the simulation base on the algorithm and data, which are presented in Figure 2.12 and Tables 1 to 3. The detailed block diagrams using in simulation are shown below in Figure 2.14 to Figure 2.18.

a. Vehicle Dynamics (refer to equations (2.1) to (2.5))

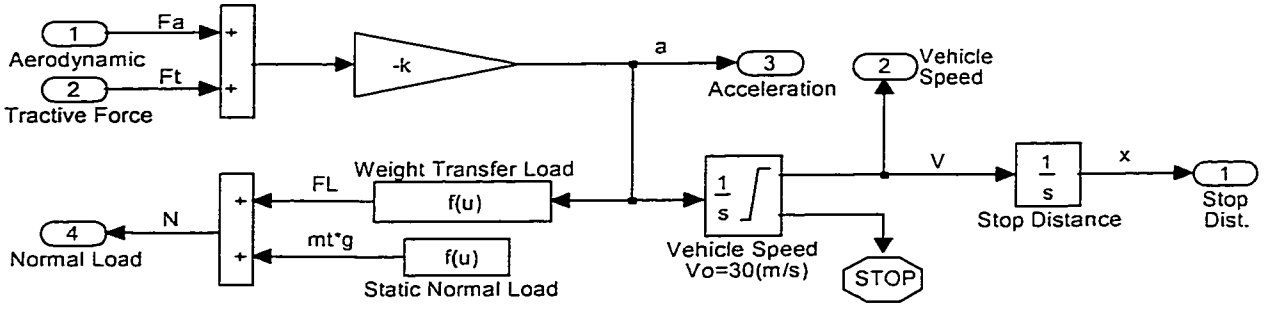

Fig. 2.14 Vehicle Dynamics

b. Wheel Dynamics (refer to equation (2.8))

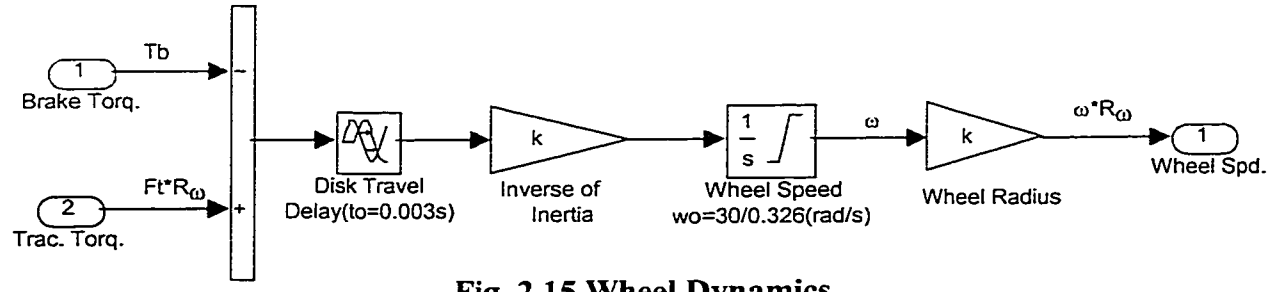

Fig. 2.15 Wheel Dynamics

c. Wheel Slip (refer to equation (2.11))

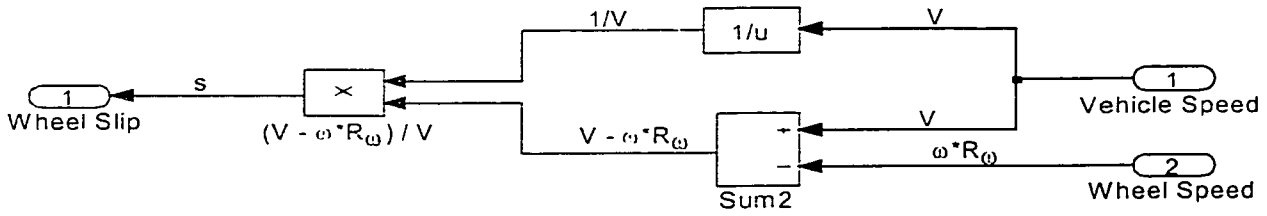

Fig. 2.16 Wheel Slip

d. Brake Actuator (refer to equations (2.33) and (2.34))

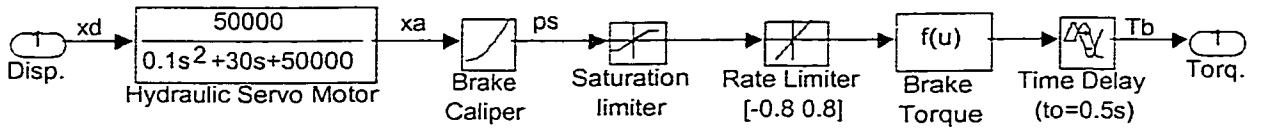

Fig. 2.17 Brake Actuator

e. Sliding Mode Optimizer (refer to equation (2.20))

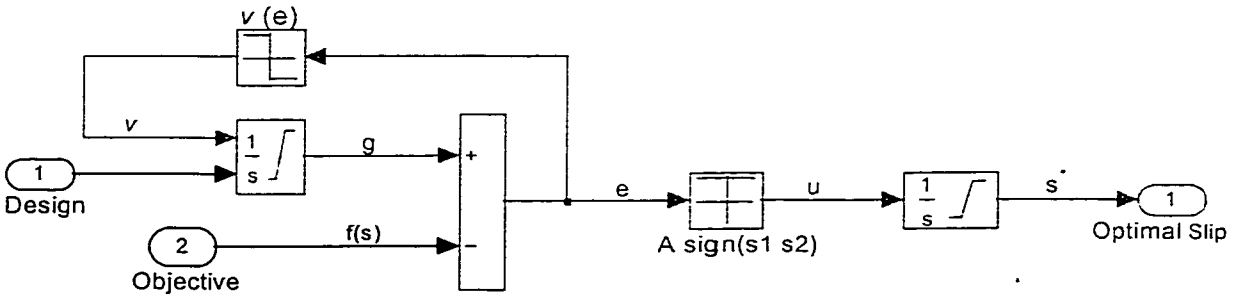

Fig. 2.18 Sliding Mode Optimizer

2.5.4 System Simulation without ABS Control

When vehicle rolls on dry asphalt surface, the typical road adhesion characteristics as described in Figure 2.8 can be used in the simulation. The road adhesion coefficient is a function of the braking slip.

For simulation, the brake torque input is assumed as shown in Figure 2.19. Initially a light brake torque of 200Nm is applied, and then the torque is stepped up from 200Nm to 3000Nm. The vehicle wheel slip response is shown in Figure 2.19. The vehicle speed, the wheel speed, acceleration and stopping distance responses are shown in Figure 2.20. The initial velocity of the vehicle is 30m/s.

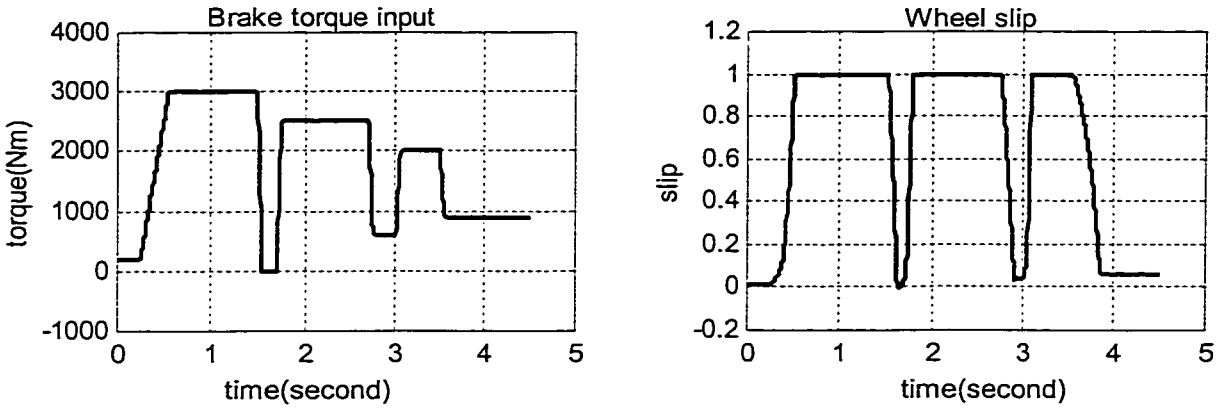

Fig. 2.19 Brake Torque and Wheel Slip without ABS

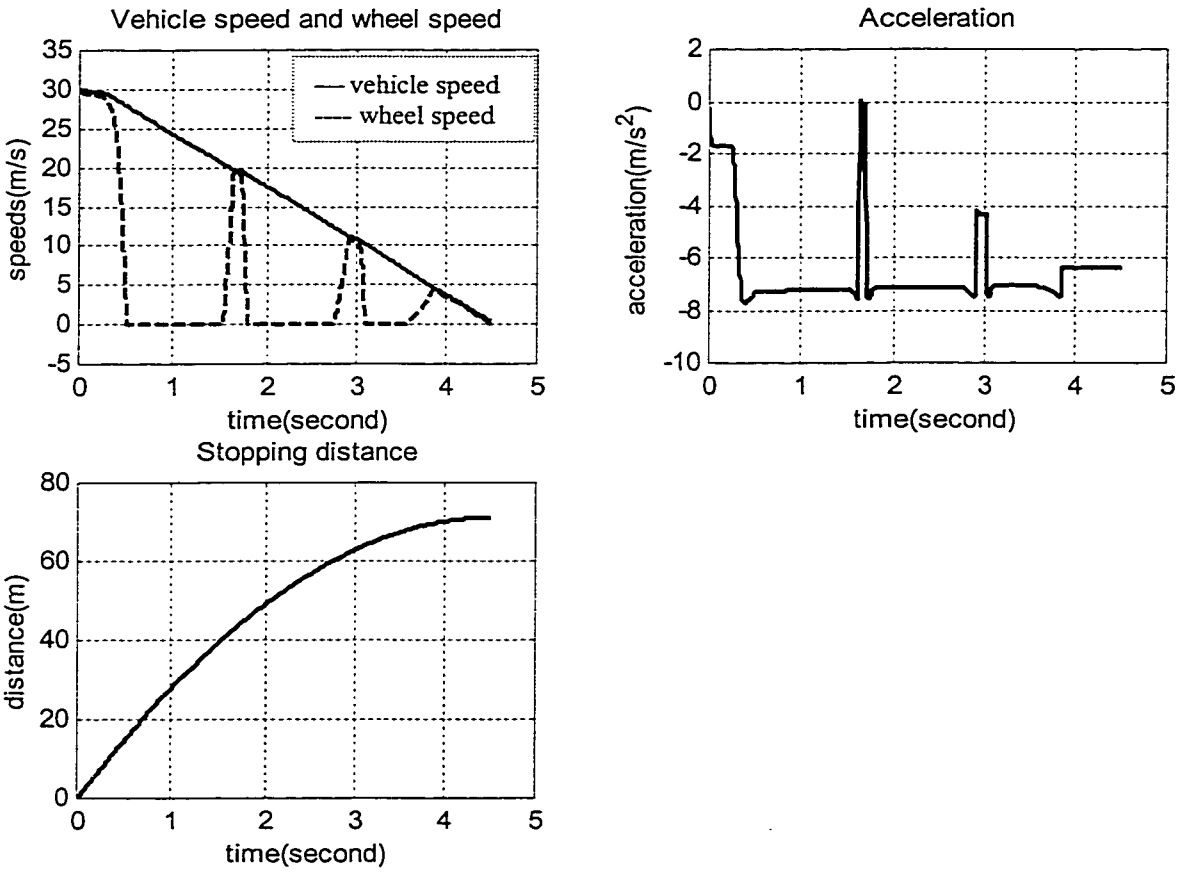

Fig. 2.20 Braking Responses without ABS

From the responses, one can see that when the brake torque is stepped up from 200 to 3000 Nm, the wheel slip increases from a nominal value around 5% to full lock-up at 100%, and when the brake torque is released. Further, by stepping the torque down from 3000 Nm to zero, the wheels unlock and regain speed that corresponds to the situation when wheel slip decreases to zero. When the brake torque increases again to 2500 Nm, the slip again increases to 100%. Hence, the simulation result shows that braking model performance is representative for a real brake system and the braking performances is highly dependent upon the brake force distribution.

2.5.5 System Simulation with ABS Control

When the vehicle rolls on dry asphalt surface, the typical road adhesion characteristic is assumed as that described in Figure 2.8. The PID controller is applied to regulate the vehicle brake torque and control the wheel slip to an optimal value. The ABS sliding mode optimizer is activated, which performs a real time search for the optimal wheel slip that corresponds to the maximum deceleration. When the initial vehicle velocities are 30 m/s, 20 m/s and 10 m/s, the brake torque input is shown in Figure 2.21 and the wheel slip, vehicle speed, the wheel speed, acceleration and stopping distance responses is shown in Figures 2.22 to 2.24. A figure 2.25 show when the brake torque input has been changed, the desired slip is changed and consequently the braking performance will be changed. Note that the brake torque input respondents to the braking force distribution, which dependents upon the correspondent to the different road conditions, but independents on the initial vehicle velocity.

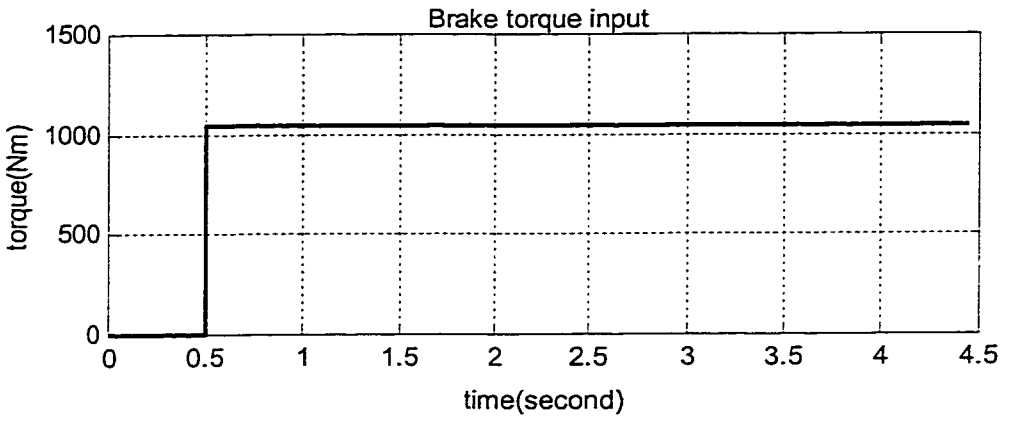

Fig. 2.21 Braking Torque Input with PID Control

a). $V_0 = 30$m/s

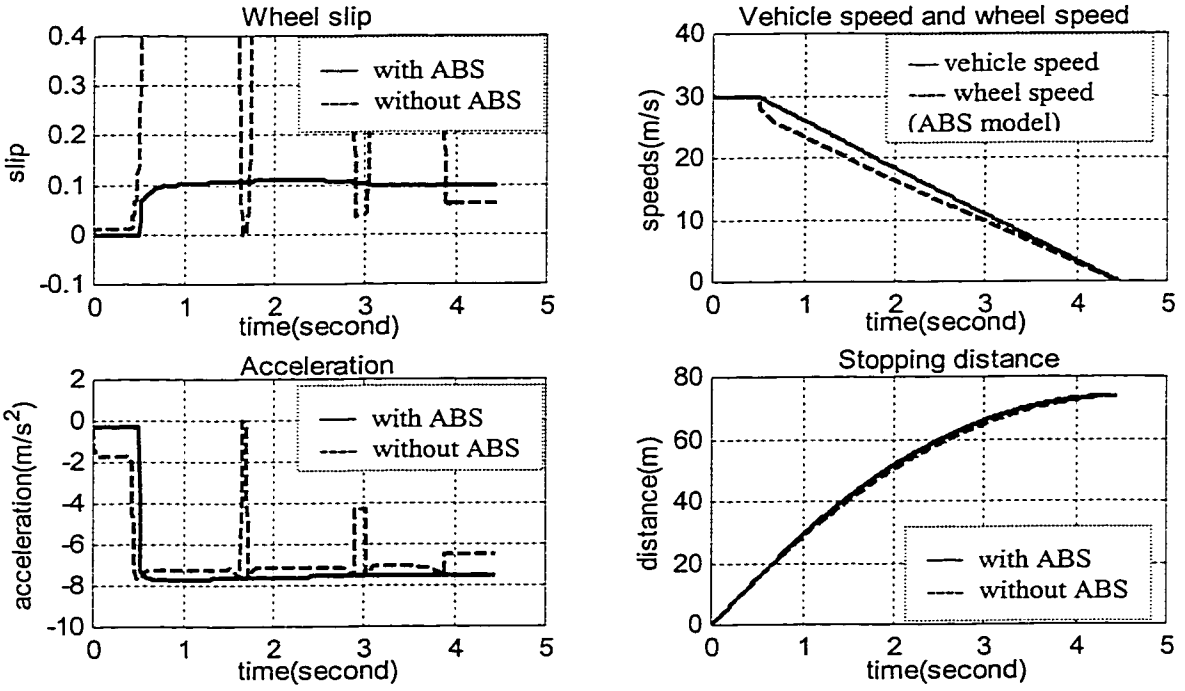

Fig. 2.22 Braking Responses with PID Control ($V_0 = 30$ m/s)

b). $V_0 = 20$m/s

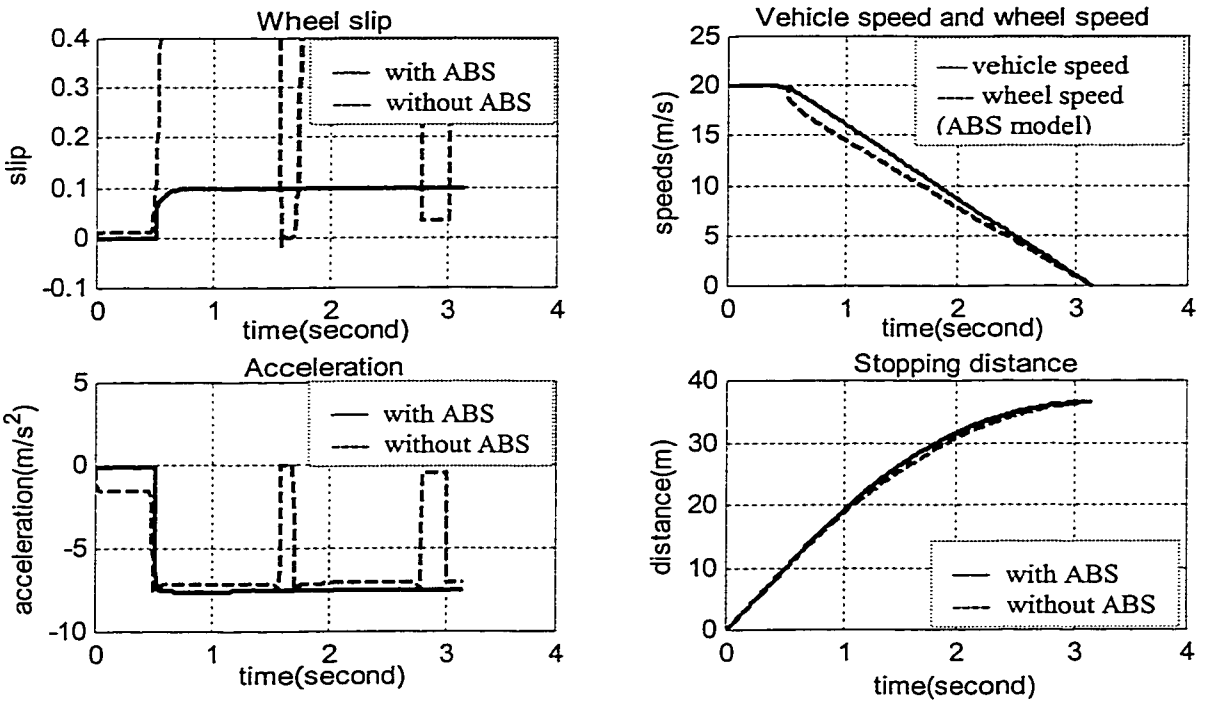

Fig. 2.23 Braking Responses with PID Control ($V_0 = 20$ m/s)

c). $V_0 = 10$m/s

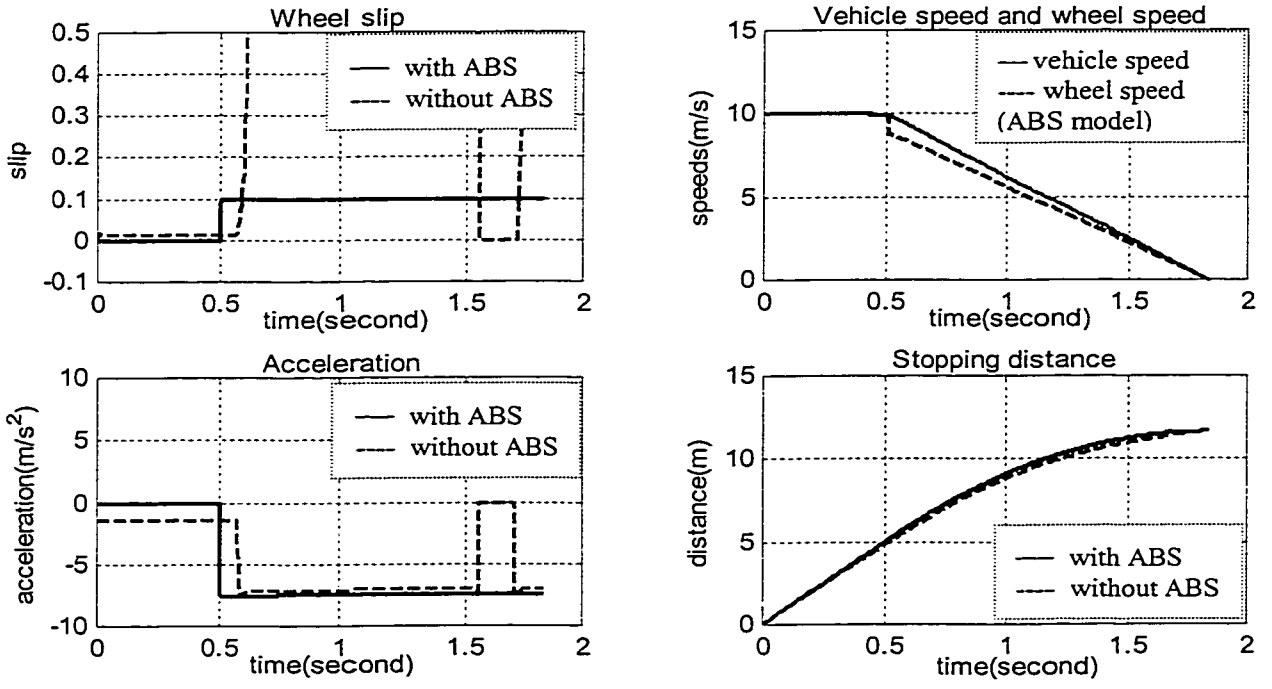

Fig. 2.24 Braking Responses with PID Control ($V_0 = 10$ m/s)

From the above responses, the stopping distance is the same when vehicle is equipped with ABS or not over the same braking period; however, when the vehicle is equipped with ABS, the average acceleration is large and held on constant to achieve the optimal slip value. From the slip plot, the optimal slip of the dry asphalt surface is about 10%, which corresponds to the typical road adhesion that is described in Figure 2.8. As results, the vehicle with ABS can avoid the wheels from being locked and make the vehicle more stable. A basic ABS braking system control by a simple strategy yields a better braking performance than the system without ABS under the same conditions.

***d).* When desired slip is 5% at $V_0 = 20$m/s**

When the vehicle moves from one surface to another surface, the braking torque input must be modified, in the case, the desired slip is changed. This would be result to change the braking performances. The responses as shown in Fig. 2.25 when the initial vehicle velocity is 20 m/s.

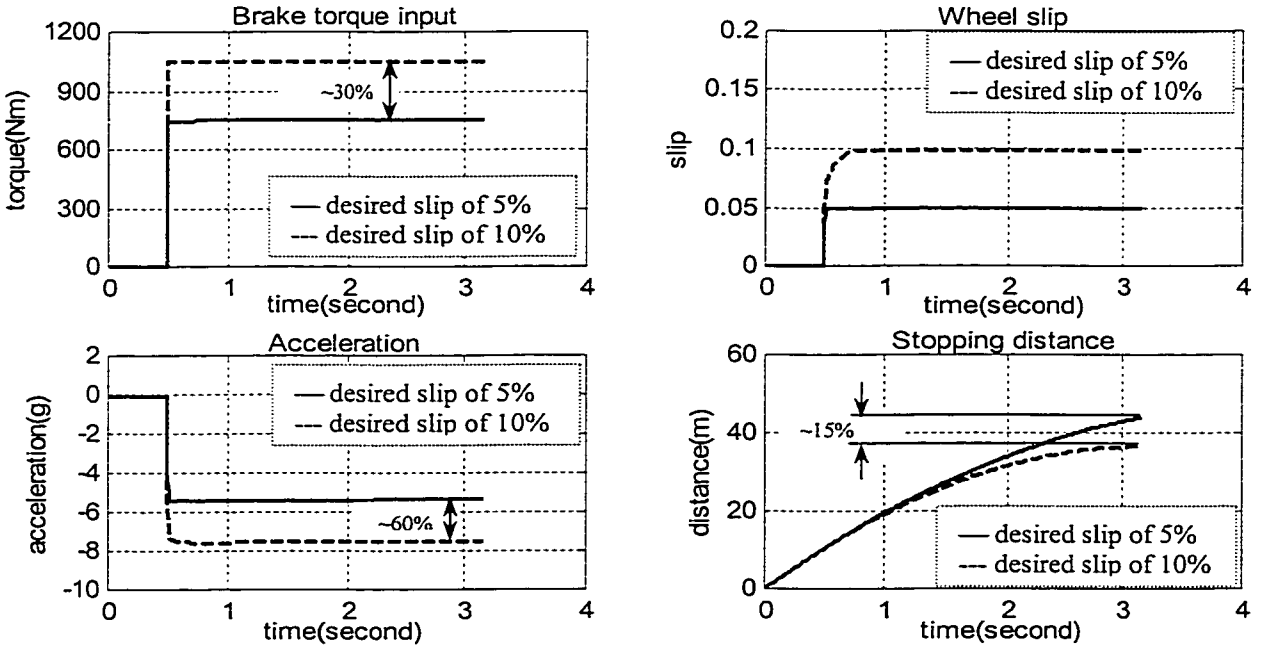

Fig. 2.25 Braking Responses with PID at Desired Slip of 5% ($V_0 = 20$ m/s)

From the responses, when the desired slip ratio changes from 10% to 5%, the brake torque reduces by 30%, consequently, the acceleration of the vehicle reduces about 60% and the stopping distance increases about 30%. Hence, one can see that when the brake torque input has been modified, the desired slip is changed and as results, the brake performances will be changed significantly.

2.5.6 Summary

In this Chapter, a basic ABS system including a PID sliding mode controller has been proposed and implemented on a quarter vehicle. The parameters that influence the performances of road vehicles with and without ABS antilock control investigated and analyses are performed to assess the effectiveness of the controller. Results of simulations are presented to illustrate the influence of the tire-to-road adhesion, the brake-force distribution and the antilock control on the stop capability and directional stability.

The simulation results clearly illustrate that the road vehicles equipped with ABS have improved the braking performances and maintain good directional stability that avoid the wheels from being lock. From the simulation analysis, however, the true ABS efficiency may be misjudged due to the different input conditions. It may be concluded below:

- The braking performances is highly dependent upon the braking force distribution and the peak tire-to-road adhesion coefficient, and on an ideal dry road condition, it is only dependent upon the locked tire-to-road adhesion coefficient;

- The real benefits of ABS are mainly related to emergency maneuvers. When a vehicle stops in emergency situations, ABS installation provides full steering control, good vehicle stability and shorter stopping distance;

CHAPTER 3

ROAD CONDITION IDENTIFICATION IMPLEMENTED IN NONLINEAR TRACKING CONTROL SYSTEM

3.1 GENERAL

The braking, steering or accelerating forces are generated by the small tire treads areas contacting the road surface and within the structure of the tire. It is well known that vehicle motions depend on tire forces and tire forces depend on vehicle motions. Tires form the interface of the vehicle and the road, are therefore their properties play a very important role in the dynamic behavior of vehicles under braking maneuvers. The braking properties of a given vehicle cannot be predicated unless the forces and moments acting at the tire road contact area are well described and integrated into the vehicle model. Many different tire models that describe forces and moments have been developed at the tire-road interface and within the tire. The efforts to deliver accurate results in relatively short computer run time are pursued. Look-up tables associated with regression techniques were applied to achieve functional relationships. Fast interpolation techniques along with data smoothing and error analysis were included in the look-up table reading routine. Once the functional relationships were established for various operating conditions of specific tires, they were further used for fast computations of the force and moment at any point of vehicle operation. The equations fit the given empirical relations over a wide range of data. The major problem associated with regression models is finding that the small errors are only encountered in the evaluation. Recently, considerable attention has been given to nonlinear regression model for tires that involve

trigonometric or other transcendental functions. The trigonometric model has come to be known as the Magic Formal (MF) tire model partly because of its complex and unusual structure, and partly because of its power to simulate many important tire performance functions with excellent accuracy.

As indicated in Chapter 2, tire longitudinal forces such as traction or braking forces as well as side forces can only be produced when a difference between the speed of the tire circumference and the speed of the vehicle relative to the road surface exists. It is common to relate tire braking force data to tire braking slip as defined before. The effectiveness of the brakes is dependent upon the road adhesion (braking friction coefficient) between tires and road. The braking friction coefficient as a function of the tire braking slip can thus vary according to road surface conditions. The relationship between wheel slip and longitudinal friction forces is usually determined from empirical relationships. In this analysis, the MF tire model is used. The ABS must perform safely under a variety of operating conditions including slippery, wet and dry roads, when vehicle is lightly or full laden, when braking while moving straight or in a curve, with new or worn brake linings, with wet or dry brakes, when braking either on smooth or rough roads. The performance of an antilock braking system relies upon a proper identification of the road surface type. When the brakes are applied on a road surface characterized by an asymmetrical left/right traction pattern, for instance, left wheels on dry asphalt, right wheels on ice, the resulting brake forces vary. This leads to yaw, which torque will impose the vehicle a tendency to spin around its vertical axis.

One of the objectives of an ABS system is to regulate the wheel slip so that road adhesion coefficient is maximized, which in turn leads to the maximum utilization of the

available braking forces and minimization of the vehicle stopping distance under stable dynamic conditions. However, the desired slip range is road surface and condition dependent. The existing ABS systems attempt to regulate the wheel slip to a range around that point where is able to maximize the braking force. For example, the optimal slip value for an icy road is different from the optimal slip value for a dry road. Therefore, in order to determine the optimal wheel slip range, the road type must be identified.

At present, there are no affordable sensors available that can accurately identify the road surface and make this information available to the ABS controller. However, the road surface type can be inferred from the vehicle's brake pressure, wheel slip measurements, and deceleration rate comparisons. Brake pressure in this type of system is determined mainly by wheel deceleration during braking where the braking pressure is controlled to increase, decrease or hold according to each specific condition. The pressure level during braking must be applied to minimize the stopping distance, providing in the same time full stability of the vehicle. Chapter 2 presents a nonlinear control system that combines a sliding mode-based optimizer and an actuator PID controller for ABS. This controller can be implemented to compute the optimal slip rate on line using data obtained from commonly available longitudinal accelerations and wheel speed sensors. This system has the ability to cope with changing system parameters, but the lack of a global stability proof is often a disadvantage of this linearized adaptive controller. Thus, giving some initial conditions in order to get the good performance on the stopping distance the system may became unstable.

In our approach, a Nonlinear Tracking Control (NTC) law is used for the servo system, which is derived from Lyapunov's stability theorem for the braking control

algorithm with the desired values of longitudinal slip calculated within the controller based on MF tire model. This approach uses a candidate Lyapunov function to synthesize both the control law and the adaptation law necessary to estimate the unknown parameters of the system. From results yield by the nonlinear tracking controller compared with those resulting from sliding model PID control system, two advanced points can be seen. The NTC system is based upon the nonlinear dynamics analysis of the hydraulic braking actuator system, so it has the ability to change the system parameters and more exactly tracks the desired trajectory. Furthermore, the NTC system can change the initial conditions for different type of roads and the system does not significantly change the pattern of stopping distance for various road conditions. Therefore, the proposed system represents a best performance of braking considering the conditions of fully stable vehicle.

3.2 MAGIC FORMULA TIRE MODEL

The Magic Formula (MF) tire model [32-35] provides a set of mathematical formulae from which the forces and moment acting from road to tire can be calculated at longitudinal, lateral and camber slip conditions, which may occur simultaneously. The Magic Formula concept is an elegant, empirical method of fitting tire data for inclusion in vehicle dynamics models. The formula gives a good representation of measured tire characteristics while certain coefficients of the model retain a physical significance, and therefore be expected to respond to road surface variations in a meaningful manner.

3.2.1 General Form of Magic Formula

The general form of the formula that holds for a given value of vertical load and camber angle is given by [33]:

$$y(x) = D\sin\{C\arctan[Bx(1-E) + E\arctan(Bx)]\}$$
$$Y(x) = y(x) + S_y \tag{3.1}$$
$$X = x + S_x$$

where *Y stands for either forces or moment*
X may represent the slip angle or longitudinal slip
S_x, S_y, B, C, D, and E are the anti-symmetric shape coefficients.

The shape coefficients must be identified from the experimental data using the nonlinear curve-fitting algorithms. For rapid execution of the iteration process during fitting and to ensure convergence, it is essential to generate initial estimates of the six coefficients that are close to their final values as shown in Figure 3.1.

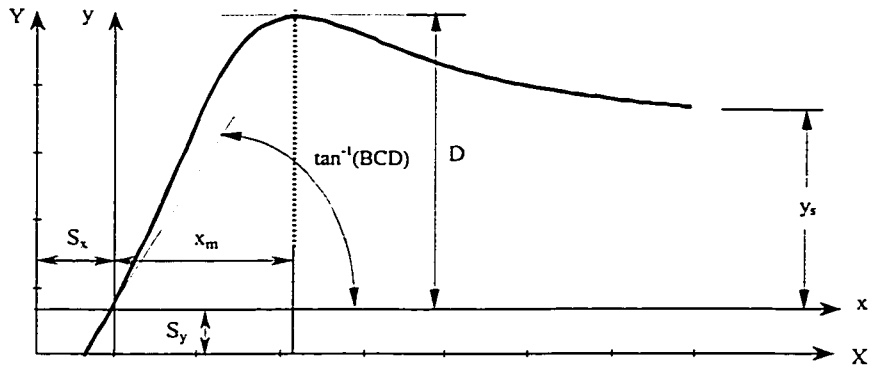

Fig. 3.1 Typical Tire Characteristic of Magic Formula

where *S_x and S_y can be estimated with reasonable accuracy directly from the experimental data for a tire*
BCD corresponds to the slope at the origin
D describes the peak value of the force or moment (y)
C can be estimated corresponding to a large value of x
B relates approximately to the slope in the linear range
E controls the slip at which the peak occurs.

3.2.2 Formulae of the Magic Tire Model for Braking

a. General formula for pure slip

$$\begin{aligned} y(x) &= D\sin\{C\arctan[Bx(1-E)+E\arctan(Bx)]\} \\ Y(x) &= y(x)+S_y \\ X &= x+S_x \end{aligned} \tag{3.1}$$

where $D = peak\ factor = y_{max}$
$C = shape\ factor = 2/\pi\ arcsin(y_s/D)$
$B = stiffness\ factor = dy/dx$
$E = curvature\ factor = (Bx_m - tan(\pi/2C)) / (Bx_m - arctan(Bx_m))$
$S_x = horizontal\ shift$
$S_v = vertical\ shift.$

b. The Lateral Force

$Y_y = F_y$ (*lateral force*)

$X_x = \alpha$ (*side slip angle*)

$D_y = \mu_{ym}F_z = (a_1F_z + a_2)F_z$

$BCD = a_3 sin(2arctan(F_z/a_4))\ (1 - a_5\ |\gamma|)$

$C_x = a_0$

$B_y = BCD_y / C_yD_y$

$E_y = a_6F_z + a_7$

$S_{xy} = a_8\gamma + a_9F_z + a_{10}$

$S_{yy} = a_{11}F_z\gamma + a_{12}F_z + a_{13}$

c. The Longitudinal Force

$Y_x = F_x$ (*longitudinal force*)

$X_x = s$ (*longitudinal slip*)

$D_x = \mu_{xm}F_z = (b_1F_z + b_2)F_z$

$BCD = (b_3F_z^2 + b_4F_z)\ \exp(-b_5F_z)$

$C_x = b_0$

$B_x = BCD_x / C_xD_x$

$E_x = b_6F_z^2 + b_7F_z + b_8$

$S_{xx} = b_9F_z + b_{10}$

$S_{yx} = 0$

Note that the coefficients above can be influenced by the vertical load on the contact patch at the tire-road interface, so they can be functions of vertical load in the above equations. Besides, the coefficients of the model retain some physical significance and can therefore be expected to react to road surface variations in a meaningful manner. This will be discussed later in this Chapter.

3.2.3 Magic Formula Optimization

The desired largest friction force could be more exactly derived from MF tire model. The greatest friction force will occur at the desired slip x^*.

Therefore, one can find

$$\left.\frac{dy}{dx}\right|_{x=x^*} = 0 \tag{3.2}$$

From Magic Formula, one has

$$\frac{dy}{dx} = \frac{BCD}{1+[Bx(1-E)+E\arctan(Bx)]^2} \left[1-E+\frac{E}{1+B^2x^2}\right]\cos\{C\arctan[Bx(1-E)+E\arctan(Bx)]\} \tag{3.3}$$

Then the Equations (3.2) and (3.3) yield

$$\cos\{C\arctan[Bx^*(1-E)+E\arctan(Bx^*)]\} = 0 \tag{3.4}$$

Hence, the optimized slip can be expressed as

$$x^* = \frac{\tan(0.5\pi/C)-E\arctan(Bx^*)}{B(1-E)} \tag{3.5}$$

The control architecture is used only when x^* finally gets convergent as shown in Fig. 3.2, which is a close loop control system.

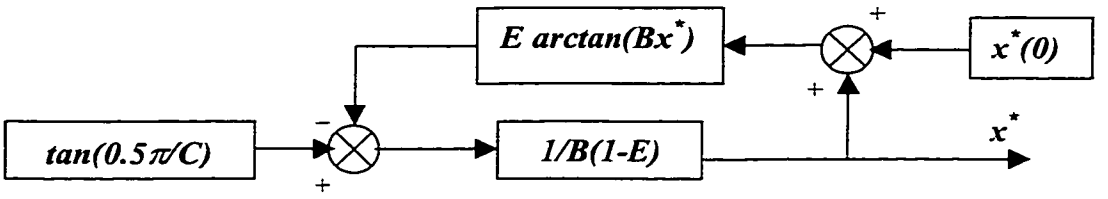

Fig. 3.2 Magic Formula Optimization

Compared sliding model optimization and magic formula optimization, as results, both of them yields very close to optimal tracking to the desired trajectory. The optimal peak slip controlled within MF model is known without error. However, MF optimization is strongly dependent on the road conditions because the required shape coefficients differ with road conditions change.

3.3 ROAD SURFACE CORRECTION OF MAGIC FORMULA

A series of μ-slip profiles for the different road surfaces are presented in Figure 2.8 and Figure 2.9, and will be generated by the tire model with optimized system variables. Further, the sensitivity of the magic formula on different road conditions is investigated for a selected tire. Thus, data of a tire on various road surfaces is measured.

The MF tire model was employed because it gives a good representation of measured tire characteristics and since certain coefficients of the model retain a physical significance, is therefore expected for them to react to road surface variations in a meaningful manner. Jagt and Parsons [79] presented the results of the measurements data of a 185/65R15 tire on different road surfaces as shown in Table 3.1.

Table 3.1 Lateral coefficients for different surface [73]

SURFACES / COEFFICIENTS	ROAD A	ROAD B	ROAD C	LAB.
a_1	–43.707	–42.026	–39.925	–35.408
a_2	1329.305	1280.406	1215.734	1086.310
a_3	1285.465	1378.389	1306.211	1502.732
a_4	8.875	8.847	8.832	8.792
a_5	0.017	0.016	0.016	0.014
a_6	–0.021	–0.025	–0.032	–0.025
a_7	–0.513	–0.428	–0.378	–0.451
a_8	–0.111	–0.132	–0.136	–0.141
a_{11}	8.210	7.977	7.542	8.122

The results of lateral force measurements were tested on laboratory as well as road surfaces. The different road surfaces of "A", "B", "C" and "Lab" present the different lateral force distributions dependent to the wheel slip with the use of a same structure tire as described in the paper [79]. The measurement results show that parameters of a_1, a_2 and a_3 in the MF change significantly from surface to surface. It had been stated that only the parameters that represent the peak lateral force (a_1 and a_2) would change to the road surface change. These parameters are related with the friction coefficient of the surface, and in fact both a_1 and a_2 do change from one surface to the other by the same percentage, illustrating load independent variation at the overall level.

According to the theory, the cornering stiffness is dependent on the construction of the tire and independent on the type of road surface. The change in parameter a_3 might be thus explained by the fact that the cornering stiffness is influenced by dynamic effects, meaning that high frequency load changes coming from road irregularities might reduce the cornering stiffness [79]. Parameter a_4 change less significant which again illustrates the variation in only the overall level of the cornering stiffness and the load

independence. Furthermore, all curve shape and camber parameters appear not to change significantly from one road surface to another.

From all of above, Jagt [79] also found that a tire model could be transferred from one surface to another by including two weighting parameters C_1, C_2 in the MF with respect to a theoretical road surface as follows

$$\begin{aligned} D^* &= C_1 \cdot D \\ (BCD)^* &= C_2 \cdot (BCD) \end{aligned} \tag{3.6}$$

where $$D = a_1 \cdot F_z^2 + a_2 \cdot F_z$$
$$BCD = a_3 \cdot \sin(2\tan^{-1}(F_z / a_4)) \cdot (1 - a_5 \cdot |\gamma|)$$

The weighting parameters C_1, C_2 different road surfaces are given as Table 3.2.

Table 3.2 Road correction factors C_1 and C_2

SURFACES	ROAD A		ROAD B		ROAD C	
	C_1	C_2	C_1	C_2	C_1	C_2
Tire A	1.226	0.776	1.213	0.843	1.176	0.872
Tire B	1.224	0.855	1.186	0.917	1.119	0.869

In the investigations, Jagt et al. show an example of measured laboratory lateral data and the MF model associated with these data and proved that an excellent characterization of the road surface can be achieved using the MF with the two correction factors for this surface.

Further investigations, proved that the same assumptions are also suitable for the longitudinal dynamics. Alleyne [120] proposed an empirical result, consequently, the parameters in MF can be written as a function of vertical load on the tire as

$$\begin{aligned} C &= 1.8 \\ D &= b_1 F_z^2 + b_2 F_z \\ B &= \frac{b_3 F_z^2 + b_4 F_z}{CDe^{a_5 F_z}} \\ E &= b_6 F_z^2 + b_7 F_z + b_8 \end{aligned} \tag{3.7}$$

The vertical and horizontal shifts S_x and S_y are used to account for offsets in the slip vs. force curves. In this investigation, both shifts are assumed to be zero. A more complete version of the MF also accounts for camber influences and combined cornering/braking maneuvers. However, for the purpose of this analysis, the model given in equations is satisfactory. The coefficients corresponding to a wet road that were used in the model and simulations [120], are given in Table 3.3.

Table 3.3 Longitudinal coefficients for wet road

b_1	b_2	b_3	b_4	b_5	b_6	b_7	b_8
-21.3	744.0	49.6	226.0	0.3	-0.006	0.056	0.486

The braking force vs. slip is shown in Figure 3.3 [120]. The maximum braking force corresponds to wet asphalt with friction coefficient ranging from 0.4 to 0.5 when the normal loads equal to 2kN, 4kN, 6kN and 8kN.

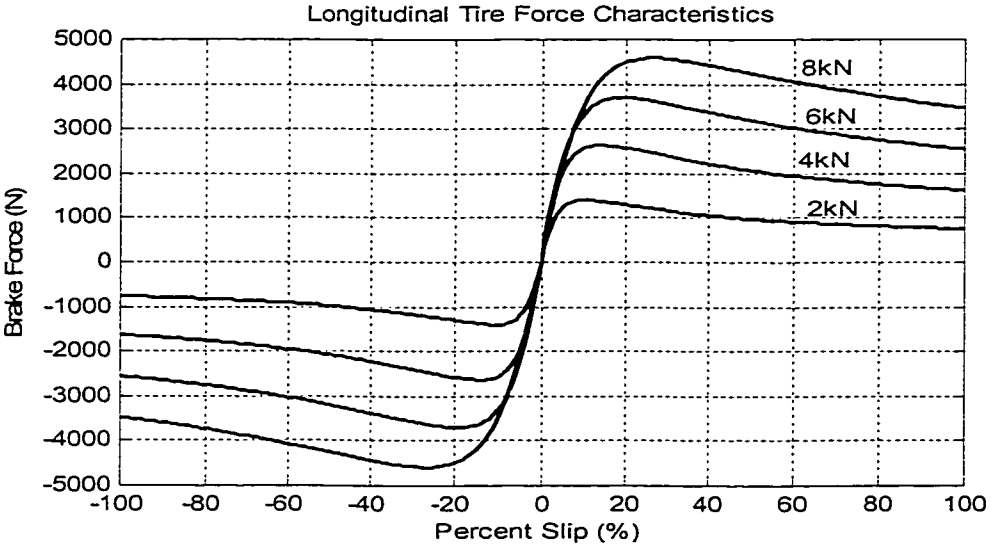

Fig. 3.3 Magic Longitudinal Force vs. Slip on Wet Surface [120]

The assumption of Jagt [79] found that the tire model could be extended from one surface to another by weighting the MF using two parameters C_1, C_2 stands for the

longitudinal forces. Given the independence of the correction factors on load, it is thus necessary to measure only a single curve on any surface to estimate the two correction factors when the MF coefficients based on laboratory data is available. From the above results, one can see the large changes in factor C_2 are related to the sensitivity of tire at high frequency load changes. It is also known from passed experience that the factor C_1 would change in time mostly due to weather, temperature and surface conditions. The effectiveness and portability in deriving the correction factors for the tire data from actual vehicle tests using standard instrumentation was investigated. The derivation of the correction factors requires data on individual tire vertical loads, lateral forces, slips and camber angles. Thus, for the initial investigation, instrumentation was chosen to measure individual tire slip angles via measurement of body sideslip and wheel steering angles relative to the body.

3.3.1 Longitudinal Force for Straight Line Braking

The typical experimental test results for this straight line braking was given in Chapter 2 (Figure 2.8). Corresponding to this typical plot, the MF coefficients corrected to different road surfaces are given in Table 3.4.

Table 3.4 Longitudinal coefficients for different surfaces

Surfaces	Dry Concrete	Wet Asphalt	Snow	Slippery Ice
b_1	−33.015	−21.3	−6.56	−3.28
b_2	1153.2	744.0	229.152	114.576
b_3	113.398	49.6	9.92	4.96
b_4	516.693	226.0	45.2	22.6
b_5	0.3	0.3	0.3	0.3
b_6	−0.006	−0.006	−0.006	−0.006
b_7	−0.056	−0.056	−0.056	−0.056
b_8	−0.486	−0.486	−0.486	−0.486

Using Alleyne's empirical results (Table 3.3), the two correction factors C_1 and C_2 for different road surfaces can results as in Table 3.5. Note that the large variation with lateral force of parameter b_4 is due to the large changing of C_2.

Table 3.5 Correction factors for different surfaces

Surfaces	Dry Concrete	Wet Asphalt	Snow	Slippery Ice
C_1	1.55	1	0.308	0.154
C_2	2.286	1	0.2	0.1

Therefore, the braking force vs. slip ratio for the corresponding coefficients of the dry concrete, snow and slippery ice surfaces, are shown in Figure 3.4 to Figure 3.6, which are used in the simulation programs. From the results of Figure 3.4 to Figure 3.6, the optimal slips are 5%-15% for dry concrete surface, 15%-35% for snow surface, 10%-30% for slippery ice surface, and the road adhesion are around 1, 0.2 and 0.08, which are in good correlation with the typical experimental test results as shown in Figure 2.8.

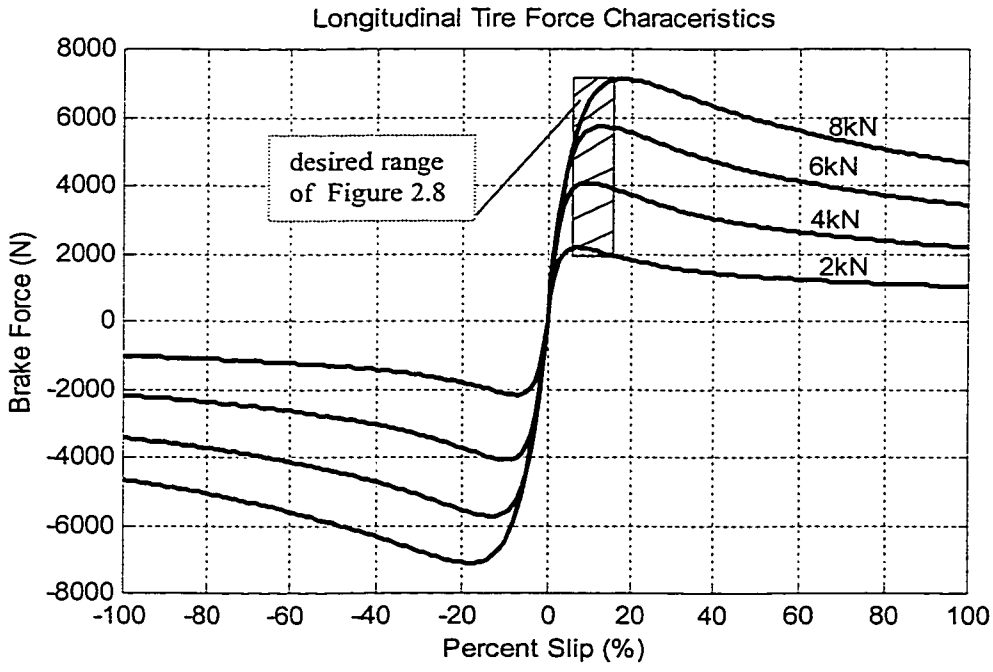

Fig. 3.4 Longitudinal Force vs. Slip on Dry Concrete Surface

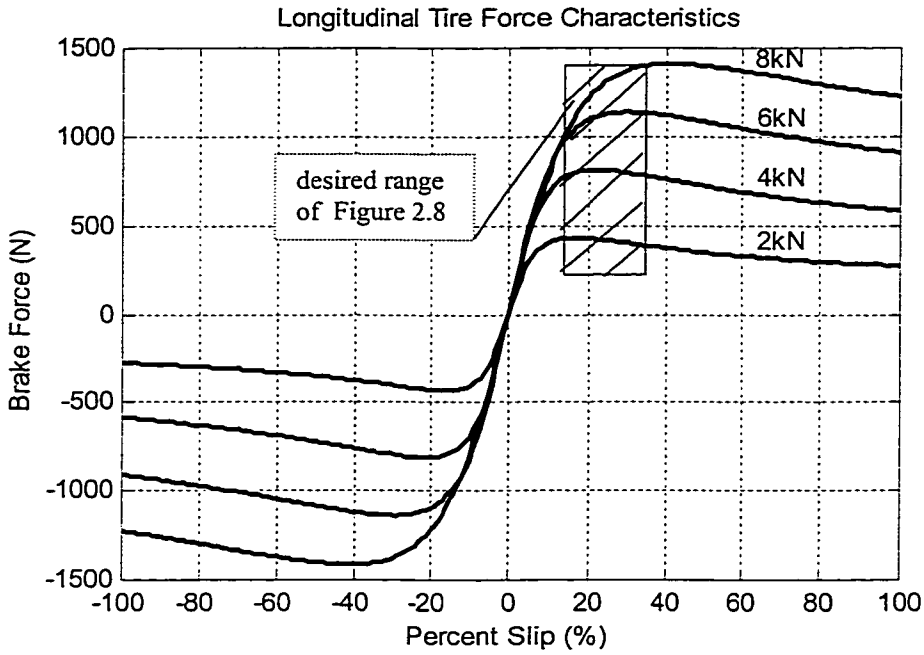

Fig. 3.5 Longitudinal Force vs. Slip on Snow Surface

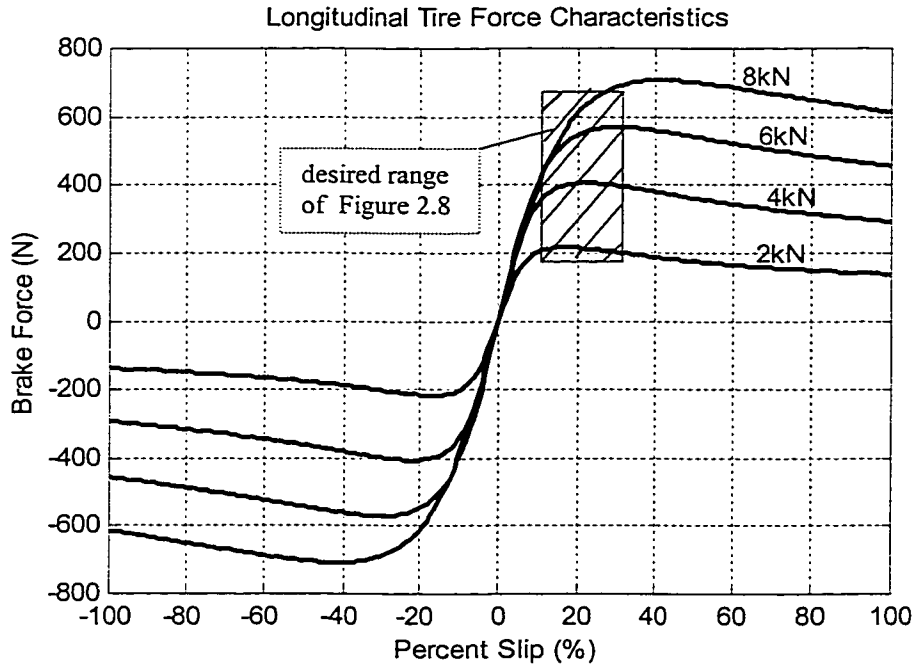

Fig. 3.6 Longitudinal Force vs. Slip on Slippery Ice Surface

3.3.2 Lateral and Longitudinal Forces while Turning

Of all the maneuvers encountered in everyday driving, one of the most critical and thus most significant for vehicle design is braking during cornering. The vehicle's response pattern must represent the optimum compromise between steering response, stability, and braking effectiveness. Improvement of cornering performance with consideration of braking is important for automobile safety. During severe braking in a turning, the ABS system should intervene early on with initially low deceleration values while the lateral acceleration is still near its maximum value permitted by the tire road friction coefficient. Therefore, it is necessary to analyze vehicle dynamics and cornering characteristics with consideration on both friction and braking forces. The more complete version of the MF also accounts for camber influences and combined cornering/braking maneuvers. However, for purposes of this analysis, the model described by Equations (3.1) and (3.2) is satisfactory.

From the typical experiment test results given in Chapter 2 (Fig. 2.8) and based on Jagt's empirical results (Table 3.1), the typical lateral coefficients for dry concrete normal road condition that are further used in this study are given in Table 3.6. More details will be presented and discussed in Chapter 4.

Table 3.6 Lateral coefficients while turning

a_1	a_2	a_3	a_4	a_5	a_6	a_7	a_8	a_{11}
-35.408	1086.31	1502.73	8.798	0.014	-0.025	-0.451	-0.141	8.122

Therefore, the normal lateral force vs. side slip angle corresponding to the correction factor coefficients further used in the braking system are shown in Figure 3.7,

which also is good correlation in well with the typical experimental test results as shown in Figure 2.9. More details are provided in Chapter 4.

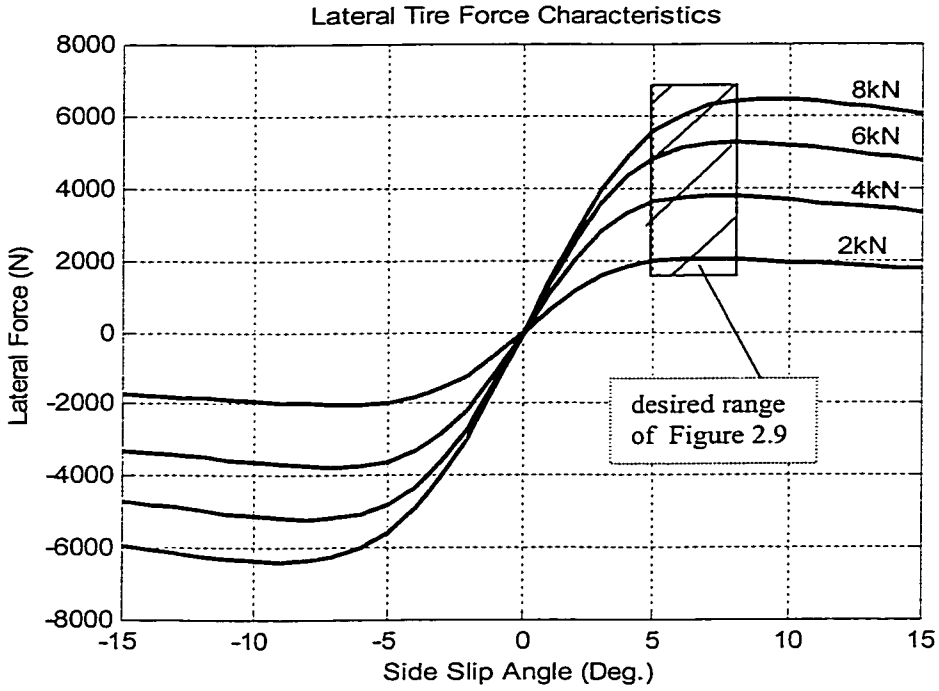

Fig. 3.7 Lateral Force vs. Slip Angle in Cornering

3.4 NONLINEAR TRACKING CONTROL HYDRAULIC SYSTEM

The hydraulic system in braking represents the power effector of the braking caliper through the braking pads on the spinning disk of the tire. The pressure on the braking pads affects the friction force and thus braking. The braking force can thus be controlled though an appropriate setting of the braking pressure in the hydraulic system. The basic hydraulic braking system of a vehicle is constituted of three main components as shown in Fig. 2.13. The hydraulic brake actuator controls the fluid flow to the brake calipers and regulate brake pressure. The other two components are brake calipers and brake pads. The brake caliper is a mechanical device that applies the pressure to the brake pad as

determined by the fluid flow caused by the hydraulic brake actuator modulation. It is important to note that the brake caliper pressure can be modeled as a nonlinear function of flow of the brake fluid, and the specific torque constant as the ratio of brake torque to caliper pressure as given by the Equation (2.34) [9].

The realization of ABS systems relies on the control of the hydraulic actuator as well as other vehicle systems. Modeling of the hydraulic actuator as a dynamic system is essential when design the ABS. In Chapter 2, a simplified actuator model was used for the actuator transfer function in conjunction with a simple nonlinear control system that combines a sliding mode-based optimizer and an actuator PID controller. This system can be implemented to compute the on line optimal slip rate, but the lack of a global stability proof is often a disadvantage for this linearized system. In the further approach, the actuator dynamics is included as a subsystem in a new integrated Nonlinear Tracking Control (NTC) system, which is developed for the hydraulic braking system. This model uses a candidate Lyapunov function to synthesize both the control law and the adaptation law is used to identify the unknown parameters of the system. The results of the simulation of this system compared with the result yield by the PID controller show that this system more exactly tracks the desired trajectory and represents the best performance of stopping distance under fully stability of the vehicle.

The analysis of hydraulic braking systems has been well documented in the literature [121, 122]. Based on the ABS system operation principles briefly illustrated in Chapter 2 (Figures 2.2-2.5), the hydraulic braking system is further considered as a part of the proposed ABS system, which are modified as Fig. 3.8. This system includes power brake source (such as accumulator, pumps, reservoir and valves), control spool valve,

hydraulic brake booster, master cylinder and solenoid valves. The hydraulic pressure to the wheels is supplied by the accumulator, and the hydraulic fluid is drained from the brakes to the reservoir. The solenoid controls the isolation/inlet valve of the hydraulic circuit to prevent the fluid flow from the master cylinder and hydraulic booster in preventing any more hydraulic pressure from reaching wheels.

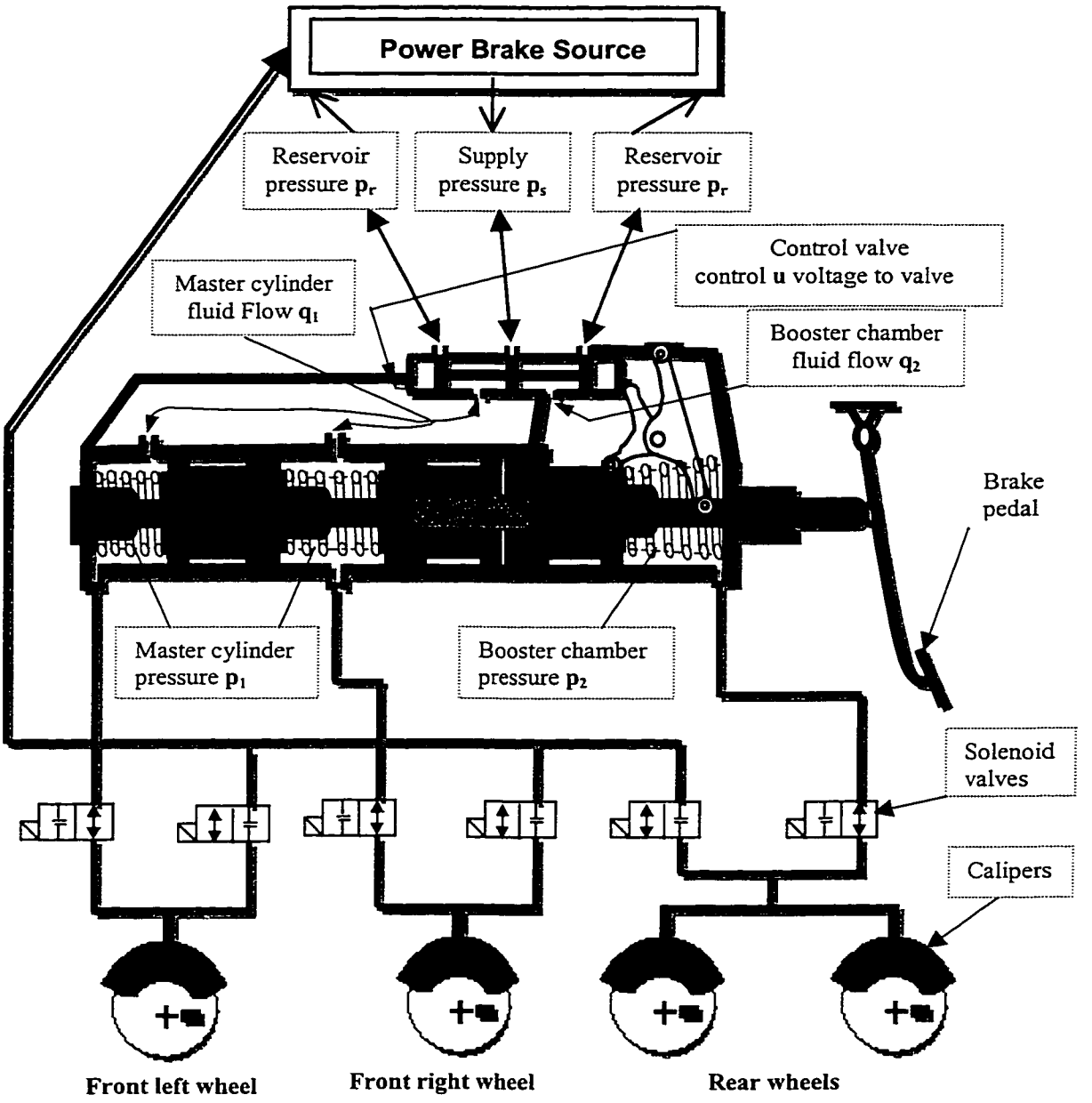

Fig. 3.8 Schematic of Hydraulic Braking System

3.4.1 Hydraulic Brake Actuator

The ABS is mostly based on two principles of braking actuation. The vacuum assist, principle uses engine vacuum, or sometimes, vacuum pressure developed by an external vacuum pump to help apply the brakes. The hydraulic assist, which is considered in presently ABS system, is shown in Figure 2.2 to Figure 2.5. The system uses hydraulic pressures developed by the power steering pump or other external pump to help apply the brakes. The hydraulic assist systems are used in braking systems provide their many advantages, including high durability and the ability to produce large forces at high speeds as discussed in Chapter 1.

Unfortunately, the dynamic characteristics of these systems are highly nonlinear and thus relatively difficult to control. The two most common approaches developed to compensate for the nonlinear behavior of hydraulic servo systems are: *i*) adaptive control; *ii*) variable structure control. Most of the adaptive controllers use linearized models for the ABS system, and hence provide only local stability. Given some initial conditions, the system model may become unstable. The variable structure control uses sliding mode controllers, where the important practical problem is the selection and tuning of the required dead band. If one selects a too small dead band, the nearly discontinuous control excites unmodeled dynamics present in the system; if the dead band is too large, a significant degradation in tracking performance occurs.

The literature review revealed that only few studies have been dedicated to the dynamics of the ABS servo braking system. Halseth [123] modeled the dynamic behavior of the vacuum booster by including the thermodynamics of the vacuum chamber and the dynamics of the power piston. Khan et al. [124] developed a complete model of the brake

servo system, and included 10 states and validated the model only for very slow brake applications. Based upon experimental results, Raza et al. [125] devised a combined actuator and braking system model for Intelligent Cruise Control (ICC) consisting of a first-order linear system with amplitude-dependent parameters. This model, however, appeared to reflect very slow actuator dynamics and did not allow for analysis of individual components. Gerdes and Hedrick [126] proposed a reduced-order model of the brake dynamics derived from a physical modeling perspective. Following the assumption of incompressible flow, a four-state model of brake hydraulics is proposed. This model provides a collection of components that can be simplified or extended as necessary to form a basis for the study of vehicle interactions with the ABS control. However, the ABS dynamics is inherently nonlinear. The nonlinearities arise from the compressibility of the hydraulic fluid and the complex flow properties of the servo valve. Friction in the hydraulic cylinder also contributes to the nonlinear behavior.

For the investigation, a new integrated Nonlinear Tracking Control (NTC) is developed for the nonlinear hydraulic braking system, which is derived from a Lyapunov analysis of the nonlinear dynamic equations. The Lyapunov-based approach separates the force control subsystem from the position tracking subsystem using a technique similar to integrator back stepping [127]. This proposed controller has provided excellent exponential stability for force and position tracking even in the presence of errors in the physical parameters without the complexity of variable structure or adaptive methods. Therefore, the proposed braking control system can maintain desired values of longitudinal slip for both front and rear wheels at pre-specified values.

3.4.2 Hydraulic Brake Actuator Dynamics

a. Hydraulic boost system

The hydraulic boost system uses pressurized fluid from the power-steering pump to obtain its power assist, as shown in Figure 3.8. The hydraulic booster is a different system from the hydraulic pressure in the brake lines. The booster assembly itself consists for a spool valve and sleeve assembly, a lever assembly, an input rod assembly, a power piston, an output pushrod, and the accumulator. The booster assembly is mounted of the same manner as a vacuum booster. Power-steering fluid flow in the hydraulic boost unit is controlled by a control valve. The control valve works as a mechanical feedback mechanism to modulate hydraulic fluid in response to force commands on the pedal.

b. Control valve dynamics

As a first step in modeling this system, assume that the control u applied to the spool valve is directly proportional to the spool position, which the dynamics of the valve motor/flapper are fast enough to be decoupled from the dynamics of the spool. Neglecting leakage in the valve, the flow into master cylinder and booster chamber [128] is given by

$$q_1 = \begin{cases} c_1 u\sqrt{p_s - p_1} & u \geq 0 \\ c_2 u\sqrt{p_1 - p_r} & u < 0 \end{cases} \tag{3.9}$$

and

$$q_2 = \begin{cases} -c_3 u\sqrt{p_2 - p_r} & u \geq 0 \\ -c_4 u\sqrt{p_s - p_2} & u < 0 \end{cases} \tag{3.10}$$

where q_1 = *master cylinder fluid flow*
q_2 = *booster chamber fluid flow*
p_s = *supply pressure*
p_r = *reservoir pressure*

u = *control applied to the spool valve*
p_1 = *pressure on master cylinder*
p_2 = *pressure on booster chamber*
c_1, c_2, c_3, c_4 = *valve orifice coefficients*

c. Brake system dynamics

As illustrated in Fig. 3.9, the brake hydraulics can be separated into two distinct circuits.

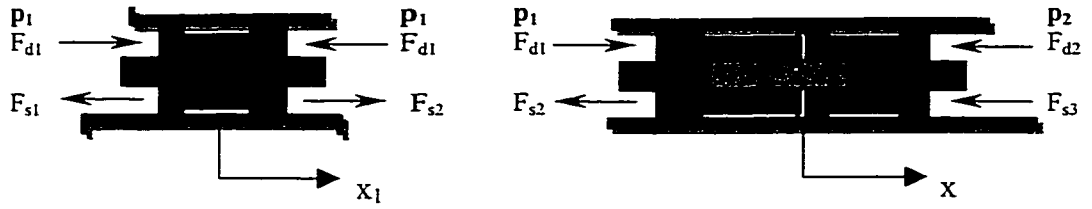

Fig. 3.9 Braking System Dynamics

Neglecting the small inertia of the pistons, the pressure in master cylinder and booster chambers are given by

$$p_1 = F_{d1} / A_1$$
$$p_2 = F_{d2} / A_2 \tag{3.11}$$

where
p_1 = *hydraulic pressure on master cylinders*
p_2 = *hydraulic pressure on booster chamber*
F_{d1} = *hydraulic force on master cylinder*
F_{d2} = *hydraulic force on booster chamber*
A_1 = *piston area in master cylinder*
A_2 = *piston area in booster chamber.*

Considering the individual force balance for the push-rod and power piston, the equations of motion become

$$F_{d1} - F_{d2} - F_{s2} - F_{s3} = m\ddot{x}$$
$$F_{s2} - F_{s1} = m_m \ddot{x}_1 \tag{3.12}$$

where
F_{s1} = *spring force on first chamber of master cylinder*
F_{s2} = *spring force on second chamber of master cylinder*
F_{s3} = *spring force booster chamber*
m = *pushrod and piston mass in booster chamber*
m_m = *piston mass in master cylinder*
x_1 = *piston position in master cylinder*
x = *piston position in booster chamber.*

The return spring forces are:

$$\begin{aligned} F_{s1} &= kx_1 \\ F_{s2} &= k(x - x_1) \\ F_{s3} &= kx \end{aligned} \tag{3.13}$$

where k = *spring constant(assume the same for the three springs)*

The inertial effects of the motion of the piston in master cylinder are quite small, relative to the forces in the master cylinder. Neglecting these inertial forces yields to

$$F_{s2} - F_{s1} = 0 \tag{3.14}$$

Combined equation (3.13), yield

$$x_1 = \frac{1}{2}x \tag{3.15}$$

Hence, the return springs forces

$$\begin{aligned} F_{s1} &= F_{s2} = \frac{1}{2}kx \\ F_{s3} &= kx \end{aligned} \tag{3.16}$$

d. Hydraulic fluid dynamics

During a typical application, hydraulic fluid applies to the booster chambers, causing the pressure to rise and forcing the diaphragm forward. From the definition of the fluid bulk modulus, the hydraulic fluid dynamics apply to the master cylinder and booster chamber yield

$$\begin{aligned} \dot{p}_1 &= \frac{\beta}{V_{11}}(-\dot{V}_{11} + q_{11}) = \frac{\beta}{V_{12}}(-\dot{V}_{12} + q_{12}) \\ \dot{p}_2 &= \frac{\beta}{V_2}(-\dot{V}_2 + q_2) \end{aligned} \tag{3.17}$$

and

$$V_{11} = \frac{1}{2}V_{10} + x_1 A_1$$
$$V_{12} = \frac{1}{2}V_{10} + (x - x_1)A_1 \tag{3.18}$$
$$V_2 = V_{20} - xA_2$$

where β = *fluid bulk modulus*
V_{11} = *total fluid volume in the first chamber of master cylinder*
V_{12} = *total fluid volume in second chamber of master cylinder*
V_1 = *total fluid volume in master cylinder*
V_2 = *total fluid volume in booster chamber*
V_{10} = *initial fluid volume in the master cylinder*
V_{20} = *initial fluid volume in the booster chamber*
A_1 = *piston diaphragm area in master cylinder*
A_2 = *piston diaphragm area in booster chamber*
q_{11} = *fluid flow to the first chamber of master cylinder*
q_{12} = *fluid flow to the second chamber of master cylinder*
q_1 = *fluid flow to master cylinder*
q_2 = *fluid flow to booster chamber.*

Combined equations (3.15), (3.17) and (3.18), one has

$$V_{11} = V_{12} = \frac{1}{2}V_1$$
$$q_{11} = q_{12} = \frac{1}{2}q_1 \tag{3.19}$$

Therefore, the equations (3.17) and (3.18) yield,

$$\dot{p}_1 = \frac{\beta}{V_1}(-\dot{V}_1 + q_1)$$
$$\dot{p}_2 = \frac{\beta}{V_2}(-\dot{V}_2 + q_2) \tag{3.20}$$

$$V_{11} = V_{12} = \frac{1}{2}V_1 = \frac{1}{2}V_{10} + \frac{1}{2}xA_1 \tag{3.21}$$
$$V_2 = V_{20} - xA_2$$

Hence, the equation of the fluid dynamics in the chambers could be written as

$$\dot{p}_1 = \frac{\beta}{V_1}(-\dot{x}A_1 + q_1)$$
$$\dot{p}_2 = \frac{\beta}{V_2}(\dot{x}A_2 + q_2) \tag{3.22}$$

3.4.3 Control Law for Hydraulic Brake Actuator

a. Piston motion modeling

The control u applied to the spool valve is directly proportional to the spool position as illustrated in the equations (3.9) and (3.10). Substituting these equations into the equation of the fluid dynamics (3.22), one obtains

$$\dot{p}_1 = \begin{cases} \frac{\beta}{V_1}\left(-A_1\dot{x} + c_1 u\sqrt{p_s - p_1}\right) & u \geq 0 \\ \frac{\beta}{V_1}\left(-A_1\dot{x} + c_2 u\sqrt{p_1 - p_r}\right) & u < 0 \end{cases}$$

$$\dot{p}_2 = \begin{cases} \frac{\beta}{V_2}\left(A_2\dot{x} - c_3 u\sqrt{p_2 - p_r}\right) & u \geq 0 \\ \frac{\beta}{V_2}\left(A_2\dot{x} - c_4 u\sqrt{p_s - p_2}\right) & u < 0 \end{cases} \tag{3.23}$$

The fluid force and spring force acting on the piston in the booster chamber yields

$$F = F_{d1} - F_{d2} - F_{s2} - F_{s3} \tag{3.24}$$

Substituting the fluid and spring forces in a differential form, yields

$$\dot{F} = \dot{p}_1 A_1 - \dot{p}_2 A_2 - \frac{3}{2}k\dot{x} \tag{3.25}$$

Combined equations (3.23), yield

$$\dot{F} = -\dot{x}\left(\beta\left(\frac{A_2^2}{V_2} + \frac{A_1^2}{V_1}\right) + \frac{3}{2}k\right) + z(x, p_1, p_2)u \tag{3.26}$$

$$z = \begin{cases} \beta\left(\frac{A_2 c_3}{V_2}\sqrt{p_2 - p_r} + \frac{A_1 c_1}{V_1}\sqrt{p_s - p_1}\right) & u \geq 0 \\ \beta\left(\frac{A_2 c_4}{V_2}\sqrt{p_s - p_2} + \frac{A_1 c_2}{V_1}\sqrt{p_1 - p_r}\right) & u < 0 \end{cases} \tag{3.27}$$

where z = *nonzero control quantity*

From the above equations, it is evident that the control signal can be adjusted to track both the force and position as desired. The problem of choosing a control input is, therefore, reduced to the problem of determining a good choice for the tracking force.

b. Controller

The control law is derived from the Lyapunov like function:

$$L(x,t) = \frac{1}{2} k_l (F - F_d)^2 \tag{3.28}$$

where L = *Lyapunov like function (assumed lower bounded by zero)*
F_d = *desired force on the piston (assumed to be a* C^1 *differentiable function)*
k_l = *function constant.*

The derivative of the function is given

$$\dot{L}(x,t) = k_l (F - F_d)(\dot{F} - \dot{F}_d) \tag{3.29}$$

It is noted that $L(x, t)$ is lower bounded by zero, which is required criterion for the stability proof. If the force in Equation (3.26) is selected such as

$$\dot{F} = \dot{F}_d - k_f (F - F_d) \tag{3.30}$$

where k_f = *positive force error gain.*

Hence, the selection provides exponential force stabilization with

$$\frac{(F(t) - F_d(t))}{(F(0) - F_d(0))} = e^{k_f t} \tag{3.31}$$

It should be noted that $(F(t) - F_d(t)) \rightarrow 0$ with time constant $\tau = 1/k_f$. The same result is obtained using Barbalat's Lemma [129]. Substituting the equation (3.30) into (3.29), the derivative of the function becomes

$$\dot{L}(x,t) = -k_f k_l (F - F_d)^2 \tag{3.32}$$

Therefore, $\dot{L}(x,t)$ is negative semidefinite, and from Barbalat's Lemma states that $\dot{L}(x,t) \rightarrow 0 \; as \; t \rightarrow \infty$. The derivative of $\dot{L}(x,t)$ becomes

$$\ddot{L}(x,t) = -2k_f k_l (F - F_d)(\dot{F} - \dot{F}_d) \tag{3.33}$$

Substituting equation (3.30) into (3.33), yield

$$\ddot{L}(x,t) = 2k_f^2 k_l (F - F_d)^2 = 4k_f^2 L(x,t) \tag{3.34}$$

Therefore, $\ddot{L}(x,t)$ is positive semidefinite and bounded. From the sufficient condition of Barbalat's Lemma, note that $(F(t) - F_d(t)) \rightarrow 0 \; as \; t \rightarrow \infty$.

From the above analysis, the combined equations (3.26) and (3.30), will yield the control signal as

$$u = \frac{1}{z}\left(\left(\dot{F}_d - k_f (F - F_d) \right) + \dot{x}\left(\beta \left(\frac{A_2^2}{V_2} + \frac{A_1^2}{V_1} \right) + \frac{3}{2}k \right) \right) \tag{3.35}$$

c. Position Tracking

Position tracking can be achieved by choosing a second-order stable system as

$$m\ddot{e} + k_v \dot{e} + k_p e = F - F_d \tag{3.36}$$

where $e = x\text{-}x_d$ *is the position error.*

It should be noticed that this system is stable in e driven by $(F\text{-}F_d)$ because $(x\text{-}x_d) \rightarrow 0$ with $(F\text{-}F_d) \rightarrow 0$.

From the equations (3.12) and (3.24), the equation of motion results in the form of

$$F = m\ddot{x} \tag{3.37}$$

Substituting (3.37) into (3.36), the desired force is given by

$$F_d = m\ddot{x}_d(t) - k_v(\dot{x}(t) - \dot{x}_d(t)) - k_p(x(t) - x_d(t)) \tag{3.38}$$

d. Equation of Motion and Friction Model

The choice of the control force F is strongly related to the fluid force and spring force in the master cylinder. The total force on the piston needs to include friction because friction in the hydraulic cylinder has a significant effect on the controller's performance, as predicted by simulations. Hence, the equation of motion (3.37) should be adjusted as

$$F - g(\dot{x}) = m\ddot{x} \tag{3.39}$$

where $g(\dot{x})$ = *Coulomb friction forces.*

The desired control force can be derived thus as

$$F_d = m\ddot{x}_d(t) - k_v(\dot{x}(t) - \dot{x}_d(t)) - k_p(x(t) - x_d(t)) + g(\dot{x}) \tag{3.40}$$

where $g(\dot{x})$ = *estimate of the friction forces.*

Subtracting (3.40) from (3.39) and writing $e = x\text{-}x_d$, equation (3.40) becomes

$$m\ddot{e} + k_v\dot{e} + k_p e = (F - F_d) + (g(\dot{x}) - g(\dot{x})) \tag{3.41}$$

The disturbance $g(\dot{x}) - g(\dot{x})$ is also bounded and since $F\text{-}F_d \rightarrow 0$, the system is stable. If one has perfect knowledge of the cylinder friction, i.e. $g(\dot{x}) = g(\dot{x})$, *then* $x \rightarrow x_d$. For bounded initial conditions, the errors can be expressed that $|e| \leq (1/k_p)|g(\dot{x}) - g(\dot{x})|$ at the steady state.

One generally accepted method is to model friction as a function of velocity [130, 131]. By measuring the friction force required to move the piston at a constant velocity, the velocity dependent friction model can be developed. Thus, a simple open loop constant control signal could be used to move the cylinder and record the friction data.

The result looks as that is shown in Figure 3.10. At high speeds Coulomb friction is dominant and the friction force is fairly constant. Stiction dramatically increases the friction at low speeds, especially when the servo distributor is moving in the positive direction [130, 131]. In the further implementation of the proposed controller, a look up table as shown in Figure 3.10 is used to model function of piston velocity [131].

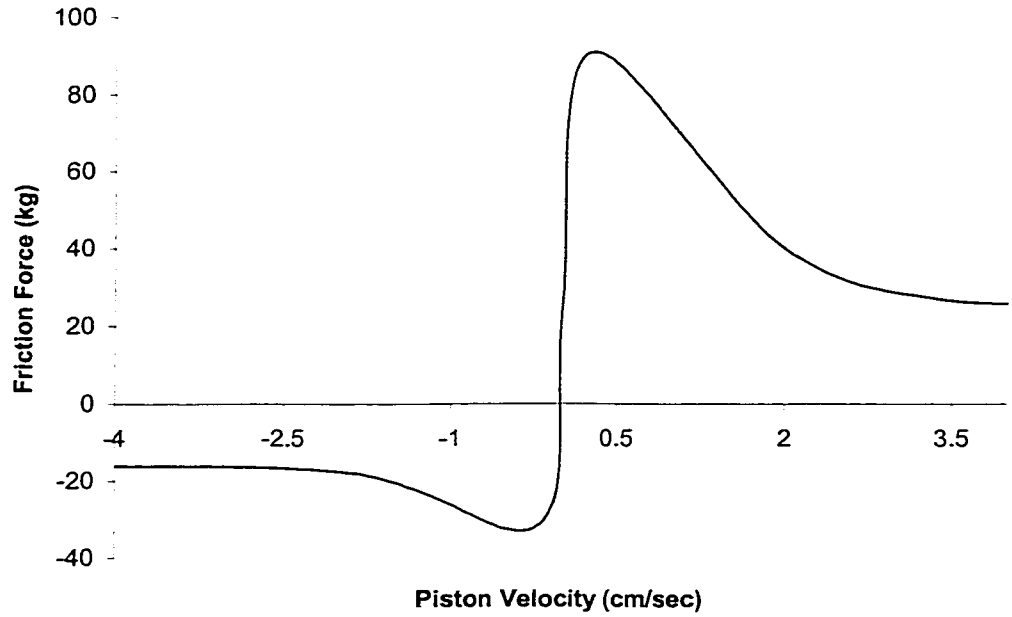

Fig. 3.10 Observed Friction Force versus Piston Velocity [130]

3.4.4 Simulation of the Hydraulic Brake Actuator

The simulation of hydraulic brake system consists of four main steps.

1. The desired trajectory information is used to determine the desired force as described by equation (3.40);
2. The control signal is found though equation (3.35);
3. The control signal is fed to the simulated spool valve which uses equations (3.9) and (3.10) as describing functions to obtain the flow rates q_1 and q_2;

4. Equation (3.22) is further used by the simulation to determine the motion of the piston and yield the new system states.

The step 1 and step 2 can be considered as control process part; the step 3 occurs at the spool valve while step 4 represents the piston motion, which can be considered with hydraulic system. Therefore, the simulation block diagram is shown in Figure 3.11.

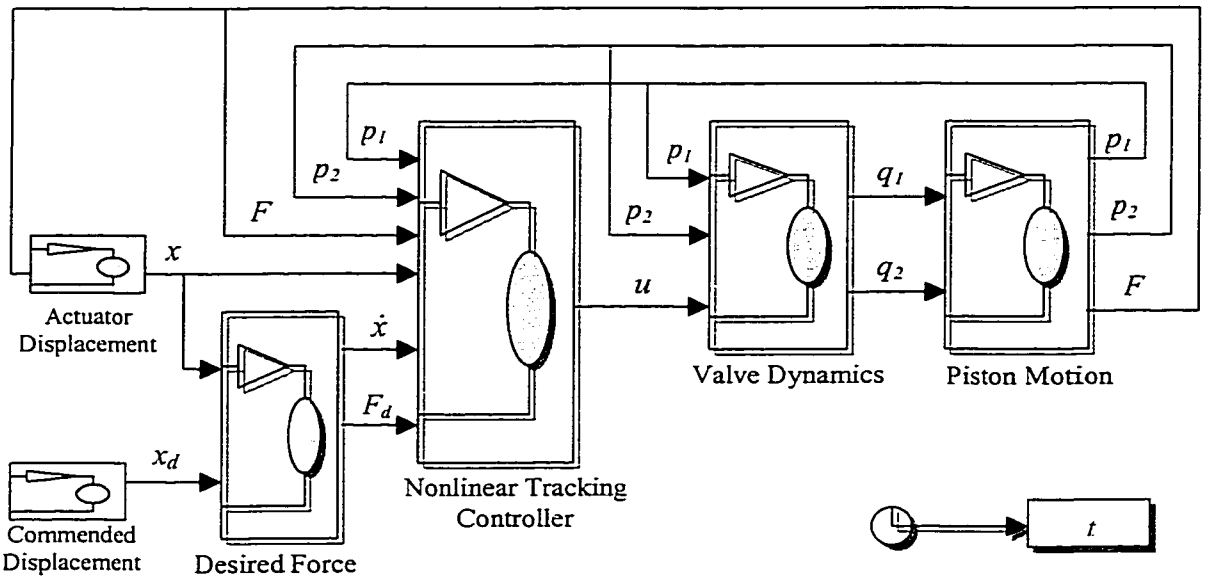

where x – *piston position;* x_d – *desired position;*
F – *piston force;* F_d – *desired force;*
p_1 – *pressure on master cylinder;* p_2 – *pressure on booster chamber;*
q_1 – *master cylinder fluid flow;* q_2 – *booster chamber fluid flow;*
u – *control signal.*

Fig. 3.11 Simulation Block Diagram of Brake Actuator

This simulation system can be used to examine the effects of errors in the system parameters or the robustness of the control system. These parameters may include the valve coefficients, system mass, friction and fluid bulk modulus terms. The introduction of errors to these parameters reduces tracking performance. The system is most sensitive to errors in the valve coefficients and friction terms, therefore, more exactly tracks the desired trajectory and more stable [130].

3.5 ABS OPTIMIZED CONTROL SIMULATION SYSTEM

The block diagram of the control system is shown in Figure 3.12. The nonlinear tracking control law requires estimates of the valve coefficients and fluid bulk modulus. Values for the valve coefficients are often provided by the manufactures, but since the simulation identified these parameters as the most critical they should be checked for accuracy. The fluid bulk modulus can significantly vary with temperature and it should be also verified.

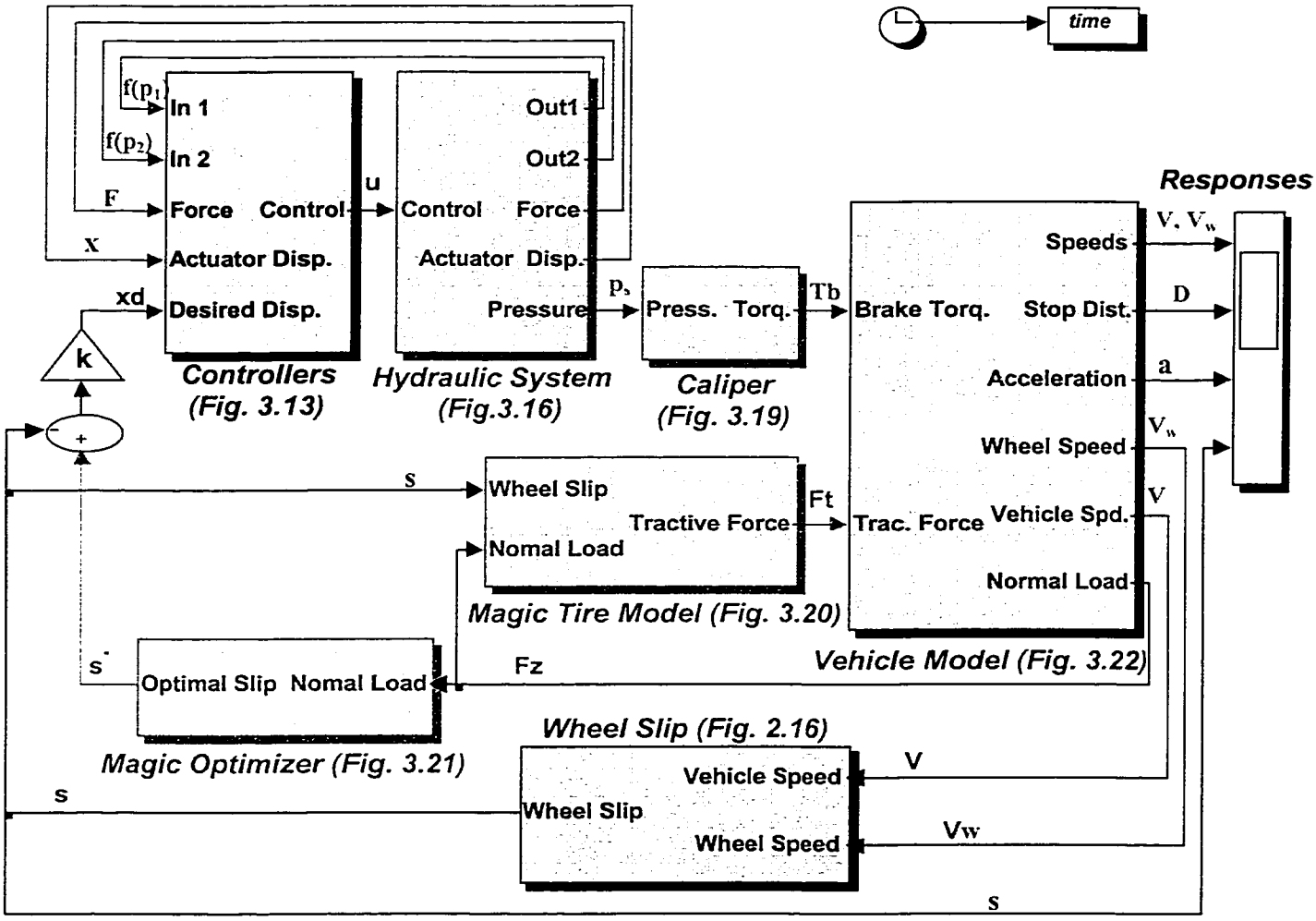

where T_b – *braking torque;* p_s – *caliper pressure;* u – *control signal;* p_1 – *cylinder pressure;* p_2 – *booster pressure;* x – *piston position;* x_d – *desired position;* F – *piston force;* s – *wheel slip;* s^* – *optimal slip;* F_z – *normal load;* F_t – *friction force;* V – *vehicle speed;* V_w – *wheel speed;* D – *stopping distance;* a – *acceleration.*

Fig. 3.12 Block Diagram of Optimal ABS Control System

3.5.1 System Simulation Inputs

The proposed nonlinear tracking control brake actuator coefficients and the vehicle dynamic parameters are given in Table 3.4. Here considering a same vehicle model with Chapter 2 and assuming the load shift from back to front is ignored. The vehicle dynamic parameters are the same as Table 2.2. An empirical value for the fluid bulk modulus could be determined from an off-line system. Given estimates for the valve parameters and fluid bulk modulus, the control law can be used to track the desired position.

Table 3.4. System parameters when implemented NTC control [9, 122]

SYM.	*VALUE*	*NAME*	*SYM.*	*VALUE*	*NAME*
L	*2.5m*	*wheel base*	p_s	*6895kPa*	*supply pressure*
h_c	*0.5m*	*centre of gravity height*	p_r	*100kPa*	*reservoir pressure*
m_{tyre}	*40 kg*	*tire mass*	C_1	*1*	*valve orifice coefficient*
m_c	*375 kg*	*quarter vehicle mass*	C_2	*1*	*valve orifice coefficient*
J_w	*1.7kgm²*	*wheel inertia*	C_3	*0.49*	*valve orifice coefficient*
R_w	*0.326m*	*wheel radius*	C_4	*0.49*	*valve orifice coefficient*
f_o	*0.01*	*basic coefficient*	A_1	*6.8cm²*	*piston area in master cylinder*
f_s	*0.005*	*speed effect coefficient*	A_2	*9.6cm²*	*piston area in booster*
K_m	*2.237*	*scaling constant*	V_{10}	*155cm³*	*fluid volume in master cylinder*
A_f	*2.04m²*	*vehicle frontal area*	V_{20}	*83cm³*	*fluid volume in booster*
C_d	*0.539*	*vehicle drag coefficient*	K_f	*96.4*	*force error gain*
V_o	*30m/s*	*initial velocity*	K_v	*9.6*	*velocity error gain*
K	*2200N/m*	*springs coefficient*	K_p	*9300*	*position error gain*
M	*0.1kg*	*servo motor prime mover mass*	β	*6.9×10^5kPa*	*fluid bulk modulus*
G	*9.81m/s²*	*gravitational acceleration*	p_o	*6.5kPa*	*initial braking pressure*
ρ	*1.23kg/m³*	*mass density of the air*			

3.5.2 Block Diagrams of the Simulation System

The optimal ABS control system block diagrams and functions are described below. The controller is conceived as a system that identifies the design force in conjunction with the

displacement of the actuator. The detailed description of the simulation system is given in Figure 3.13 to Figure 3.22.

***a).* Desired Force and Nonlinear Tracking Controller**

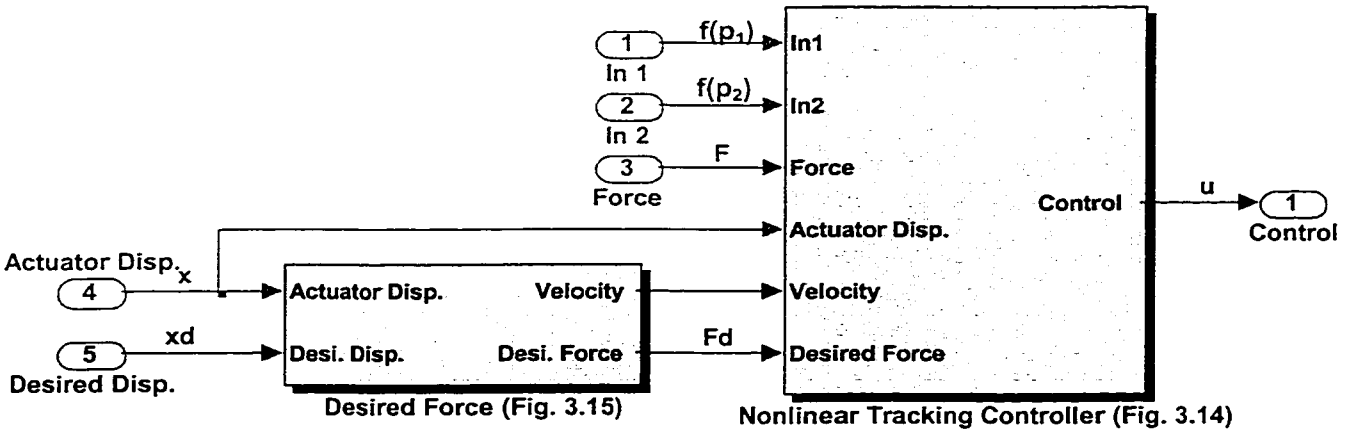

Fig. 3.13 Controller

i). Nonlinear tracking Controller (refer to equations (3.27) and (3.35))

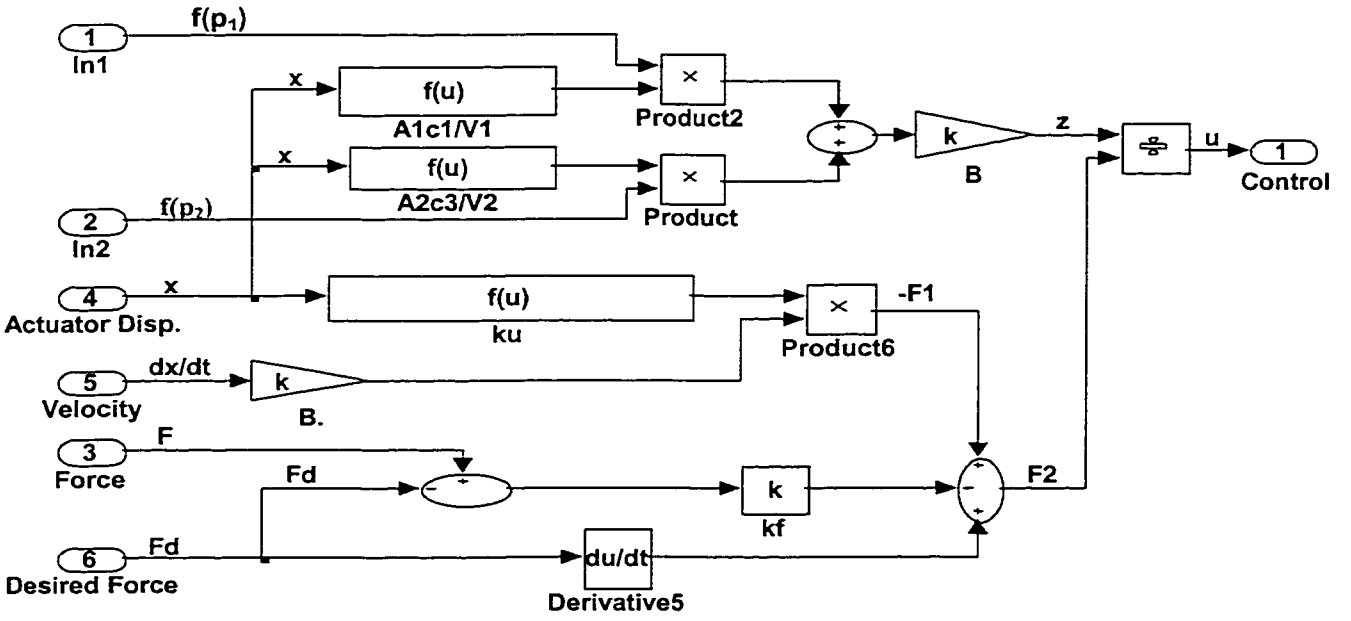

Fig. 3.14 Nonlinear Tracking Controller

ii). Desired force (refer to equations (3.38))

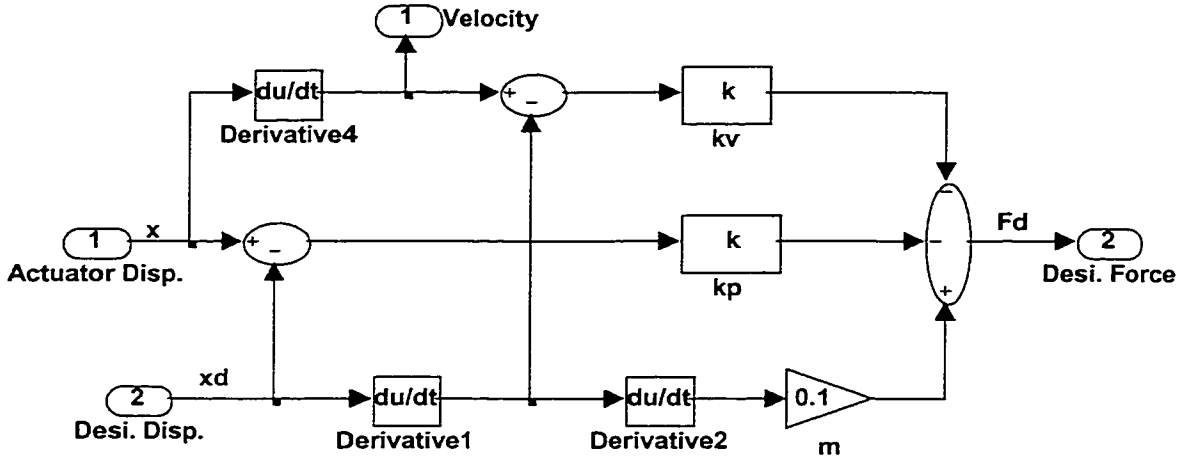

Fig. 3.15 Desired Force

***b).* Hydraulic System**

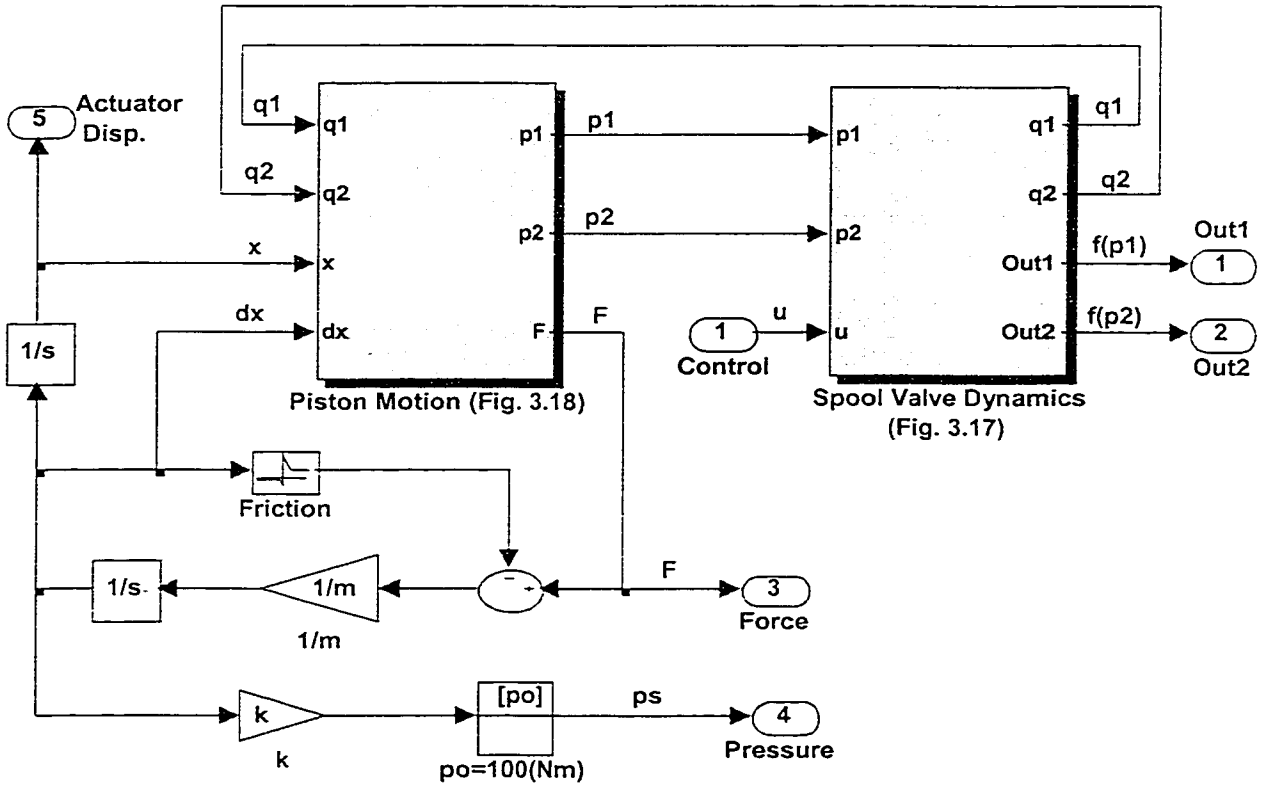

Fig. 3.16 Hydraulic System

i). Spool valve dynamics (refer to equations (3.9) and (3.10))

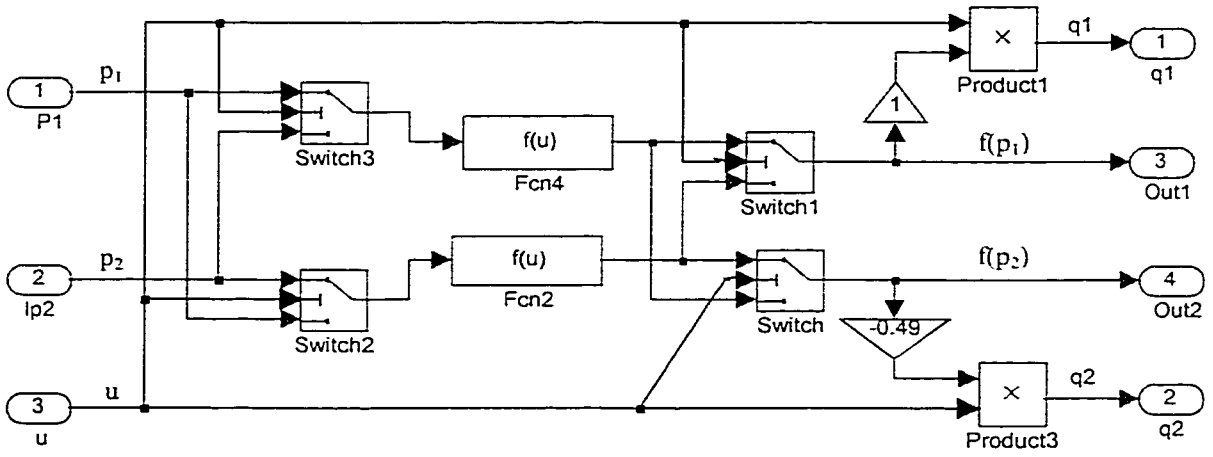

Fig. 3.17 Spool Valve Dynamics

i). Piston motion (refer to equations (3.23) and (3.25))

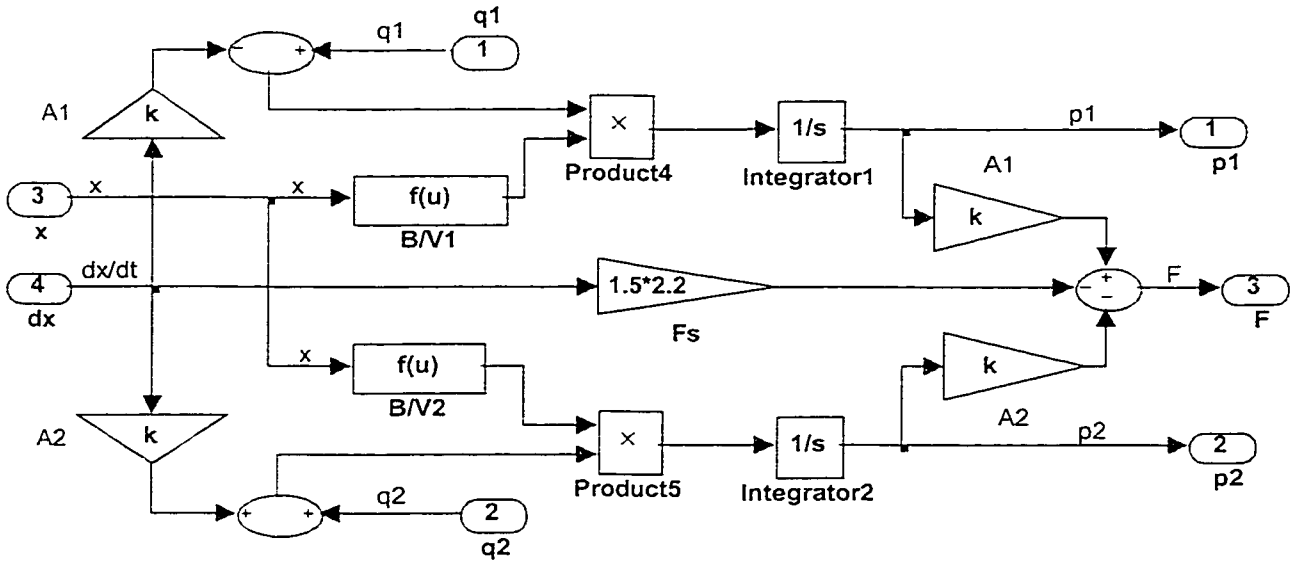

Fig. 3.18 Piston Motion

c). Braking Caliper (refer to equation (2.34))

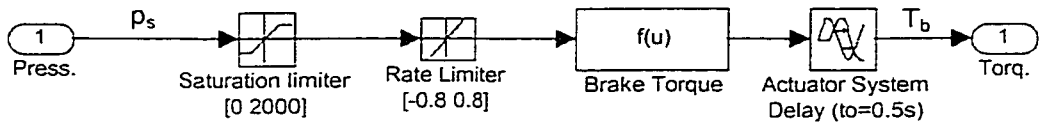

Fig. 3.19 Caliper

d). Magic Formula Tire Model (refer to equations (3.1) and (3.6))

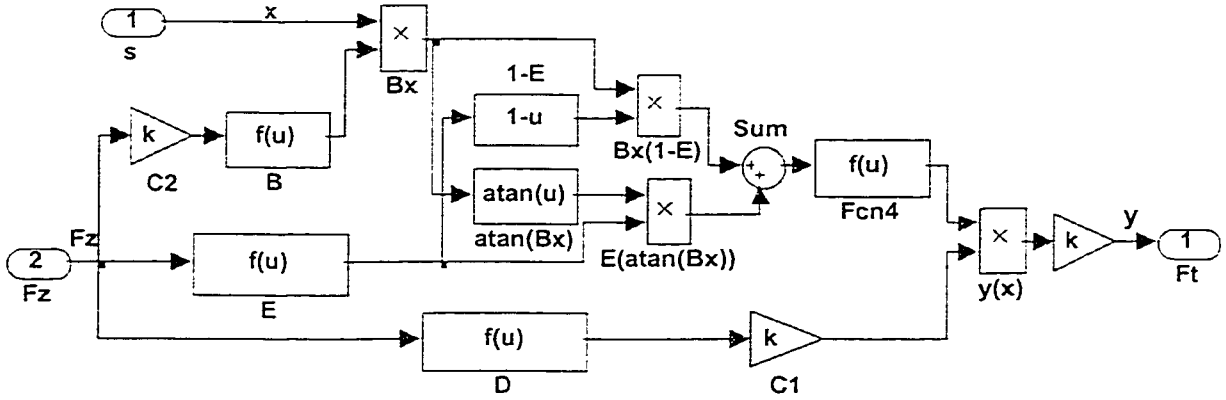

Fig. 3.20 Magic Formula Tire Model

e). Magic Formula Optimizer (refer to equations (3.5))

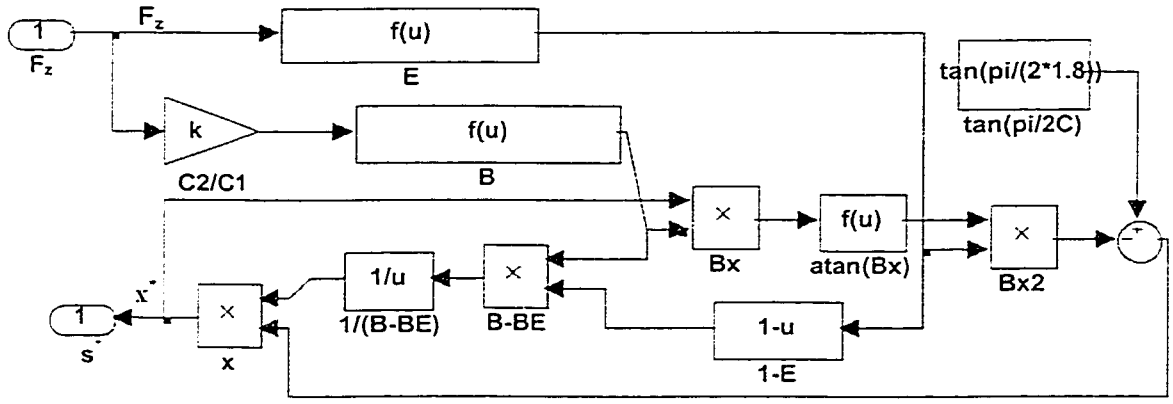

Fi 3.21 Magic Formula Optimizer

f). **Vehicle and Wheel Dynamics** (refer to figure (2.12))

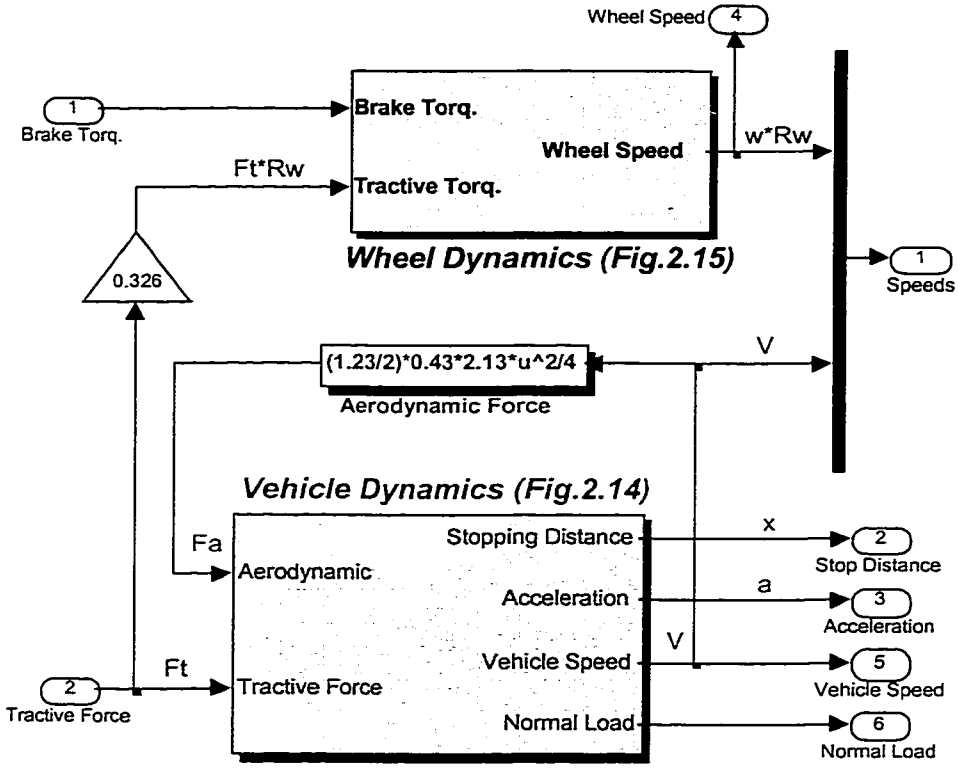

Fig. 3.22 Vehicle Model

The details of wheel slip, vehicle dynamics and wheels dynamics have been described in Chapter 2 and are further used in this simulation.

The simulation of the proposed system consists of four main parts:

1. Hydraulic braking system and nonlinear tracking control as described by Figures (3.13), (3.16) and (3.19);
2. Vehicle and wheel dynamics is modeled as shown in Figure (3.22);
3. Magic Formula tire model and optimization as shown in Figures (3.20) and (3.21);
4. Figure (2.16) is further used in simulation to determine the slip ratio of the wheels and yield the new system states.

3.5.3 System Simulation Compared with PID Control System

The simulation results can be compared with sliding mode PID control, which was implemented in Chapter 2. From the typical experimental characteristic of the tire as shown in Figure 2.8, the optimal slip of dry surface is about 9% –12%. Consider with the time delay, the braking is applied at time t_0 = 0.5 second when the vehicle moves at forward speeds of 30m/s (108km/h), 20m/s (72km/h) and 10m/s (36km/h). The wheel slip, vehicle speed, the wheel speed, acceleration and stopping distance responses are shown in Figures 3.23 to 3.25.

a). V_0 = 30m/s

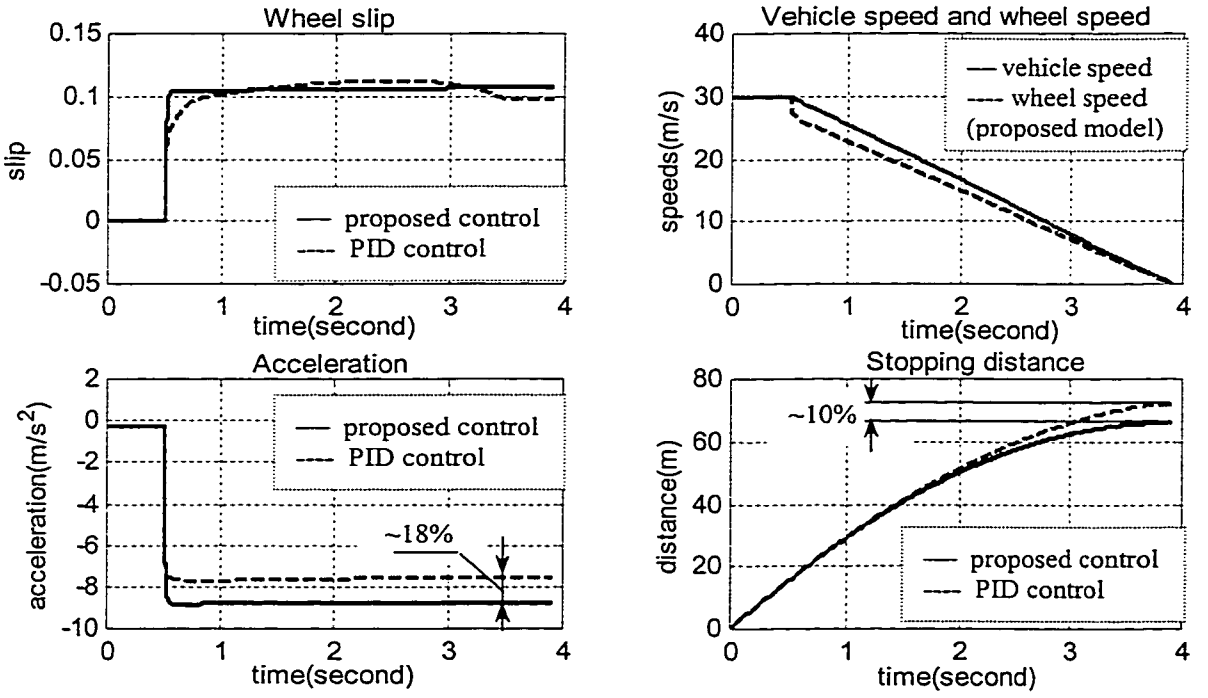

Figure 3.23 Braking Responses at Forward Speed of 30m/s

From the responses, when a vehicle moves at a forward speed of 30m/s, in the case of proposed control system vs. PID system, the wheel slip can keep the most adequate

constant value for braking. However, the PID system has small variation due to the rigidity of the controller that will affect the performances. The stopping distance of sliding mode PID system is about 73.5m/s, and it is about 66.5m/s of the proposed control system, which reduces by 10%. The average deceleration is about 8.5m/sec^2 for the proposed system, which increases from PID control system about 18% due to the continue optimization of the slip. Hence, the proposed system performances better representation on vehicle stopping distance and deceleration.

b). V_0 = 20m/s

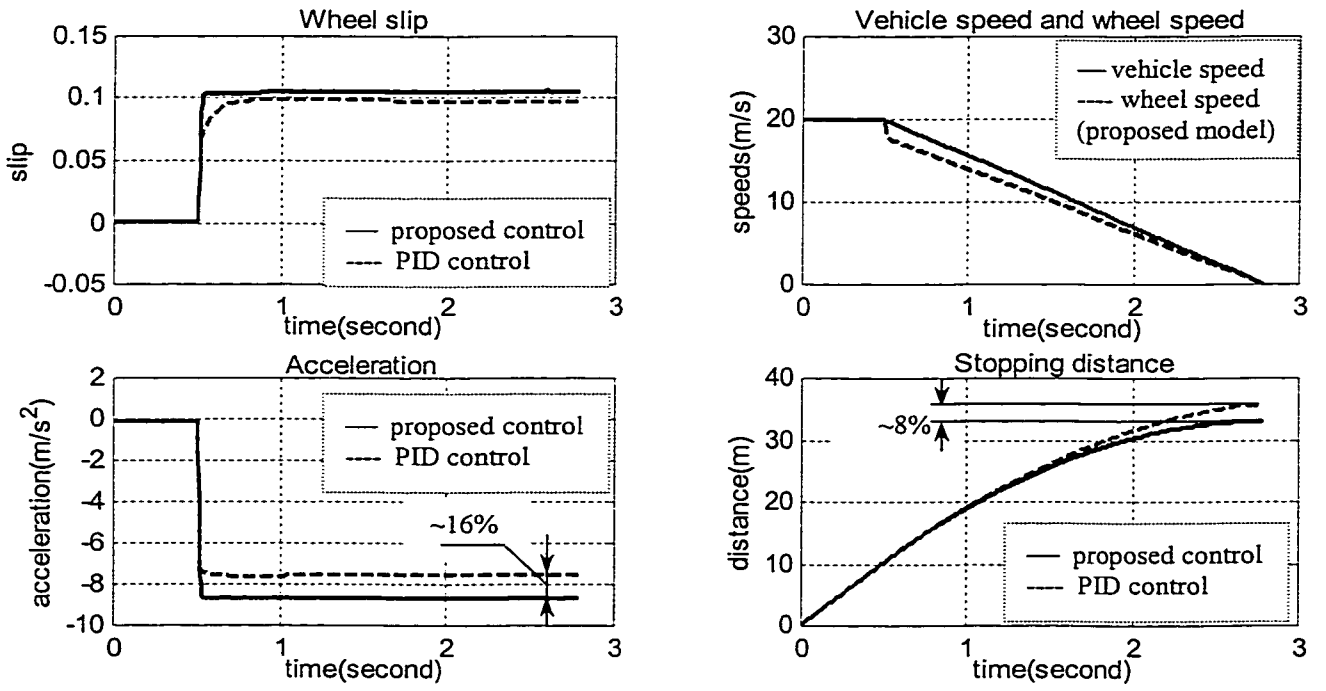

Figure 3.24 Braking Responses at Forward Speed of 20m/s

From the responses, when a vehicle moves at a forward speed of 20m/s, the stopping distance reduces by 8% and the average deceleration increases about 16% from

PID control system when proposed controller is implemented to the system, which due to the proposed controller can adjust the slip to achieve the optimal value quickly.

c). $V_0 = 10$m/s

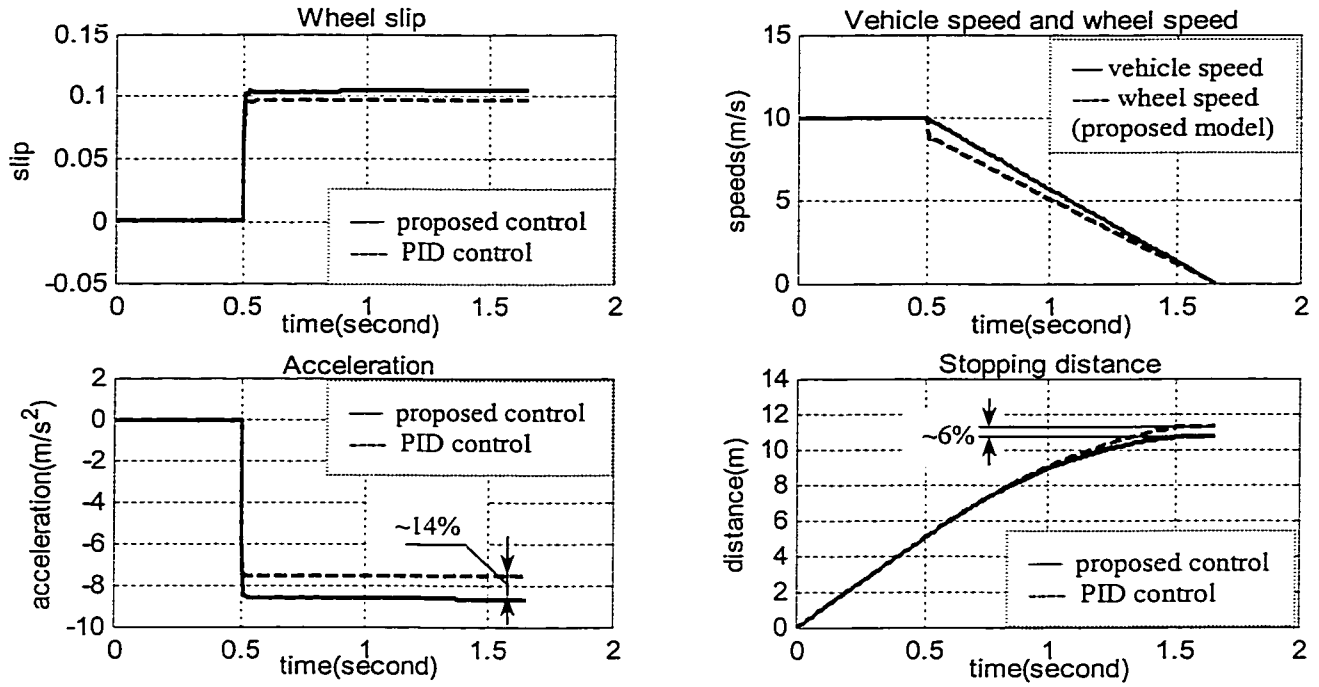

Figure 3.25 Braking Responses at Forward Speed of 10m/s

From the responses, when a vehicle moves at a forward speed of 10m/s, the stopping distance reduces by 6% and the average deceleration increases about 14% from PID control system when proposed controller is implemented to the system.

In conclusion, from Figs. 2.23-2.25, the stopping distances of the proposed system are smaller than that when implementing PID control, mainly at high-speed. The proposed system performances better representation for vehicle stopping distance and deceleration on dry roads. The reason is duo to the proposed system is based upon the dynamic analysis of the hydraulic braking system, so it more stable exactly tracks the desired trajectory.

3.5.4 System Simulation of Different Road Conditions

The performance of an ABS relies upon a proper identification of the road surface type. When the vehicle drive on snow road or ice road surfaces, the road brake force characteristic reduces significantly from dry concrete conditions as shown in Figure 3.4 to Figure 3.6. In order for the vehicle to operate in a stable manner, the controller must be able to adapt very quickly to this type of disturbance. The Magic Formula coefficients for different surfaces are shown in Table 3.4 and the correction factors C_1, C_2 for different surfaces are given in Table 3.5.

***a).* Vehicle moves on snow road**

Consider with the time delay, the braking is applied at time t_0 = 0.5 second when the vehicle moves at a forward speed of 20 m/s. The wheel slip increases to the optimal slip of 24% as experimental measured in Figure 2.8. The responses are shown in Figure 3.26.

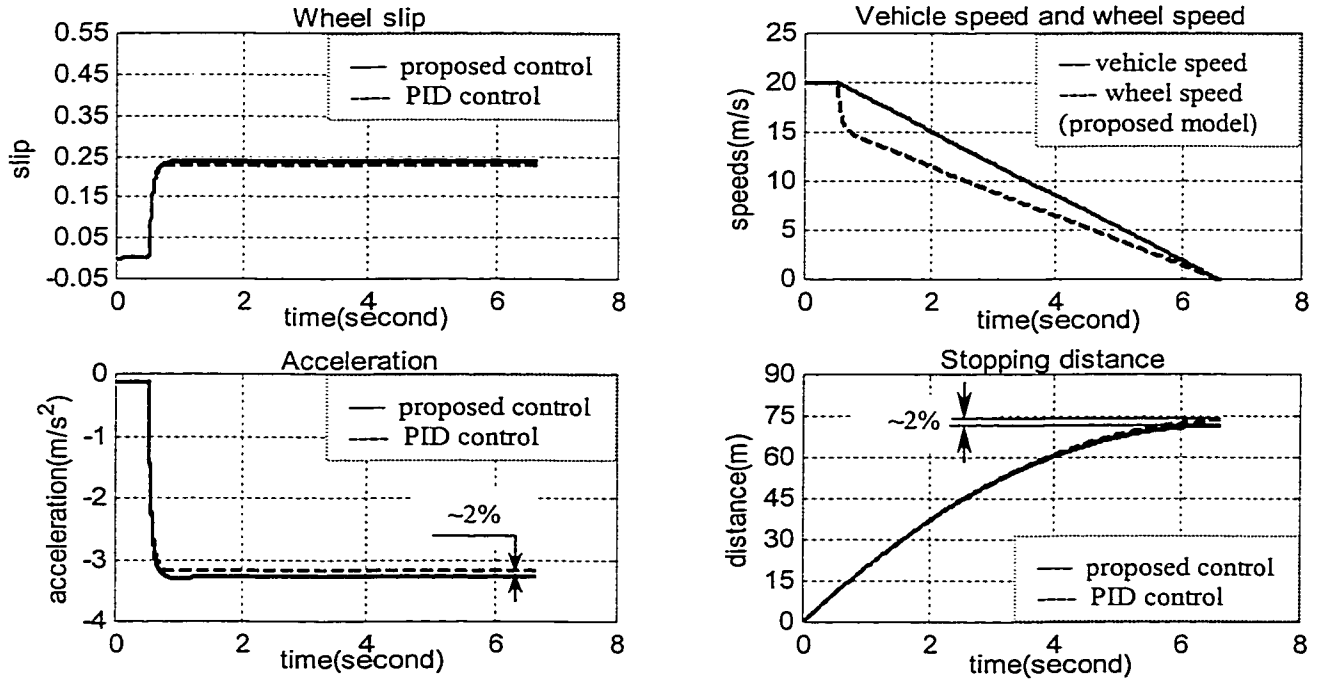

Figure 3.26 Braking Responses on Snow Road

From the responses, the ABS of proposed system adjusts well for snow roads. The stopping distance is about 73 m and the deceleration is about 3.2 m/s^2. The NTC presents a good performance when the vehicle drives on snow road; however, the brakes have less efficient on snow roads than on dry roads when controller is modified. This reason due to the friction force becomes very small and greatly affects the braking performance on snow roads.

b). Vehicle moves on icy road

Consider with the time delay, the braking is applied at time t_0 = 0.5 second when the vehicle moves at a forward speed of 20 m/s. The wheel slip increases to the optimal slip of 19% as experimental measured in Figure 2.8. The responses are shown in Figure 3.27.

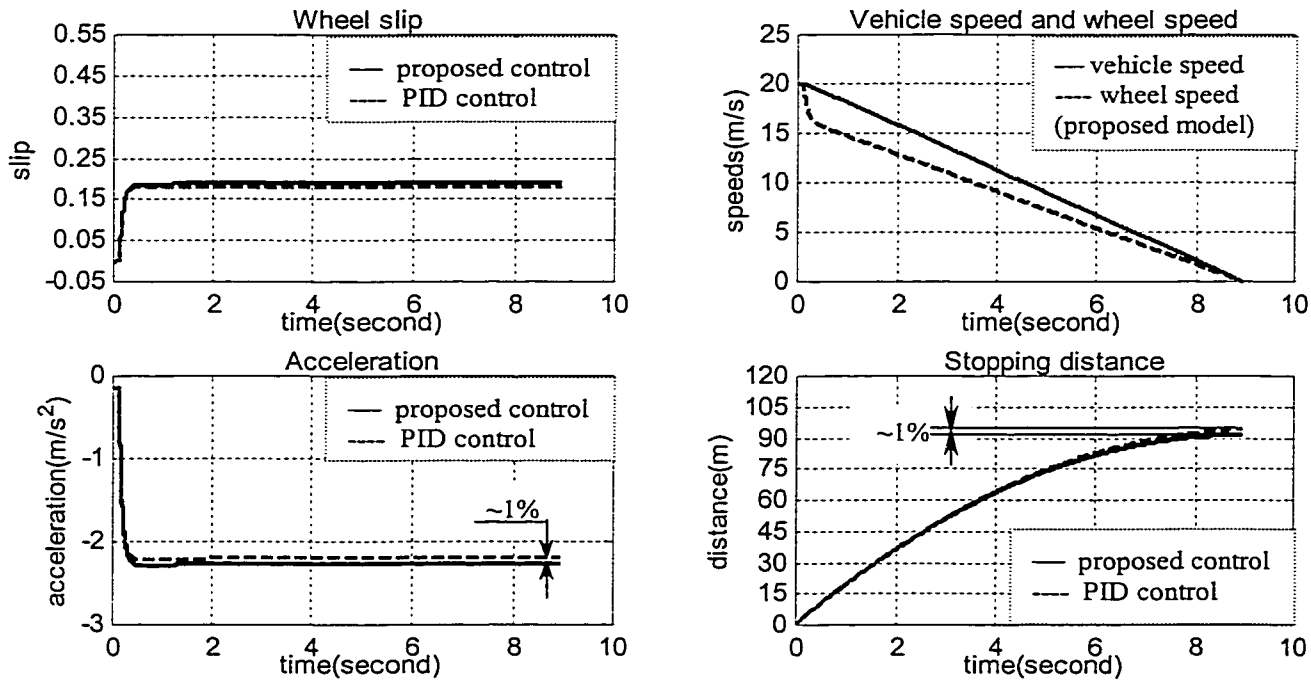

Figure 3.27 Braking Responses on Icy Road

From the responses, the ABS of proposed system adjusts well for icy road. The stopping distance is about 92 m and the deceleration is about 2.2 m/s^2. The NTC presents a good performance when the vehicle drives on icy road. The brakes have much less efficient on icy roads than on snow and dry roads when proposed control instead of PID control is implemented to the system.

In conclusion, the ABS control system does not significantly change the pattern of stopping distance under different road conditions. The NTC presents well in braking performances when the vehicle drives on different road surfaces. However, NTC can not greatly improve the braking performances from PID control for the snow and icy surfaces due to the friction forces very small.

3.5.4 Summary

In this Chapter, a new integrated NTC is developed for the hydraulic braking system, which used Lyapunov's stability theorem for the braking control algorithm with the desired values of longitudinal slip calculated in the real time. The MF tire model derived for different road conditions, are compared for validation with the available measured data. Examples of simulation were presented to illustrate the influence of the different road conditions, the brake-force distribution and the antilock control on the stop capability for the straight line braking. It is indicated that the optimum distribution of the friction and braking forces is necessary to achieve more robust vehicle directional stability, controllability and response to the drive braking performance.

Compared the simulation results, the ABS with proposed system can improve the braking performances. The adoption of ABS control on road vehicles will not

significantly change the stopping distance pattern on dry road surfaces, however, on wet snowing and slippery icy road surfaces, where wheel lock results in slippage, loss of stability and loss of steering control may occur more frequently. The proposed system using nonlinear tracking control combined with MF tire model provides a good control for the different road conditions. From results yield by the NTC compared with those resulting from sliding model PID control system, the proposed control system is based upon the nonlinear dynamic analysis of the hydraulic braking actuator system can change the system parameters, which more exactly tracks the desired trajectory. As a result, the proposed system performances better representation on vehicle stopping distance and deceleration for different road conditions mainly when vehicles move at high speeds. Furthermore, the proposed system has the ability to change the initial conditions for different type of roads which would not significantly change the pattern of vehicle stopping distance, deceleration and wheel slips for various road conditions, which represents the best braking performances under vehicle stability conditions.

CHAPTER 4

VEHICLE DYNAMICS VALIDATION AND ABS OPTIMIZED CONTROL SYSTEM

4.1 GENERAL

In the previous chapters, wheel lockup has been considered only as a boundary phenomenon in braking. However, the wheel steering of the vehicle seriously affects the braking performances during turning. An advanced braking system design must consider the interaction of the steering system to the overall dynamics of the vehicle. The control law was defined to reduce the longitudinal slip to a pre-selected value that maximizes the braking capability of the vehicle. Directional stability in conjunction with control issues was not yet addressed directly. However, during emergency maneuvers, when hard braking is combined with severe steering, normally stable (understeering) vehicles, even those equipped with ABS, can spin out due to a change of the vehicles to an unstable oversteering condition. Hence, retention of vehicle stability and steering ability, which are related to vehicle safety, are generally more important than minimizing stopping distance. Some of the vehicle subsystems might be designed and developed independently of each other. The dynamics of these subsystems, however, often interact. Lockup of front wheel causes loss of the ability to steer the vehicle, which will generally continue to move straight ahead despite the any steering inputs, or drifting to the side in response to cross-slope or side winds. While the braking process may considerably influence to the vehicle handling characteristics, braking in a turning maneuver increases the demand for both longitudinal and lateral resistant forces.

It is well recognized that the real wheel lockup first places a motor vehicle in an unstable condition. Once the wheels lock up, any small disturbances will initiate a rotation of the vehicle. When the brakes are applied on a road surface by an asymmetrical left or right traction pattern, the resulting brake forces vary, and the vehicle is lead to yaw. The front wheels, which yaw with the vehicle, develop a cornering force that enhances the capability to rotation, such that the yaw angle continues to grow. The vehicle is again stable only when it has completely "switched ends". On long vehicles (some heavy vehicles) the rotational accelerations are usually slow enough that the driver can apply corrective steer and prevent the full rotation. However, on smaller passenger cars, it is generally accepted that the average driver cannot readily control the vehicle in such a harsh driving situation. Thus there is a "rule of thumb" among automotive designers to states that a front brake bias constitutes the preferred design, which the rear wheels never lock first up before front wheels do.

Many control devices, such as Four-wheel Steering control system, have already been applied successfully to car production on certain models, and have contributed to the safety of automotive transportation. Four-wheel steering or active rear wheel braking systems have extensively been investigated and developed over the past two decades to improve their handling and stability characteristics. In particular, various active control systems for rear wheel steering have been developed by feed forward or feedback compensations for sideslip motion in the vehicle body. The improvement of handling and stability results in quite a good effect on driver steering maneuver, the so-called closed loop performance of the driver-vehicle system. The improvement is limited when assume a linear dynamic system because of the decrease of cornering stiffness of tires during

large lateral or longitudinal accelerations. In addition to the lateral wheel load transfer at the wheels during cornering there is also an axle load transfer from rear to front when braking in a curve. The axle load transfer causes the side slip angle to decrease at the front and increase at the rear. As a result of the brake forces, which due to tire deformation, the effective centre of tire contact shifts and the steering torque is reduced. An additional steering angle of the rear wheels may improve vehicle maneuverability and stability [18]. During the interval when the brake forces increase the driver has to initially reduce the steering wheel angle considerably; if the driver fails to do so, the vehicle would leave the road on the inside of the curve. When the braking force is further increased, the influence of front-to-rear axle braking balance plays the major role. The brake balance is generally set up for straight-line braking. The situation of braking while turning is usually neglected. However, this aspect becomes particularly important in the case of a non-constant brake balance. Most passenger cars have a fixed linear front-to-rear brake balance.

Of all the maneuvers encountered in everyday driving, one of the most critical is braking during turning. Braking and turning cause longitudinal and lateral weight transfer, which change the distribution of normal forces on the tires. This will, in turn, affect the dynamic properties of the tire and the motion of the vehicle. The vehicle's response pattern must represent the optimum compromise between steering response, stability, and brake effectiveness. Bosch [132] has defined a reference axis system as shown in Figure 4.1. This system is a right-hand orthogonal axis system fixed to a vehicle such that with the vehicle moving steadily on a level road, the x-axis is substantially horizontal, points forward and is in the longitudinal plane of symmetry, while the vehicle

could roll about x-axis. The y-axis points to driver's right about which the vehicle could pitch. The z-axis points to downward, and the vehicle's rotation is called yaw.

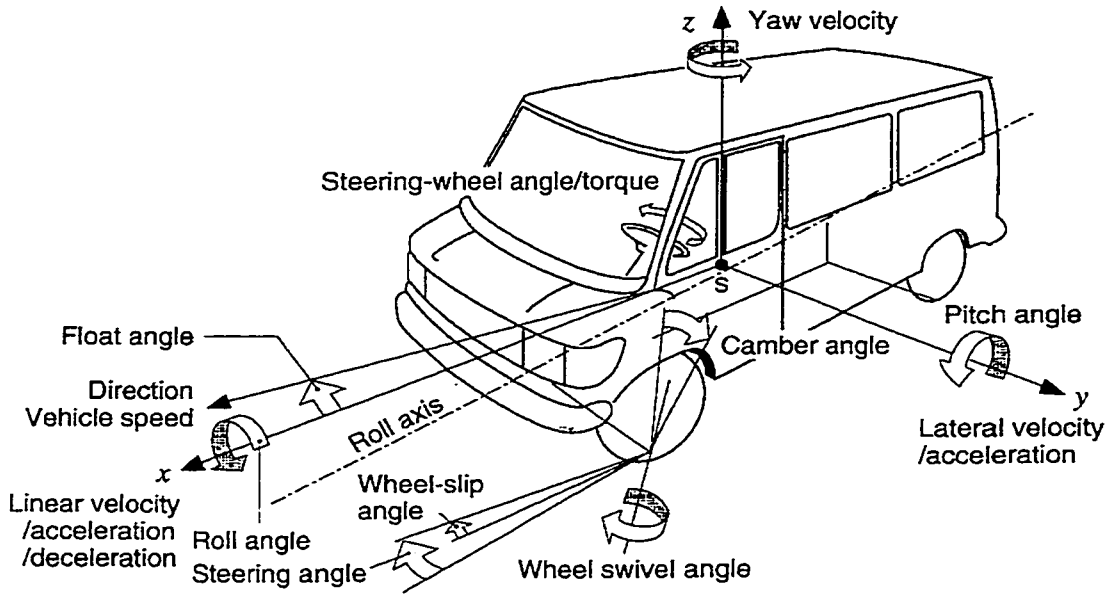

Fig. 4.1 The Axis Braking System during Cornering [132]

The main criteria employed in evaluating vehicle dynamics are:

- steering-wheel angle
- lateral acceleration
- linear acceleration/deceleration
- yaw velocity
- float and roll angles

Additional data are employed to verify and confirm the other available information on specific points of the vehicle performance:

- linear and lateral velocity
- steering angles at front and rear wheels

- slip angles at all wheels
- force applied at steering wheel.

As mentioned before [115], a more complex model of a vehicle does not necessarily yield more accurate results. However, the Bicycle Model would not consider the effect of the lateral weight transfer, and thus is not suitable for investigating the lateral dynamics of a vehicle under the turning and braking conditions. Thus, the choice of vehicle model relies mostly on the objectives of the analysis. In this dissertation research, a simple and credible model of a vehicle is proposed to facilitate its integration with an adequate vehicle ABS braking system is considered. A nonlinear Yaw-plane Four-wheel steering control model with a Limited Roll motion (YFLR), which incorporate nonlinear cornering characteristics through the Magic Formula [MF] tire model, and compliance of the braking column is proposed in this study. The model is thus initially developed to study the braking responses of the vehicle, which account for the effect of weight transfer. This model incorporates eight degrees of freedom (DOF): longitudinal and lateral velocities, yaw rate, roll angle and rotational velocity for each wheel. Pitch motions and vertical bounce motions of the sprung mass are assumed to be small and thus neglected.

Improvement of cornering performance with consideration of braking is important for automobile safety. Therefore, it is necessary to analyze vehicle dynamics and cornering characteristics with consideration of friction and braking forces. One of the scopes of the current research is to develop more sophisticated control algorithms that can handle highly nonlinear dynamics. Tire cornering characteristics add complexity to vehicle dynamics, because they exhibit saturation and unknown tire road contact

conditions. As shown before, the Sliding Mode control appears to be a very appropriate tool for this type of problem due to its flexible nonlinear modeling structure and the special consideration to modeling errors. The problem of control saturation, however, is not easy to be solved and needs very careful consideration. The traditional sliding mode controller can perfectly track a desired target trajectory even in the presence of unknown disturbance only if there is no related saturation and disturbances. When saturation does occur, the loss of controllability can induce system instability. In order to cope with saturation, Kaminaga, M. and Hedrick, J. K. proposed a method that employs an "Intelligent Sliding Surface" in their work [133]. The sliding surface is dynamically changed based on the observation of the system controllability. When controllability is decreasing, the sliding surface is relaxed from the control reference in order to limit the input and to preserve the controllability of the system.

The objective of ABS system is to maintain the longitudinal slip for each tire at a pre-selected value that will maintain braking effectiveness while simultaneously assuring improved directional stability and control by varying the pre-selected longitudinal slip values as functions of front wheel steer angle. By specifying a smaller value of desired longitudinal slip for the rear tires as compared with the front tires, the capacity of the rear tires to sustain lateral forces is increased, thus delaying the onset of "spin out" and providing a greater margin of stability during combined hard braking and steering maneuvers. The driver input commands are the front wheel steering angle and the brake torque. Braking system dynamics (from master cylinder to the wheel cylinders) are approximated by a first order lag with a time constant of 0.05 sec. Neither driver nor steering system dynamics are considered. The simulated maneuver, response to

simultaneous steps in both braking torque and front wheel steering angle, corresponds to a sudden reaction by the driver to a perceived emergency.

4.2 VEHICLE DYNAMICS

A nonlinear Yaw-plane Four-wheel steering model considers with Limited Roll motion (YFLR) used in this study. The system has eight degrees of freedom: longitudinal and lateral velocities, yaw rate, roll angle and rotational velocity for each wheel.

A free body diagram of this vehicle model is shown in Fig. 4.2.

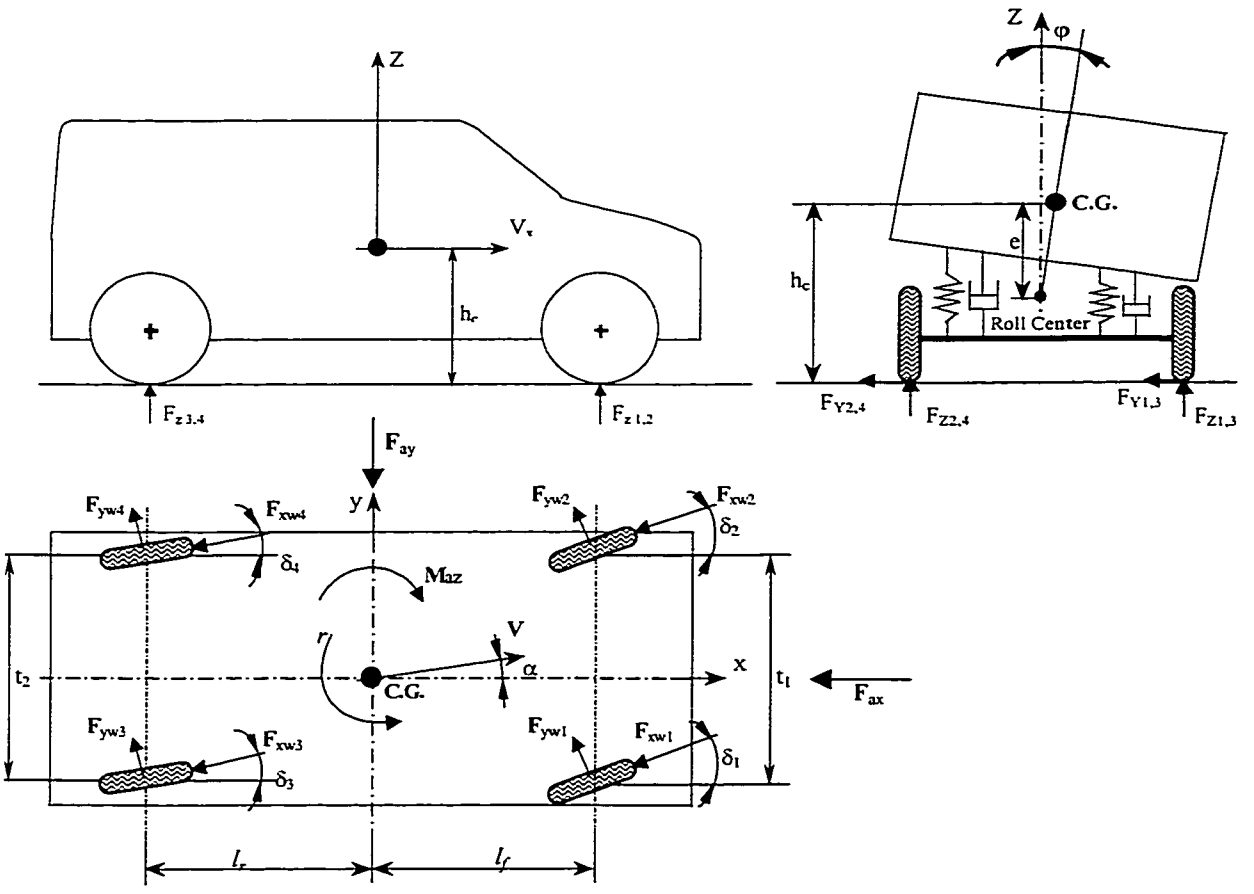

Fig. 4.2 Nonlinear Yaw-plane Four-wheel Steering Model with Limited Roll Motion for Braking

4.2.1 Four-wheel Steering Control Model

Four-wheel Steering Control (4WSC) systems have been investigated and developed over the last two decades to improve vehicle handling and stability characteristics. Several vehicular manufactures (Nissan, Honda, Mazda, Mitsubishi, Toyota, Daihatsu, BMW) introduced additional rear wheel steering for automobiles, and a second actuator is becoming available for vehicle steering dynamics.

Vehicle performance in turning can be enhanced by actively steering the rear wheels as well as the front wheels. An additional steering angle of the rear wheels may improve vehicle maneuverability and stability [36, 92]. Steering of the rear wheels, in addition to steering of the front wheels, makes it possible to reduce the vehicle sideslip angle at the center of gravity of the vehicle to zero. This greatly improves maneuverability at low speed and stability at high speed. To achieve this, the rear wheels are steered in opposite phase as that of the front wheels at low speed and in the same phase at high speed as shown in Figure 4.3 [92].

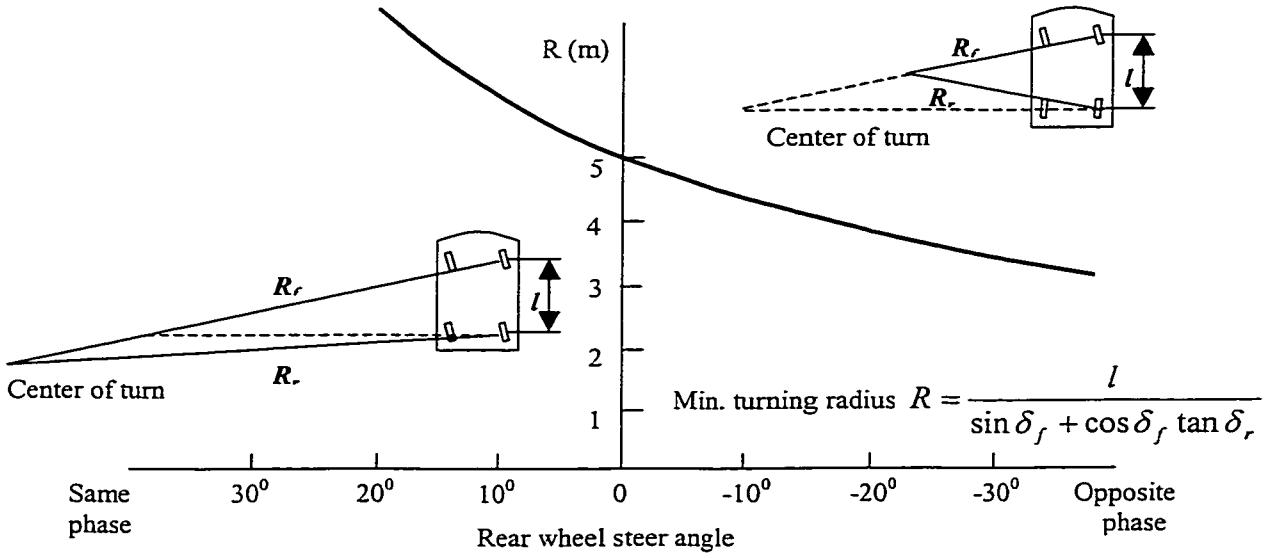

Fig. 4.3 Effect of Four-wheel Steering on Minimum Turning Radius

From Figure 4.3, when a turning maneuvers is performed with the 4WSC vehicle, the rear wheels are steered in the opposite phase from that of the front wheels at low speed, which leads to a reduction in the turning radius. By steering the rear wheels out-of-phase with the front wheels to reduce the turn radius one can improved the turning performance, thus improving maneuverability and cornering stability. Tight turning with small radius is a maneuver performed in a parking road at speeds of 5-10 km/h (2-3 m/s). However, when one talks about dynamics, one must consider the situation of higher speeds. This involves quasi-static state and the angles of the front & rear wheels in the same sign to increase the turn radius, thus improving vehicle stability. When analyzing the stability of the vehicles, it is referred to higher speeds and considered only the above situation with its consequences.

In general, 4WSC systems yield a quicker response with better damping of the yaw oscillation that occurs along with initiation of a turn. As a result, this system will provide better controllability and stability.

4.2.2 Nonlinear Yaw-plane Four-wheel Steering Model

The vehicle lateral and yaw directional response characteristics can be well evaluated through development of a nonlinear Yaw-plane Four-wheel Steering (YFS) model. The Four-wheel Steering Control (4WSC) model greatly improves maneuverability and stability of the vehicle. Nonlinear Yaw-plane (NYP) model, on the other hand, yields lateral and yaw directional response of a reasonable accurate manner for the vehicle. The YFS model consists of lateral, longitudinal and yaw motions as shown in Figure 4.4.

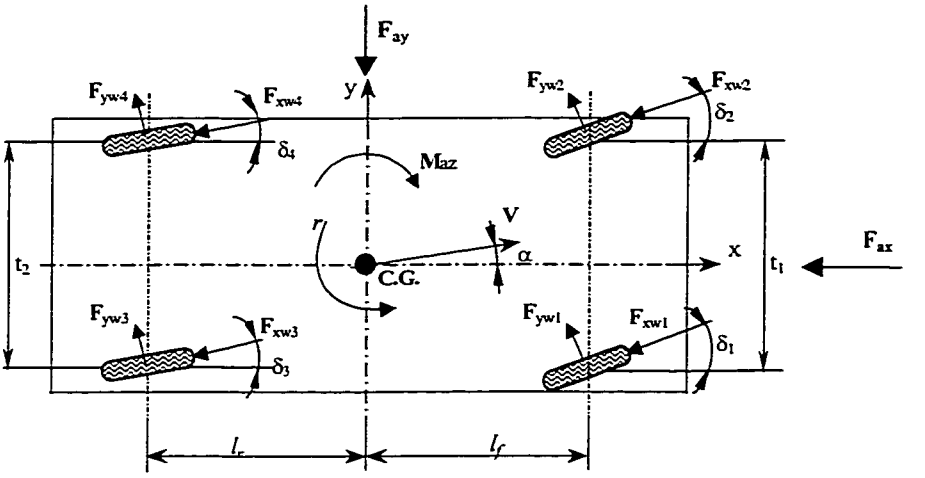

Fig. 4.4 Nonlinear Yaw-plane Four-wheel Steering Model

The vehicle is assumed to be negotiating a turn with constant radius on a banked track. It is also assumed that the lateral motion of the vehicle is only due to the tire forces exerted on the body of the vehicle. From Fig. 4.4, the equations of motion can be expressed as follows:

$$m(\dot{V}_y + V_x r) = \sum F_{yi} - F_{ay} \tag{4.1}$$

$$m(\dot{V}_x - V_y r) = \sum F_{xi} - F_{ax} \tag{4.2}$$

$$J_z \dot{r} = \sum M_{zi} - M_{az} \tag{4.3}$$

where

m = *vehicle mass*
V_x = *longitudinal velocity*
V_y = *lateral velocity*
r = *yaw rate*
F_{xi} = *tire force components along x-axis*
F_{yi} = *tire force components along y-axis*
M_{zi} = *yaw moment about the c.g of the vehicle.*
F_{ax} = *longitudinal aerodynamic force*
F_{ay} = *lateral aerodynamic force*
M_{az} = *yawing moment by aerodynamic*
J_z = *yaw moment of inertia of the vehicle.*

The yaw moment is given by,

$$\sum M_{zi} = l_f(F_{y1} + F_{y2}) - l_r(F_{y3} + F_{y4}) + \frac{t_1}{2}(F_{x1} - F_{x2}) + \frac{t_2}{2}(F_{x3} - F_{x4}) \tag{4.4}$$

where l_f = *distance from vehicle cg to front axial.*
l_r = *distance from vehicle cg to rear axial.*
t_1 = *distance between front wheels*
t_2 = *distance between rear wheels.*

The aerodynamic forces and moments exhibit high nonlinear behaviour, which can be expressed as a function of the angle-of-attack. The literatures [134] and [135] have been described a new technique which successfully has been applied to determine the aerodynamic forces and moment acting on an aircraft as a function of the aircraft state (e.g., velocity and angle-of-attack). This technique could be applied to ground vehicles.

The longitudinal aerodynamic force acting on the vehicle is

$$F_{ax} = \frac{\rho}{2} C_l A_f V_x^{\,2} \tag{4.5}$$

where ρ = *mass density of the air*
C_l = *longitudinal drag coefficient*
A_f = *frontal area of vehicle.*

The lateral wind components will also impose a side force on the vehicle attempting to change its direction of travel [136].

$$F_{ay} = \frac{\rho}{2} C_s A_f (V_x^2 + V_y^{\,2}) \tag{4.6}$$

where C_s = *side force coefficient*
A_s = *frontal area of vehicle.*

Note that the frontal area, rather than the side area are used in the equation (4.6), which is weighted by side force coefficient C_s. The side force coefficient C_s is zero at zero

relative wind angle, and grows nearly piecewise linearly with the angle from zero to 20 degrees. The slope of the gradient varies somewhat with vehicle type, but will typically be in the range of 0.035/deg to 0.06/deg [137]. Hence, C_s can be expressed as

$$C_s = k_s \alpha \tag{4.7}$$

where k_s = *slope of side force coefficient*
α = *relative wind angle.*

The side force acts on the body at the center of pressure, which is normally located ahead of the center of gravity such that the vehicle has the tendency to yaw from the wind. In the wind tunnel the side force is measured in the ground plane at the mid-wheelbase position.

The lateral force caused by a side wind does not normally act at the mid wheel base position, which produces a yaw moment. The yaw moment of the aerodynamic force is quantified by the equation [136],

$$M_{az} = 1/2\rho(V_x^{\ 2} + V_y^2)C_{YM} A_f L \tag{4.8}$$

where C_{yM} = *yaw moment drag coefficient*
L = *wheel base length of vehicle.*

The yaw moment coefficient varies with wind direction, starting at zero for zero relative wind angles and grows almost linearly up 20-degree angle. The slope of the coefficient at small angles ranges from 0.007/deg to 0.017/deg [137]. Hence, yaw moment drag coefficient is expressed as,

$$C_{YM} = k_{YM} \alpha \tag{4.9}$$

where k_{YM} = *slop of yawing moment drag coefficient*

From Figure 4.4, the tire forces components, respectively, can be calculated by the following transformation:

$$\begin{bmatrix} F_{xi} \\ F_{yi} \end{bmatrix} = \begin{bmatrix} \cos\delta_i & -\sin\delta_i \\ \sin\delta_i & \cos\delta_i \end{bmatrix} \begin{bmatrix} F_{xwi} \\ F_{ywi} \end{bmatrix} \tag{4.10}$$

where F_{xwi} = *longitudinal tire force along wheel axis*
F_{ywi} = *lateral tire force along wheel axis*

Note that the differences of the steering angles are very small between left and right wheels in front or rear especially at the high speed of the vehicle, hence assume:

$$\delta_1 = \delta_2 = \delta_f \tag{4.11}$$

$$\delta_3 = \delta_4 = \delta_r \tag{4.12}$$

where δ_f = *front wheel steering angle*
δ_r = *rear wheel steering angle.*

Substituting Equations (4.10)-(4.12) into Equations (4.1), (4.2) and (4.3), the differential equations of the vehicle motion become:

$$\begin{aligned} m(\dot{V}_y + V_x r) = &\sum_{i=1}^{2}(-F_{xwi}\sin\delta_f + F_{ywi}\cos\delta_f) \\ &+ \sum_{i=3}^{4}(-F_{xwi}\sin\delta_r + F_{ywi}\cos\delta_r) - F_{ay} \end{aligned} \tag{4.13}$$

$$\begin{aligned} m(\dot{V}_x - V_y r) = &\sum_{i=1}^{2}(-F_{xwi}\cos\delta_f - F_{ywi}\sin\delta_f) \\ &+ \sum_{i=3}^{4}(-F_{xwi}\cos\delta_r - F_{ywi}\sin\delta_r) - F_{ax} \end{aligned} \tag{4.14}$$

$$\begin{aligned} J_z\dot{r} = &(l_f\cos\delta_f - \frac{t_1}{2}\sin\delta_f)F_{yw1} + (l_f\cos\delta_f + \frac{t_1}{2}\sin\delta_f)F_{yw2} \\ &-(l_r\cos\delta_r + \frac{t_2}{2}\sin\delta_r)F_{yw3} - (l_r\cos\delta_r - \frac{t_2}{2}\sin\delta_r)F_{yw4} \\ &-(l_f\sin\delta_f + \frac{t_1}{2}\cos\delta_f)F_{xw1} - (l_f\sin\delta_f - \frac{t_1}{2}\cos\delta_f)F_{xw2} \\ &+(l_r\sin\delta_r - \frac{t_2}{2}\cos\delta_r)F_{xw3} + (l_r\sin\delta_r + \frac{t_2}{2}\cos\delta_r)F_{xw4} - M_{az} \end{aligned} \tag{4.15}$$

From Equations (4.13) and (4.15), it can be seen that the longitudinal force F_{xwi} affects not only the longitudinal performance but also the lateral and yaw motions of the vehicle. It is therefore desirable to control the longitudinal force of each tire to meet the

driver commands and keep the vehicle in dynamic equilibrium. F_{xwi}, and F_{ywi} are the tire longitudinal and lateral braking forces, which can be obtained though the Magic Formula, as described in Chapter 3,

$$y(x) = D\sin\{C\arctan[Bx(1-E) + E\arctan(Bx)]\}$$

where Y = *for either forces or moment*
X = *the slip angle or longitudinal slip*
B, C, D, E = *functions of the normal loads.*

Because the vertical suspension has small affect on the normal loads and the wheel treads are changed a little from front to rear, assume the vehicle without vertical suspension, and the wheel treads

$$t_1 = t_2 = t \tag{4.16}$$

From Figure 4.2, considering the load shift caused by the longitudinal acceleration and the lateral acceleration, for the most case of the vehicle traveling on a smooth road, the normal loads are calculated as:

$$F_{z1} = \left(\frac{mgl_r + m\dot{V}_x h_c}{2(l_f + l_r)}\right) + \left(\frac{m\dot{V}_y h_c}{2t}\right) \tag{4.17}$$

$$F_{z2} = \left(\frac{mgl_r + m\dot{V}_x h_c}{2(l_f + l_r)}\right) - \left(\frac{m\dot{V}_y h_c}{2t}\right) \tag{4.18}$$

$$F_{z3} = \left(\frac{mgl_f - m\dot{V}_x h_c}{2(l_f + l_r)}\right) + \left(\frac{m\dot{V}_y h_c}{2t}\right) \tag{4.19}$$

$$F_{z4} = \left(\frac{mgl_f - m\dot{V}_x h_c}{2(l_f + l_r)}\right) - \left(\frac{m\dot{V}_y h_c}{2t}\right) \tag{4.20}$$

where $F_{z1,2}$ = *normal loads on front wheels*
$F_{z3,4}$ = *normal loads on rear wheels*
h_c = *height of car cg. above road.*

The forces predicted by the tire model depend on the instantaneous value of the normal reaction force of the road on the tire. The normal forces will then change due to the longitudinal and lateral accelerations.

4.2.3 Roll Motion of the Model

To develop the most complete and accurate model of vehicle dynamic behavior, it is necessary to rely on more comprehensive vehicle models that simulate both yaw and roll response. Long vehicle, in general, the experience certain roll motion due to centrifugal actions arising from a steering maneuver, In small vehicle, the roll motion is due to compliance of suspension and tires. When a vehicle turns, the weight is transferred from the inside wheels to the outside wheels. The magnitude of this weight transfer is a function of mass, speed, yaw rate, and location of the center of mass. This weight transfer must be balanced by the roll moment produced by the suspension. A conventional suspension would yield front and rear roll stiffness and damping. Given roll stiffness and damping, roll displacement and velocity must be present to yield roll moments. Therefore, adequate treatment of such vehicles would require the inclusion of roll dynamics mode as shown in Figure 4.5.

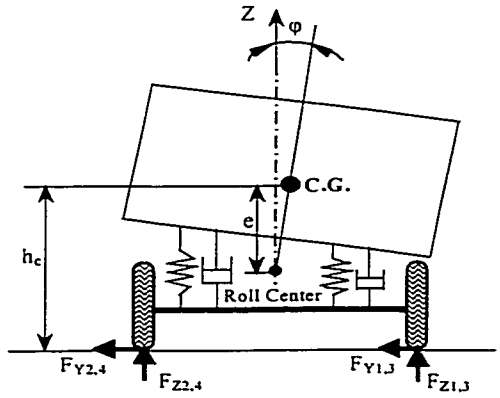

Fig. 4.5 Roll Motion of the Model

The static roll stability limit of a vehicle is frequently characterized by its rollover threshold, defined as the maximum lateral acceleration to which the vehicle can withstand without rolling over in a steady turning maneuver.

The related equation to roll mode is

$$J_x\ddot{\varphi} + m_b e(\dot{V}_y + V_x\psi) = \sum M_x \tag{4.21}$$

where m_b = *vehicle sprung mass*
e = *the distance from the roll center to the sprung mass center*
J_x = *roll moment of inertia*
φ = *roll angle*
$\dot{\varphi}$ = *roll rate*
ψ = *yaw angle.*

The roll moment produced by the suspension can be expressed as [31]:

$$\sum M_x = -K_\varphi\varphi - C_\varphi\dot{\varphi} + m_b ge\sin\varphi \tag{4.22}$$

where K_φ = *roll stiffness*
C_φ = *roll damping.*

Therefore, the roll motion equation becomes

$$J_x\ddot{\varphi} + m_b e(\dot{V}_y + V_x\psi) = -K_\varphi\varphi - C_\varphi\dot{\varphi} + m_b ge\sin\varphi \tag{4.23}$$

Four-wheel Steering Control (4WSC) vehicles invariably steer the rear wheels in same direction as front wheels at high speed to improve the responsiveness in transient cornering. The 4WSC also steer the rear wheels in the opposite direction at low speed to enhance cornering response. However, it may contribute to the increase in the potential for rollover. Therefore, to analyses the braking dynamics, it is necessary to include the roll motion of the 4WSC vehicle.

4.2.4 Wheel Dynamics

Consider the free body diagram of wheel i due to braking, which is shown in Figure 4.6. It is clear that the rolling resistance force is very smaller than the friction force and thus can be neglected.

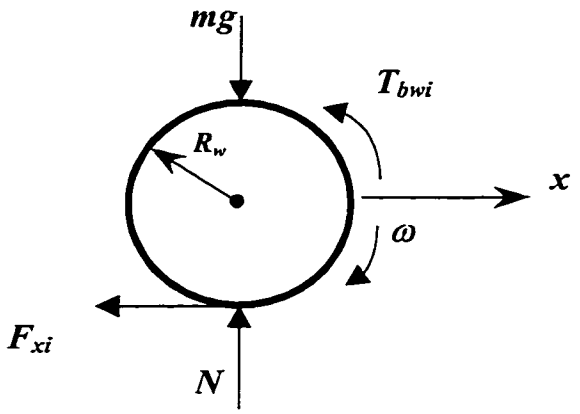

Fig. 4.6 Free Body Diagram of Wheel *i*

Hence, for the wheel i, the sum of torque about the axis is

$$F_{xwi}R_w - T_{bwi} = J_w\dot{\omega}_i \tag{4.24}$$

where ω_i = *angular velocity of wheel i*
J_w = *inertia of the wheel about the axle*
R_w = *wheel radius*
T_{bwi} = *applied braking torque.*

The nonlinear tire forces are evaluated using the slip angle and the longitudinal slip for each tire. It is known that tire forces are nonlinear functions of the slip angle and the slip ratio. They are also dependent on the vertical load (which may vary due to the longitudinal and lateral load transfer) and also the coefficient of friction on the tire-road contact patch. The top view schematic of a tire i during combined cornering and braking maneuvers is shown in Figure 4.7.

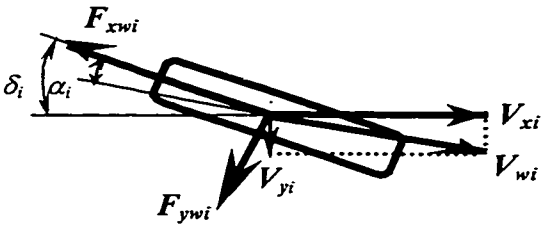

Fig. 4.7 Top View of Wheel *i*

The slip angles are defined as the angles between the longitudinal axis and the direction of travel of the centre of tire contact, which is expressed as follows:

$$\alpha_1 = \delta_f - \tan^{-1}\left(\frac{V_y + l_f r}{V_x + \frac{1}{2}t_1 r}\right) \tag{4.25}$$

$$\alpha_2 = \delta_f - \tan^{-1}\left(\frac{V_y + l_f r}{V_x - \frac{1}{2}t_2 r}\right) \tag{4.26}$$

$$\alpha_3 = \delta_r - \tan^{-1}\left(\frac{V_y - l_r r}{V_x + \frac{1}{2}t_1 r}\right) \tag{4.27}$$

$$\alpha_4 = \delta_r - \tan^{-1}\left(\frac{V_y - l_r r}{V_x - \frac{1}{2}t_2 r}\right) \tag{4.28}$$

The values of the longitudinal slip are

$$s_i = (V_{wi}\cos\alpha_i - \omega_i R_w)/(V_{wi}\cos\alpha_i) \tag{4.29}$$

where $V_{w1,2}$ = *estimated magnitudes of front axle velocities*
$V_{w3,4}$ = *estimated magnitudes of rear axle velocities*

The magnitudes of the velocities of axles can be calculated by

$$V_{w1} = \left[(V_y + l_f r)^2 + \left(V_x + \frac{1}{2} t_1 r \right)^2 \right]^{1/2} \tag{4.30}$$

$$V_{w2} = \left[(V_y + l_f r)^2 + \left(V_x - \frac{1}{2} t_2 r \right)^2 \right]^{1/2} \tag{4.31}$$

$$V_{w3} = \left[(V_y - l_r r)^2 + \left(V_x + \frac{1}{2} t_1 r \right)^2 \right]^{1/2} \tag{4.32}$$

$$V_{w4} = \left[(V_y - l_r r)^2 + \left(V_x - \frac{1}{2} t_2 r \right)^2 \right]^{1/2} \tag{4.33}$$

4.3 OPTIMIZED CONTROL SYSTEM

In this study, Nonlinear Track Control (NTC), Four-wheel Steering Control (4WSC) and Variable Slip-ratio Control (VSC) are implemented to the simulation. The NTC is developed for the hydraulic braking system, which uses Lyapunov's stability theorem for the braking control algorithm with the desired values of longitudinal slip calculated within the controller based on steering wheel angle. The 4WSC is developed for the yaw-plane four-wheel steering vehicle model, which the rear wheel steering angles set as functions of the front wheel steering angles and vehicle yaw rate. The VSC is developed for the corning characteristics with the balance of longitudinal forces and lateral forces. The three controllers are independent but are coupled through the states of the longitudinal and lateral tire forces. Considering the tire friction ellipse, the control systems are designed using model matching control theory to make the vehicle performance follow a desired dynamic model even during large decelerations or lateral accelerations.

4.3.1 Four-wheel Steering Control Law for Vehicle Model

Rear wheel steer is accomplished by mechanical, hydraulic or electronic means [138]. Normally, the rear-wheel steering angles are functions of the front steering angles. The specific control law used for the 4WSC in this study was originally proposed by Whitehead [94]. 4WSC system is a combination of vehicle yaw rate, front wheel steering angle and determines the rear wheel angle required to maintain zero side slip angle during steady state cornering. The primary reason for required minimum sideslip angle is that with small or zero sideslip angles, the car has not spun out and lost directional control.

This control scheme was proposed originally for applications to a linear vehicle model to control speed. However, Xia and Law [139] applied the same control strategy to a nonlinear vehicle model and showed that significant improvement in directional control and stability may be possible. The proposed control law is given by

$$\delta_r = \left(\frac{mV_x}{C_{ar}} - \frac{l_r}{V_x} + \frac{C_{af} l_f}{C_{ar} V_x} \right) r - \frac{C_{af}}{C_{ar}} \delta_f \tag{4.34}$$

where C_{af} = *front per axle cornering stiffness*

C_{af} = *rear per axle cornering stiffness*

From the equation, one can see that the rear wheel steering angle is set out-of-phase with the front wheel steering angle and coordinate a combination of vehicle yaw rate to minimize the side slip angle to becoming zero. For this system, it is necessary to measure yaw rate and use the resulting signal in the control law.

The front and rear turn radii, R_f and R_r, as shown in Figure 4.3, are related by the expression:

$$R_f \cos\delta_f = R_r \cos\delta_r \tag{4.35}$$

4.3.2 Nonlinear Tracking Control and System Optimization

The NTC Law for braking actuator used in this study was described in Chapter 3. The hydraulic servo system controls the fluid flow to the brake caliper and regulates brake pressure. The NTC system provides the best possible performances for the given track controller, which is described by

$$m\ddot{e} + k_v\dot{e} + k_p e = F - F_d + \Delta(g) \tag{4.36}$$

where e = *position error of the piston*
F = *piston force*
F_d = *desired force*
$\Delta(g)$ = *friction disturbance.*

because $e \to 0$ as $F - F_d \to 0$.

The NTC controller is derived as:

$$u = \frac{1}{z}\left(\left(\dot{F}_d - k_f(F - F_d)\right) + \dot{x}\left(\beta\left(\frac{A_2^2}{V_2} + \frac{A_1^2}{V_1}\right) + \frac{3}{2}k\right)\right) \tag{4.37}$$

The tire characteristics using MF tire model was also described in Chapter 3. The optimal peak slip is controlled using MF tire model, where slip is measured without error and peak slip is established with precision. The greatest friction force lead to peak slip s^*, which can be found from

$$\left.\frac{dF_t}{ds}\right|_{s=s^*} = 0 \tag{4.38}$$

As may be seen in the Magic Formula, when there is "weight transfer" from rear to front wheels during braking, the lateral force capability of the rear tires is reduced. The force capability is further reduced as longitudinal slip increases due to braking. This may eventually lead to spin out and loss of control of the vehicle. By setting the desired

longitudinal slip of the nonlinear tracking control system at the rear tires to a lower value than at the front, this loss of lateral force capability may be offset and the stability of the vehicle maintained under simultaneous hard braking and steering conditions.

An analysis is conducted and results with different combinations of desired front and rear slip angles are used in this study to achieve the best vehicle braking performance. The controller at each wheel is designed to track a desired longitudinal slip value that is specified as a function of front wheel steering angle.

It is assumed that braking at each axle of the vehicle is controlled independently, and the peak slip may differ for each wheel. The control gains are assumed same for each axle. For simplicity, no control dynamics or drive models are included. The control system is activated during severe braking, when the applied torque would cause wheel lock of one or both axles. Peak slip is re-iterated at each time step, based upon the actual value corresponding to maximum longitudinal force when both front and rear slip angles are zero. During combined steering and braking maneuvers, peak slip is defined as that value corresponding to maximum longitudinal force when slip angle is equal to the steering input. In conducting these simulations, sufficient braking torque was commanded to result in actuation of the nonlinear track control system and steer angle was increased to the point where spin out occurred. The results indicated that the actual slip values could be controlled such that they well tracked the varying values.

4.3.3 Variable Slip-ratio Control Law for Cornering

The cornering force at each tire is strongly affected by the wheel load transfer caused by the lateral and longitudinal accelerations. Moreover, the strong braking forces especially

on a slippery road can easily cause the wheels to lock, which decreases the cornering stiffness so much that the vehicle may easily become dangerously unstable.

While more longitudinal traction force is desired during straight driving, more lateral force is desired during cornering in order to be able to turn without lateral slippage, and thus to increase the vehicle stability. Typical characteristics of tires (Figure 2.8) shows that the longitudinal friction coefficient decreases and the location where the coefficient peaks, shifts to higher slip region as the slip angle increases. It also shows that the lateral friction coefficient decreases as the slip increases, and vice-versa. Thus, it is desirable to have a lower value of the slip during cornering than during driving straight. If the slip is too low, a significant portion of the traction force will be lost, which is also not desirable. Therefore, there should be an optimal way to balance the longitudinal and lateral forces.

In the proposed control strategy, the slip is given as a function of the wheel slip angle that is estimated from measurements of the vehicle velocity, the yaw rate, and the steering angle, as given in equations (4.39). From Figure 3.3, as the slip angle increase, the slip at which the longitudinal force reaches its maximum value increases. Therefore, in order to achieve the maximum longitudinal force, the slip should be increased as the slip angle increases. However, this would result in a small lateral force and reduce the cornering capability, which may cause the vehicle instability. It is proposed, therefore, that the target slip should be rather reduced in order to increase the lateral force when the slip angle is large. Therefore, the optimal slip value s_o must be smaller than the peak value s^*.

The variable slip ratio control scheme regulates wheel slip during cornering by varying the slip ratio as a function of slip angle. The control law is in the form of:

$$s_o = K(\alpha)\, s^* \tag{4.39}$$

where $K(\alpha)$ = *function of slip angle.*

$K(\alpha)$ can be obtained from test measurements [31] as shown in Figure 4.8, which is used in the proposed controller.

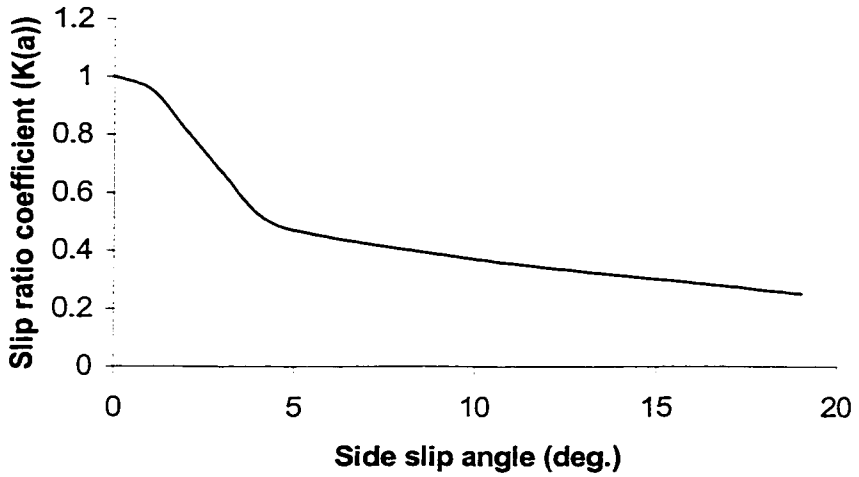

Fig. 4.8 Slip Ratio Coefficient [31]

4.4 Optimized System Simulation

In this section, a combined steering and braking maneuver on dry concrete surface is simulated for different forward speeds of the vehicle. Based on the above analysis, a YFLR of the vehicle, incorporating nonlinear MF tire model and compliance of the braking column is used in the simulation. Pitch and bounce motions of the sprung mass are assumed to be small and are thus neglected. The three controllers – NTC, 4WSC and VSC are implemented together through the states of the longitudinal and lateral tire

forces to impose the vehicle performance follow a desired dynamic model even during large decelerations or lateral accelerations. Various simplifying assumptions are associated with the vehicle and tire models, the hydraulic braking system and the control laws. The most significant assumptions adopted in the simulation are listed below:

- The vehicle is assumed to move on a horizontal surface with uniform friction characteristics;
- The pitch and vertical motions of the vehicle traveling on a perfectly smooth road are small and hence neglected;
- The roll motion of the sprung masses occur about their respective roll centers, which are located at fixed distances beneath the sprung masses;
- The roll motions of the unsprung masses are assumed to be negligible due to the large vertical stiffness of tires, while the effective radii of all the tires are considered to be identical;
- The contributions due to suspension lash are small assumed to be zero;
- The steering angle developed at the left and right wheel is considered to be identical, assuming parallel steering;
- The rolling resistance force is small and is neglected;
- The wheel camber angles are assumed small and hence the influence of wheel camber on lateral force generation is neglected;
- The unsprung mass is assumed to be rigidly attached to their respective sprung masses, thus, the suspension of the vehicle is assumed rigid;
- The properties of left and right tires of an axle are considered represented by a single composite tire, and the cornering stiffness of each axle is the sum of the cornering stiffness of the tires mounted on that axle;

- The aerodynamics forces act at the c.g. of the vehicle;
- Neglect the fluid leakage in the valve, cylinder, booster and the hydraulic circuits;
- Assume that the control u applied to the spool valve is directly proportional to the spool position, which the dynamics of the valve motor/flapper are fast enough to be decoupled from the dynamics of the spool;
- Neglect the small inertia of the pistons in the master cylinder and braking booster;
- The friction in cylinder and booster are consider as the functions of the velocity of the piston;
- The brake caliper pressure is modeled as a nonlinear function of displacement of the brake fluid and that the specific torque constant is the ratio of braking torque to caliper pressure;
- The vehicle is initially moving straight forward, therefore, the initial yaw rate and rear steering angle of the vehicle equal zero;
- The commands of the combined braking and steering from driver are interpreted as the simultaneous application of step inputs in the front steering angle and deceleration.

Based on the above assumptions and note that $t_1 r$ and $t_2 r$ are much smaller than V_x, hence the equations (4.24) to (4.33) can be further simplified as:

The side slip angle of the front wheels is

$$\alpha_f = \alpha_1 = \alpha_2 = \delta_f - \tan^{-1}\left(\frac{V_y + l_f r}{V_x}\right) \tag{4.40}$$

The side slip angle of rear wheels is

$$\alpha_r = \alpha_3 = \alpha_4 = \delta_r - \tan^{-1}\left(\frac{V_y - l_r r}{V_x}\right) \tag{4.41}$$

The velocities of front wheels is

$$V_{wf} = V_{w1} = V_{w2} = \left[(V_y + l_f r)^2 + V_x^2\right]^{1/2} \tag{4.42}$$

The velocities of rear wheels is

$$V_{wr} = V_{w3} = V_{w4} = \left[(V_y - l_r r)^2 + V_x^2\right]^{1/2} \tag{4.43}$$

The longitudinal slips of front wheels is

$$s_f = s_{1,2} = (V_{wf}\cos\alpha_f - \omega_{1,2}R_w)/(V_{wf}\cos\alpha_f) \tag{4.44}$$

The longitudinal slips of rear wheels is

$$s_r = s_{3,4} = (V_{wr}\cos\alpha_r - \omega_{3,4}R_w)/(V_{wr}\cos\alpha_r) \tag{4.45}$$

From equation (4.24), the wheel speeds

$$\dot{\omega}_{1,2} = \frac{1}{J_w}(F_{xw1,2}R_w - T_{bw1,2}) \tag{4.46}$$

$$\dot{\omega}_{3,4} = \frac{1}{J_w}(F_{xw3,4}R_w - T_{bw3,4}) \tag{4.47}$$

Note that the longitudinal forces F_{xwi} and lateral forces F_{ywi} can be obtained from Magic Formula (MF) tire model. The equations of motion (4.13) - (4.15) for nonlinear Yaw-plane Four-wheel Steering (YFS) model and the equation of motion (4.23) for Roll Motion are solved simultaneous for the simulation. The equations (4.17) - (4.20) can be used for the normal loads and the aerodynamic forces are calculated using relationships (4.5) - (4.9).

4.4.1 System Simulation Inputs

A simulation program that consists of the proposed braking system, vehicle model and model matching controllers is described by using MATLAB and SIMULINK. The implemented dynamic parameters of the brake system and vehicle are given in Table 4.1.

Table 4.1. System parameters with the YFLR model [31] [9] [122]

SYM.	VALUE	NAME	SYM.	VALUE	NAME
m	1660 kg	vehicle mass	V_0	30m/s	initial velocity
m_b	1500 kg	vehicle sprung mass	C_{af}	65.1 kN/rad	cornering stiffness of front tire
m_f	40 kg	front tire mass	C_{ar}	54.1 kN/rad	cornering stiffness of rear tire
m_r	40 kg	rear tire mass	A_f	$2.13m^2$	vehicle frontal area
g	$9.81m/s^2$	gravitational acceleration	C_l	0.539	longitudinal drag coefficient
l_f	1.0 m	distance from front to C.G.	k_s	0.05/deg	slop of side force coefficient
l_r	1.45m	distance from rear to C.G	k_{YM}	0.012/deg	slop of yaw moment coefficient
l	2.45m	wheel base length	ρ	$1.23kg/m^3$	mass density of the air
h_c	0.533m	centre of gravity height	f_0	0.01	basic coefficient
t	1.524m	wheel tread length	f_s	0.005	speed effect coefficient
e	0.39m	roll center	K_m	2.237	scaling constant
R_w	0.326m	wheel radius	M_{pm}	0.1kg	servo motor prime mover mass
J_x	$460\ kgm^2$	roll moment of inertia	B_{ft}	$30N/ms^{-1}$	fluid viscous friction coefficient
J_z	$2400\ kgm^2$	yaw moment of inertia	K_{ft}	50000N/m	fluid stiffness coefficient
J_t	$4.07kgm^2$	tire moment of inertia	K_t	1.7	specific torque constant
J_e	$0.241kgm^2$	engine inertia	K_φ	38.40 kNm/rad	roll stiffness
ζ	10.0	transmission gear ratio	C_φ	1756Nms/rad	roll damping coefficient

4.4.2 Steering Input while Turning

In order to investigate the effect of the proposed controller on the improvement of handling and stability on braking and turning condition, the transient response is evaluated, in the case when a driver operates the steering wheel to execute at the front wheels a maneuver as shown in Figure 4.9.

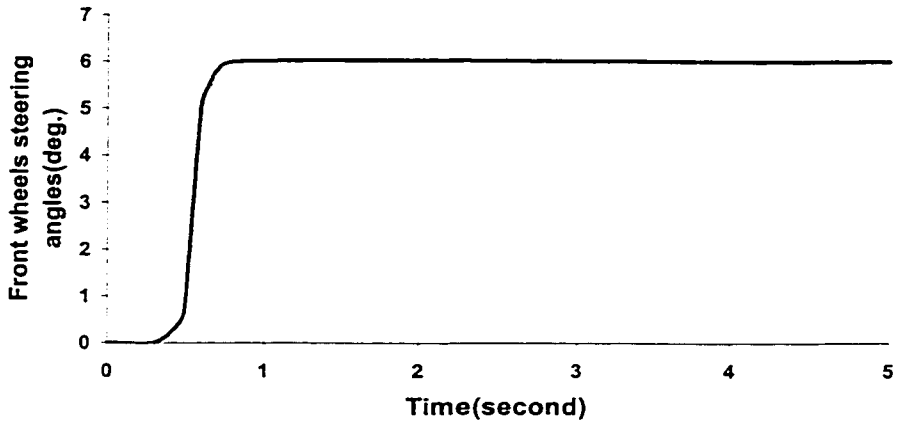

Fig. 4.9 Steering Wheel Angle Input

Figure 4.9 shows the animation of the J-turn behavior of the vehicles. The maneuver consists of a rapid steering from 0 to 6 degree, which is initiated at time 0.3 second and lasts for 0.3 second. During braking, different decelerations are considered for the vehicle running on the different road conditions at various speeds. For the rear steering angles, the four-wheel control law is given by [139]

$$\delta_r = \left(\frac{mV_x}{C_{\alpha r}} - \frac{l_r}{V_x} + \frac{C_{\alpha f} l_f}{C_{\alpha r} V_x} \right) r - \frac{C_{\alpha f}}{C_{\alpha r}} \delta_f \tag{4.48}$$

The parameters of the desired model are calculated from the baseline vehicle parameters in Table 4.1. The vehicle is controlled by the model matching controller with the desired model.

4.4.3 Block Diagrams of the Simulation System

The analysis is carried out using MATLAB/SIMULINK programs where the constitutive equations and the data of Table 4.1 are implemented. The block diagrams is shown in Figure 4.10 and is detailed in Figure 4.11 – Figure 4.23.

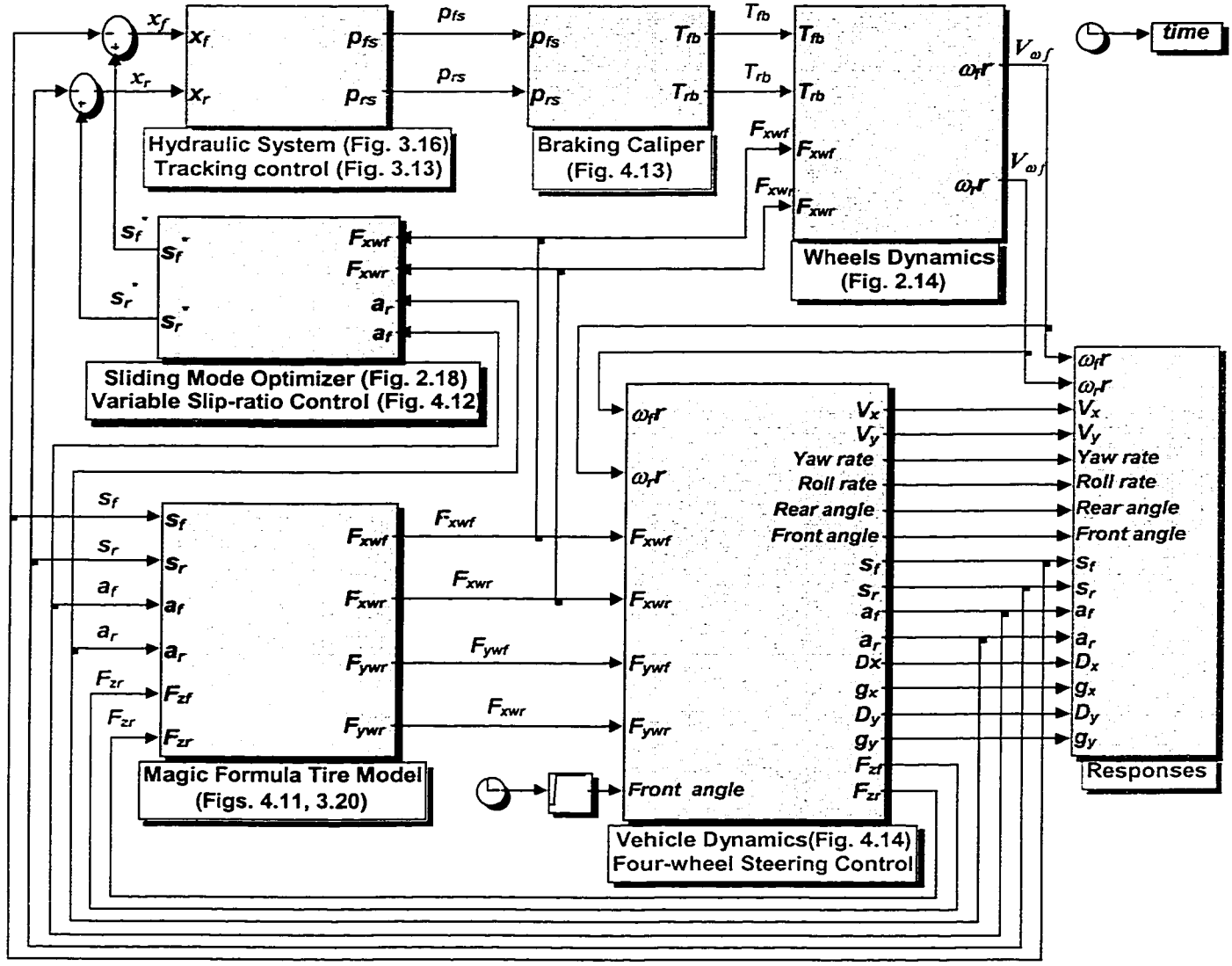

where T_{fb} – *braking torque on front wheels;* p_{fs} – *pressure of front calipers;* x_f – *piston position for front wheels;*
T_{rb} – *braking torque on rear wheels;* p_{rs} – *pressure of rear calipers;* x_r – *piston position for rear wheels;*
s_f^* – *optimal slip of front wheels;* s_f – *front wheel slip;* F_{zf} – *normal load on front wheels;*
s_r^* – *optimal slip of rear wheels;* s_r – *rear wheel slip;* F_{zr} – *normal load on rear wheels;*
a_f – *front wheel slip angle;* D_x – *longitudinal stopping distance;* a_x – *longitudinal acceleration;*
a_r – *rear wheel slip angle;* D_y – *lateral stopping distance;* a_x – *lateral acceleration;*
V_x – *longitudinal velocity of vehicle;* $V_{\omega f}$ – *front wheels velocity;* ω_f – *angular velocity of front wheels;*
V_y – *lateral velocity of vehicle;* $V_{\omega r}$ – *rear wheels velocity;* ω_r – *angular velocity of rear wheels;*
r – *wheel radius;* F_{ywf} – *lateral tire force of front axis;* F_{ywr} – *lateral tire force of front axis;*
F_{xwf} – *longitudinal tire force along front axis;* F_{xwr} – *longitudinal tire force along rear axis.*

Fig. 4.10 Simulation Diagram of ABS Optimized Control System
(Nonlinear Tracking, Four-wheel Steering and Variable-slip Ratio Controls;
Nonlinear Yaw-plane Vehicle model with Limited Roll Motion;
Magic Formula Tire Model and Sliding Optimizer)

The details of hydraulic system, nonlinear tracking, sliding mode optimizer, wheel dynamics and longitudinal Magic Formula tire force have been described in Chapter 2 and Chapter 3 and are further used in this simulation:

- Hydraulic system as shown in Fig. 3.16;
- Nonlinear tracking control as shown in Fig. 3.12;
- Sliding mode optimizer as shown in Fig. 2.18;
- Wheel dynamics as shown in Fig. 2.14;
- Longitudinal Magic Formula tire force as shown in Fig. 3.19.

Other simulation diagrams are described below:

a). **Magic Formula lateral tire force** (refer to equation (3.1)):

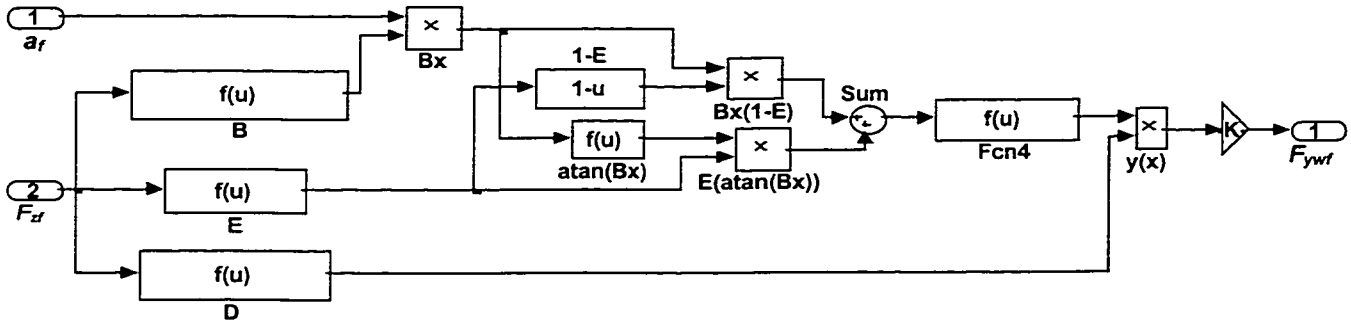

Fig. 4.11 Magic Formula Lateral Tire Force

b). **Sliding mode optimizer and Variable-slip ratio control** (refer to equation (4.39))

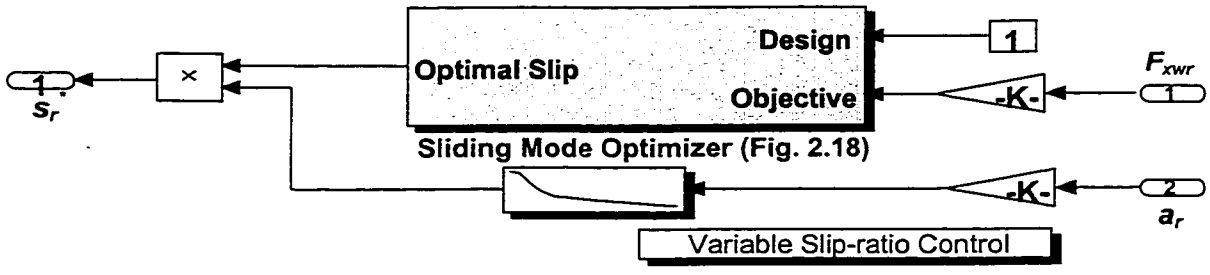

Fig. 4.12 Sliding Mode Optimizer and Variable Slip-ratio Control

c). **Braking caliper** (refer to equation (2.34))

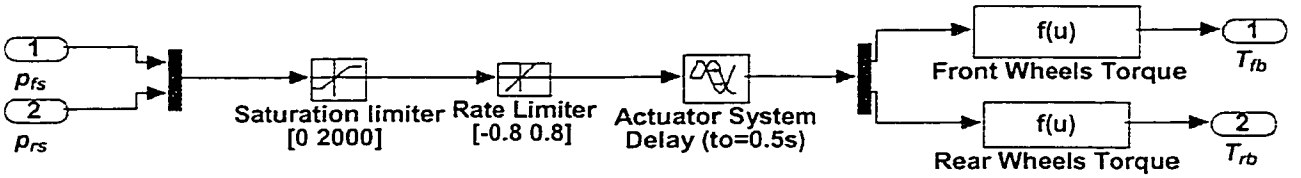

Fig. 4.13 Braking Caliper

d). **Vehicle dynamics model and Four-wheel steering control**

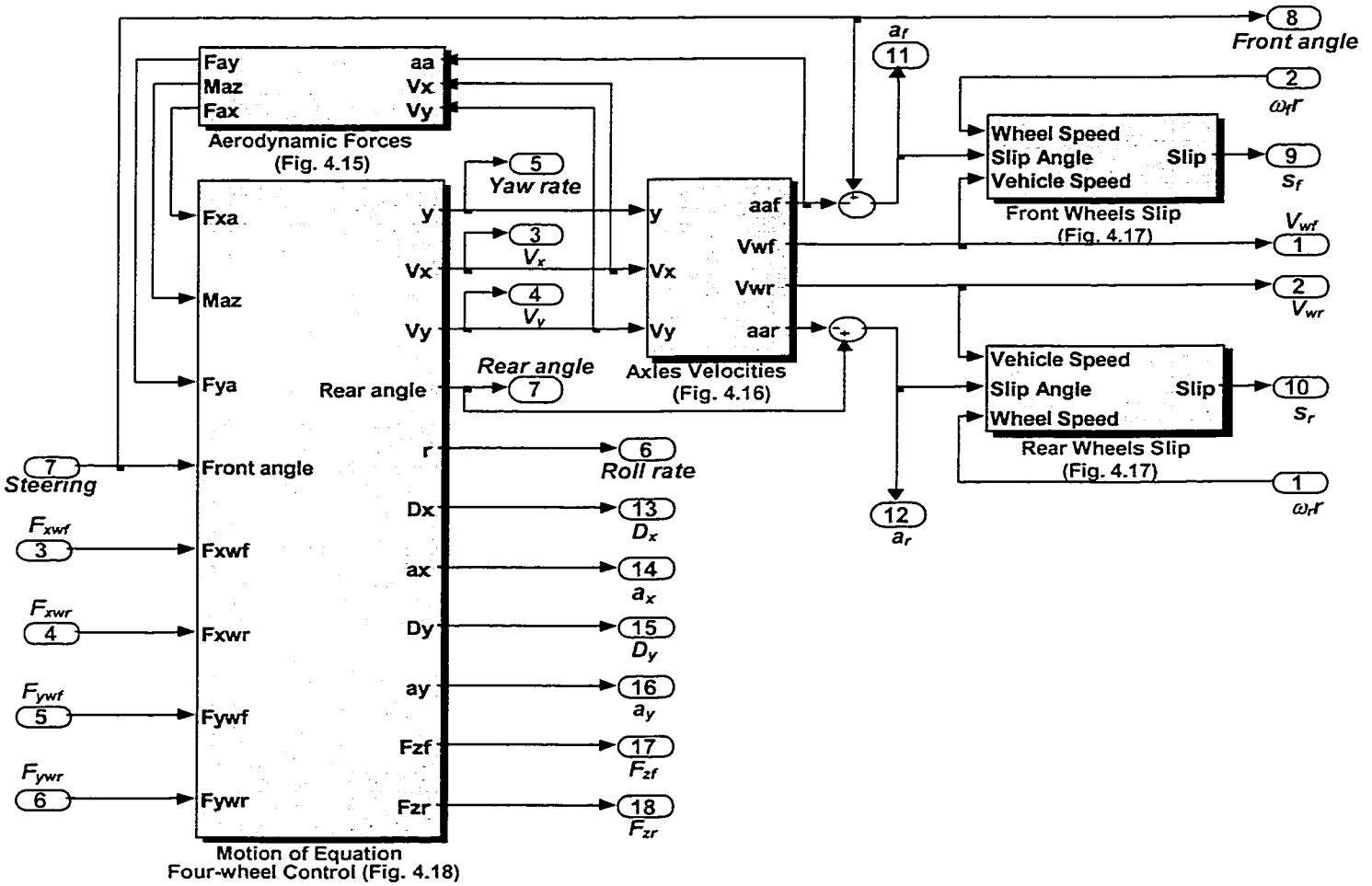

Fig. 4.14 Vehicle Dynamics Model and Four-wheel Steering Control

i). Aerodynamic forces (refer to equations (4.5) to (4.9))

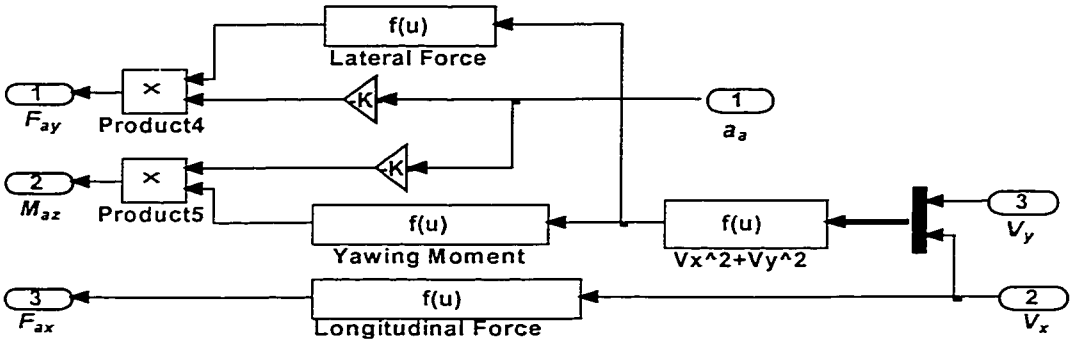

Fig. 4.15 Aerodynamic Forces

ii). Axles velocities (refer to equations (4.40) to (4.43))

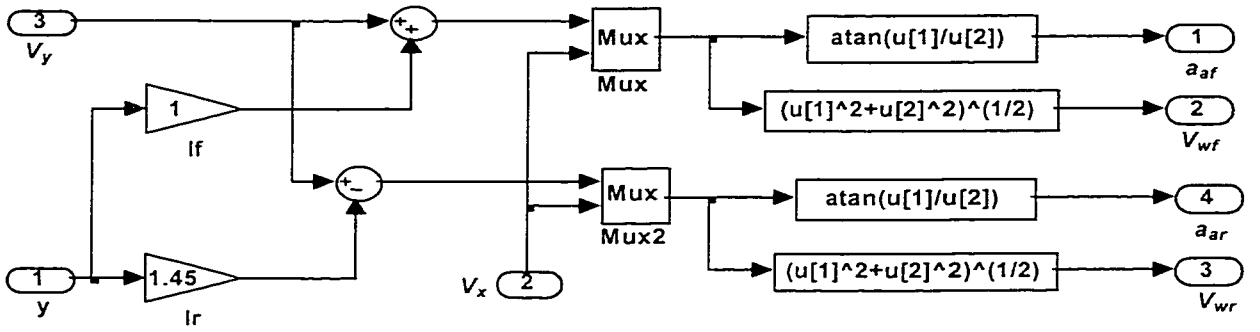

Fig. 4.16 Axles Velocities

iii). Front or rear wheels slip ((refer to equations (4.44) and (4.45)):

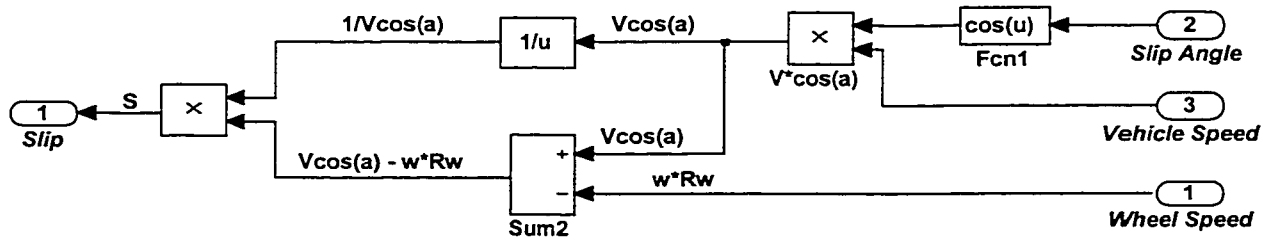

Fig. 4.17 Front or Rear Wheels Slip

iv). Motion of equation and Four-wheel steering control (equations (4.13) to (4.20))

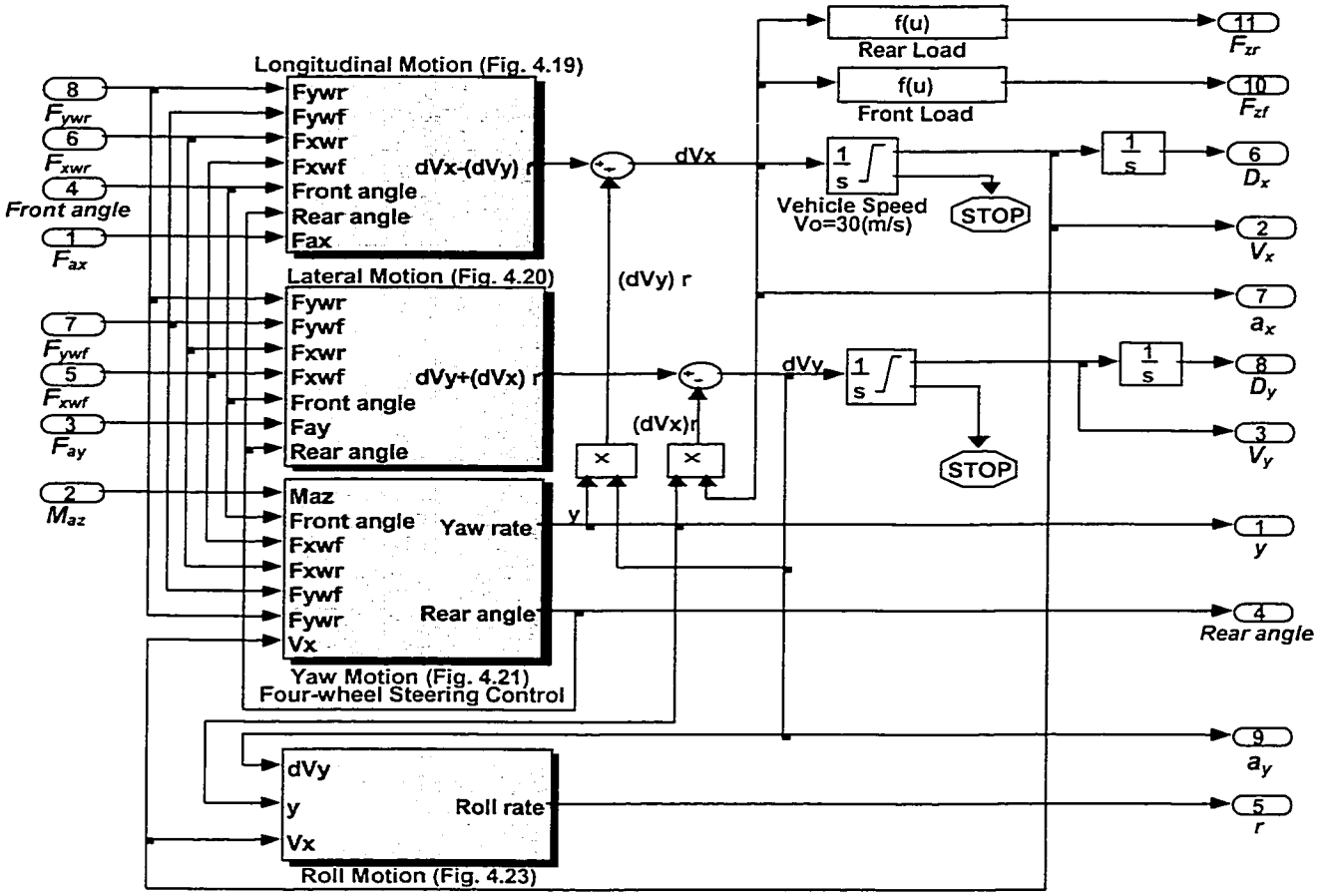

Fig. 4.18 Motion of Equation and Four-wheel Steering Control

1). Longitudinal motion (refer to equation (4.14)):

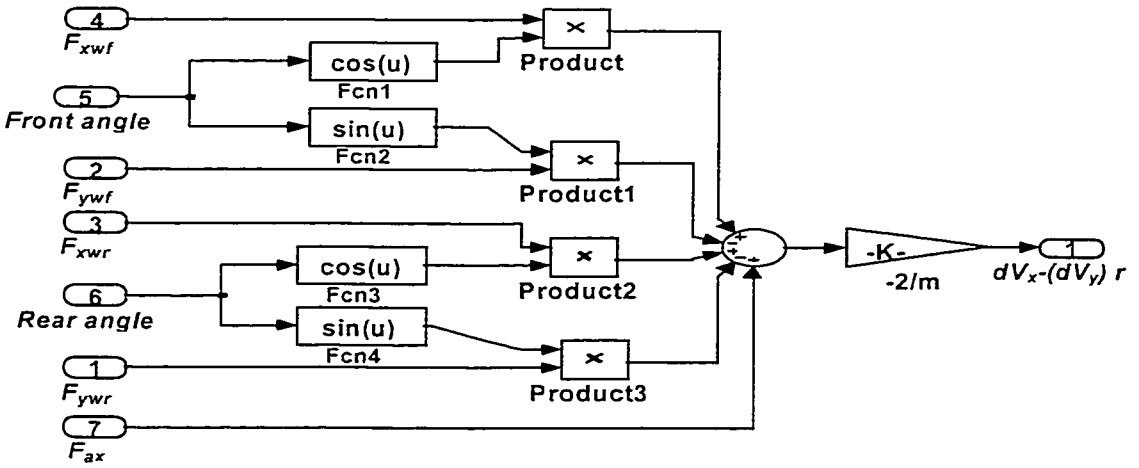

Fig. 4.19 Longitudinal Motion

2). Lateral motion (refer to equation (4.13)):

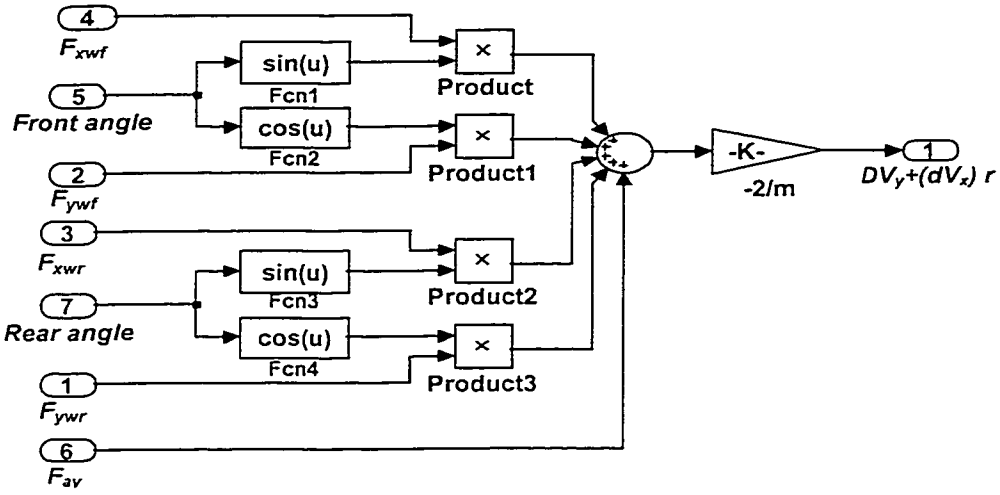

Fig. 4.20 Lateral Motion

3). Yaw motion and Four-wheel steering control (refer to equation (4.15)):

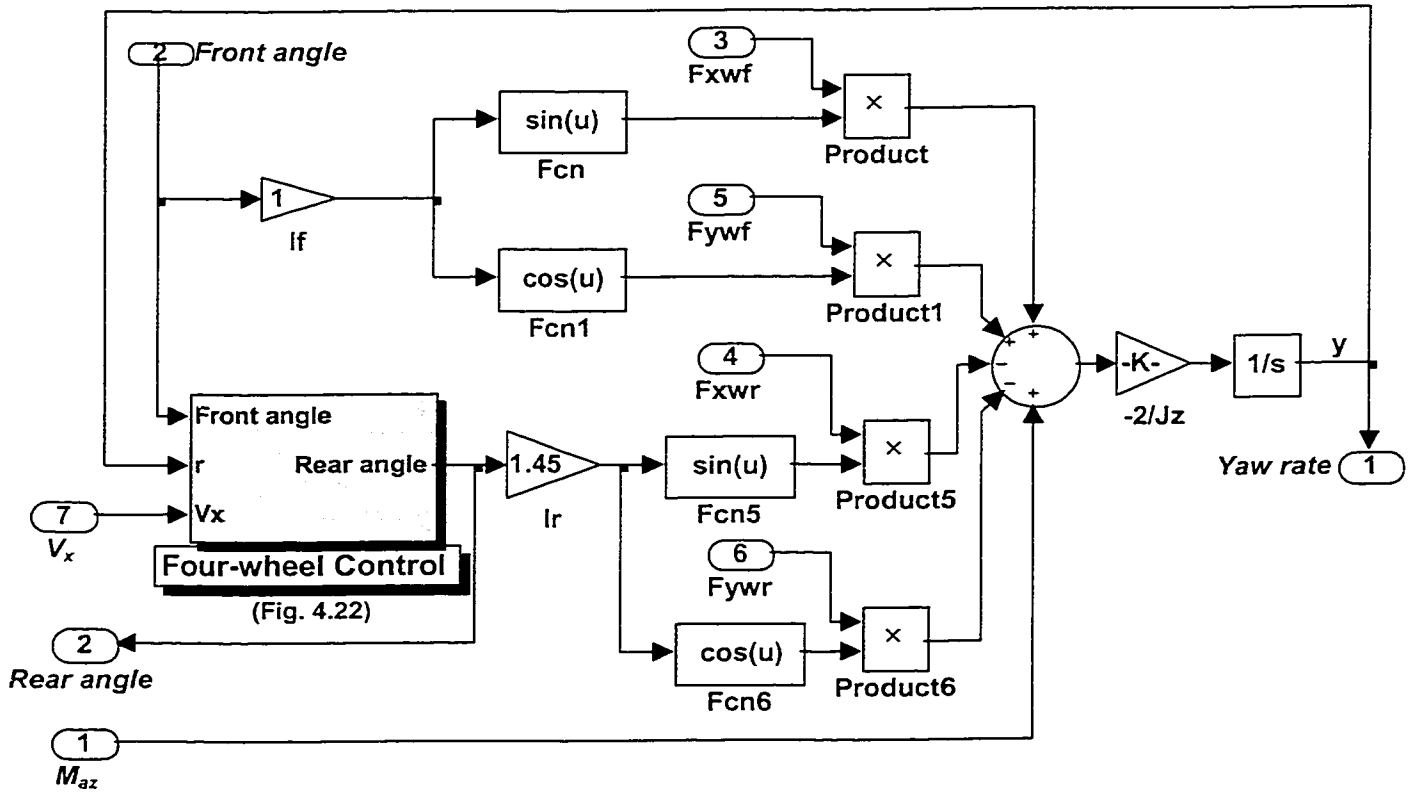

Fig. 4.21 Yaw Motion and Four-wheel Steering Control

* Four-wheel Steering Control (refer to equation (4.34)):

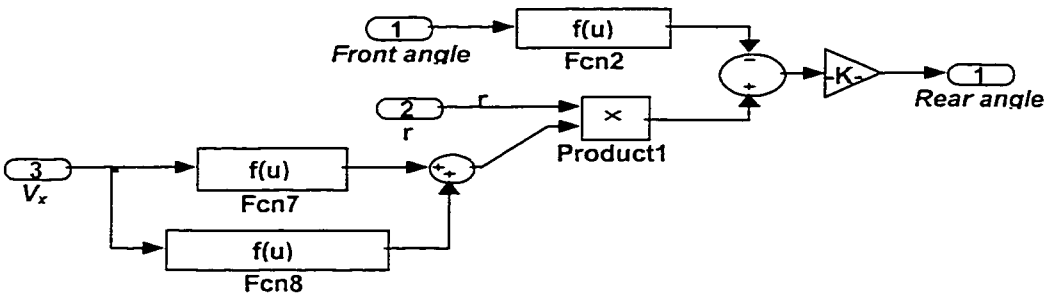

Fig. 4.22 Four-wheel Steering Control

4). Roll motion (refer to equation (4.23)):

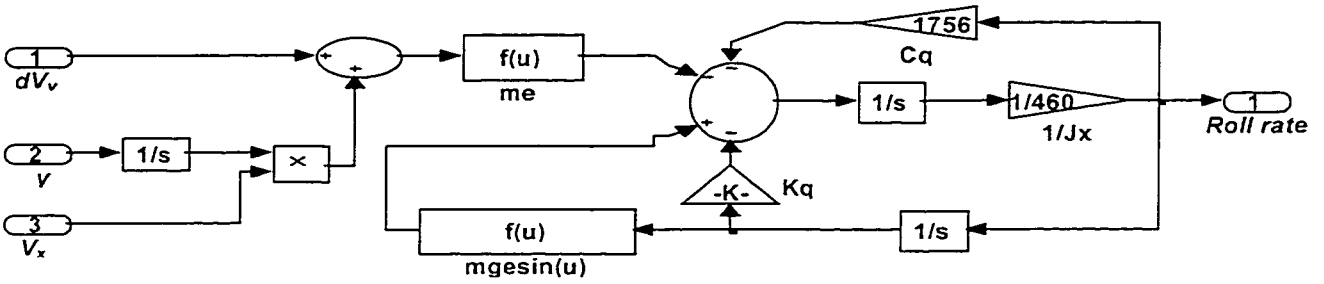

Fig. 4.23 Roll Motion

From the block diagrams, the simulation of the system can be concluded as:

1. The braking pressure and braking torque have been controlled by the integrated hydraulic Nonlinear Tracking control system as described by Figures 3.13, 3.16, 3.19 and 4.13.
2. The hydraulic braking system gets the feedback signal from the errors between the wheel slip ratios and the optimal slip ratios, which are determined by Figures 4.17, 2.18 and 4.12 where the Variable-slip Ratio control law controls the balance of the longitudinal friction forces and lateral friction forces.
3. The longitudinal friction forces and lateral friction forces are obtained by the Magic Formula (Figures 4.11 and 3.19).

4. The Four-wheel Steering control is used in the Yaw/Roll Four-wheel steering system of the vehicle as found though Figures 4.14 to 4.23.
5. The braking torque and friction forces are applied to the wheel rotors to avoid the wheels lock up and maintain the vehicle directional stability as shown in Figures 2.15 and 2.17.

Note that this electronic feedback control system can be integrally implemented with electronic components. As a cycle, when wheel lock is detected, the pressure in one or more of the braking cylinders is reduced until the wheel speed exceeds a predetermined value, at which time the pressure is again increased. The system continues this cycle until the vehicle completely stops.

4.4.4 System Simulation Responses

The performances of the proposed control scheme are compared with the system when PID control is implemented as described in Chapter 2.

Simulation results are generated for cases where vehicle drive on dry concrete road and when the vehicle moves at forward speeds of 30m/s (108km/h), 20m/s (72km/h) and 10m/s (36km/h). The considered vehicle parameters and brake actuator dynamic properties as listed in Table 4.1 when a driver operates the front wheels as shown in Figure 4.8. Assuming the vehicle is initially moving straight forward and consider the time delay when the braking is applied at time $t_0 = 0.5$ second. The responses are shown in Figures 4.24 to 4.29, which represent the significantly improving of both braking performances and stability when the proposed is implemented.

a). V_0 = 30m/s

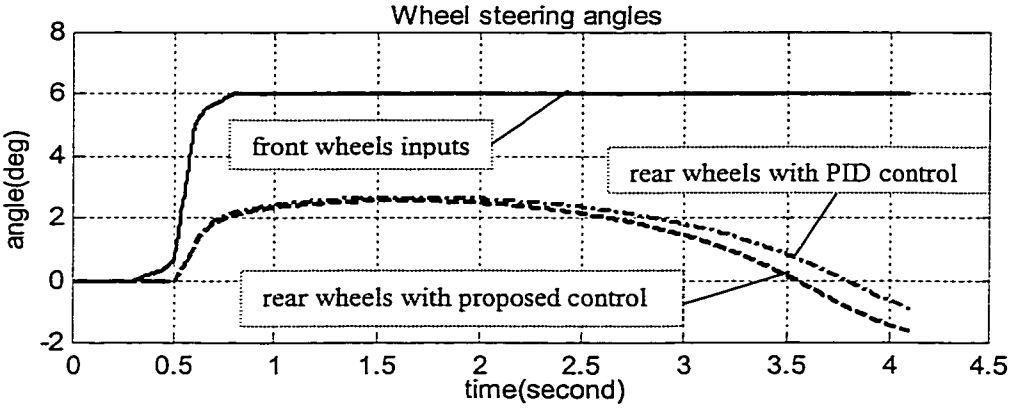

Fig. 4.24 Front and Rear Steering Angles (V_0=30m/s)

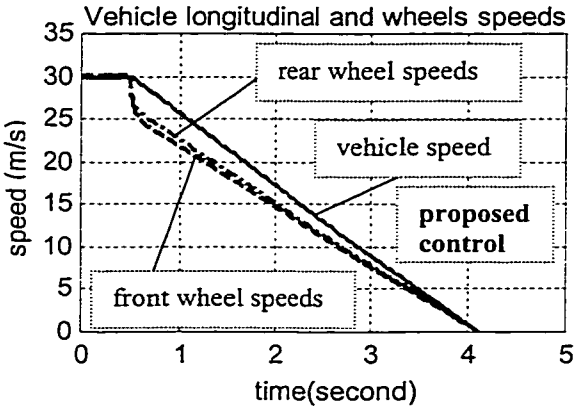

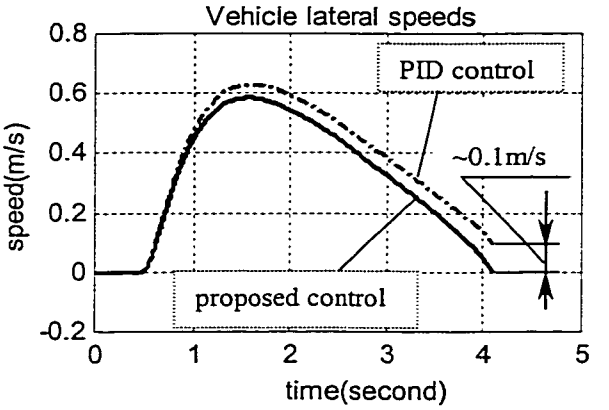

Fig. 4.25 Vehicle and Wheel Speeds (V_0=30m/s)

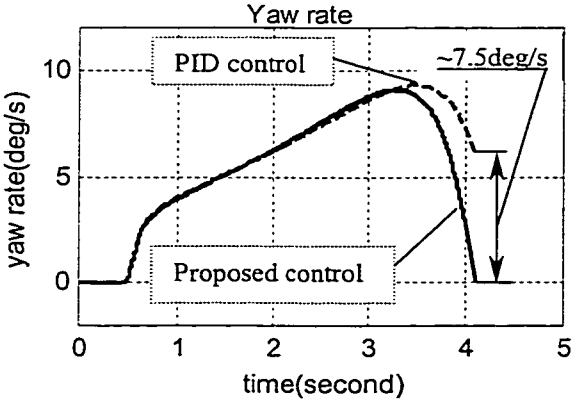

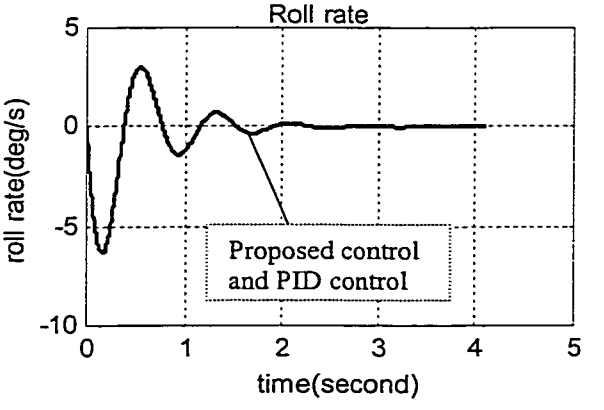

Fig. 4.26 Vehicle Yaw Rate and Roll Rate (V_0=30m/s)

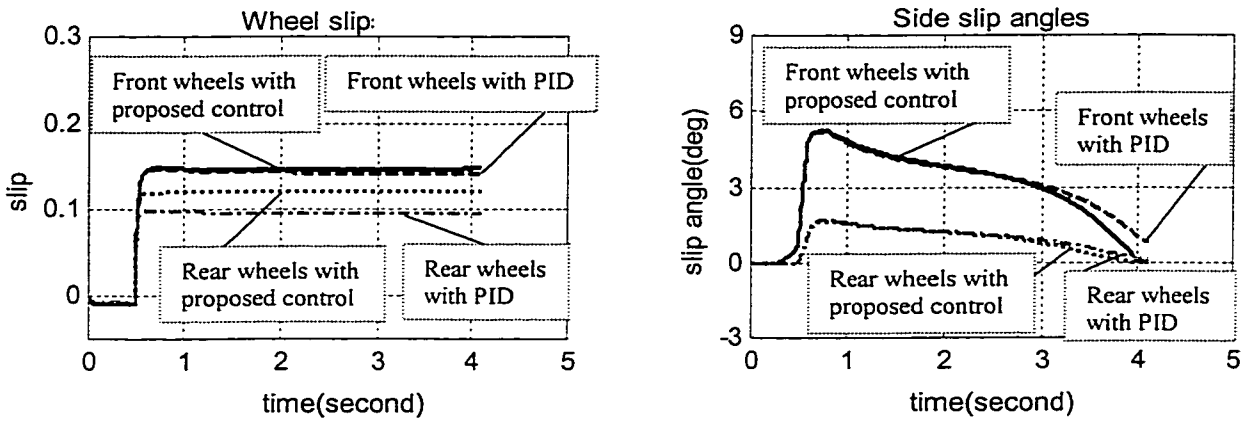

Fig. 4.27 Wheel Slip and Side Slip Angles (V_0=30m/s)

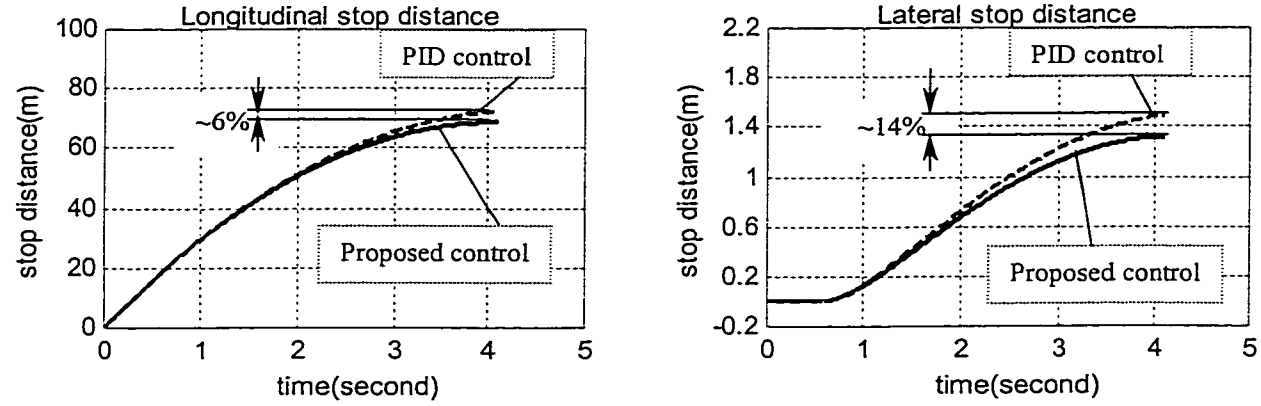

Fig. 4.28 Vehicle Stopping distance (V_0=30m/s)

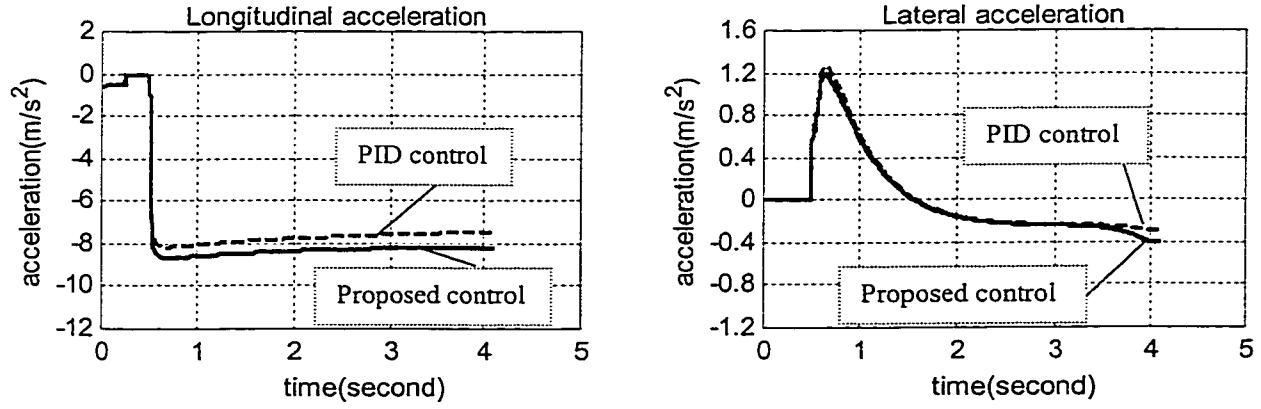

Fig. 4.29 Vehicle Accelerations (V_0=30m/s)

Figures 4.24 shows the rear wheel steering angles correspond to the front wheel steering angles. The results show that, at beginning when braking applied, the difference in the rear steer angle is small between the two control systems. As the velocity of the vehicle is reduced with time, the proposed system only need smaller rear steering angle than PID system. However, when the velocity of the vehicle continues reducing to zero, the rear wheels steering angle increase to 1.8 degree in an opposite direction with front wheels. As results, Figures 4.25 and 4.26 show that the proposed system reduces the yaw rate by 7.5deg/s and lateral speed about 0.1m/s from PID system. Figure 4.27 shows that the difference between front wheel slip and rear wheel slip is about 0.025 with proposed control, which is smaller than the one of 0.05 with PID control. The results also show that the slip angles are further reduced when proposed control implemented. From the responses of Figures 4.28, the proposed system shorts the both longitudinal and lateral stopping distances by 6% and 14% because the average decelerations are increased than that with PID control, which can be seen in Figures 4.29.

***b).* $V_0 = 20$m/s**

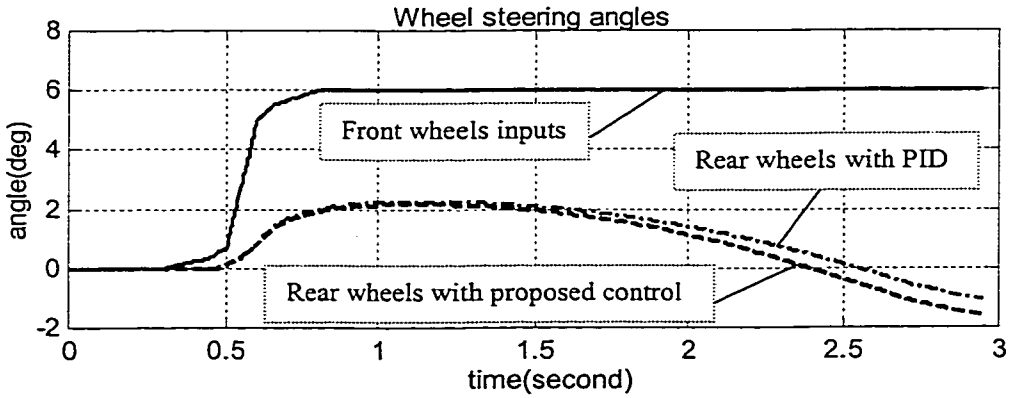

Fig. 4.30 Front and Rear Steering Angles (V_0=20m/s)

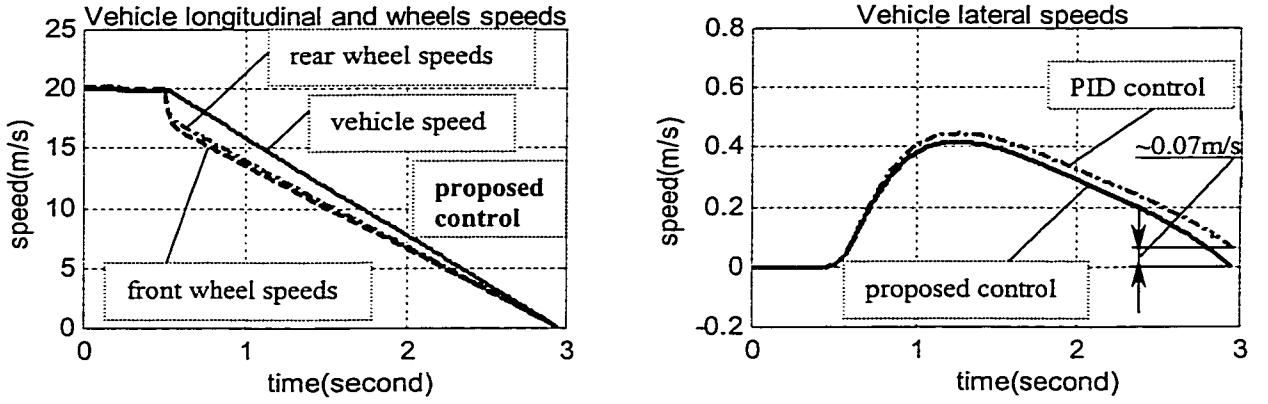

Fig. 4.31 Vehicle and Wheel Speeds (V_0=20m/s)

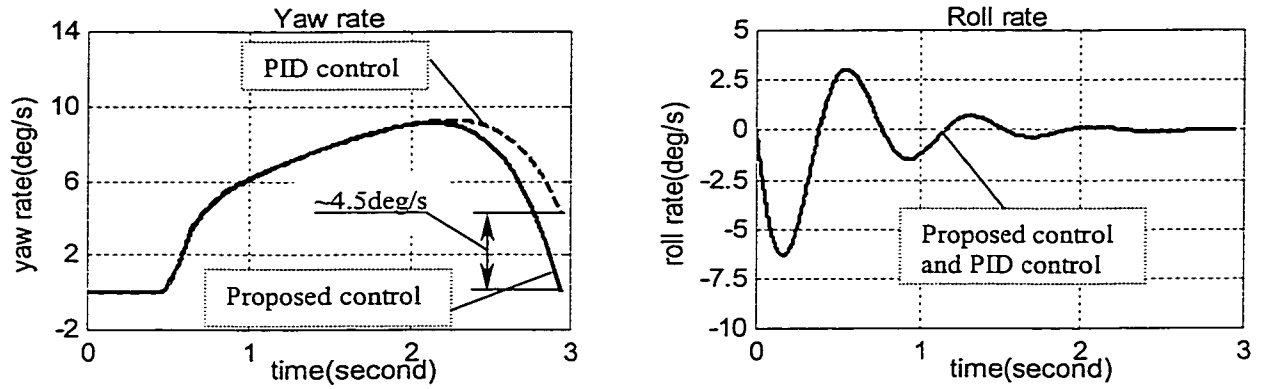

Fig. 4.32 Vehicle Yaw Rate and Roll Rate (V_0=20m/s)

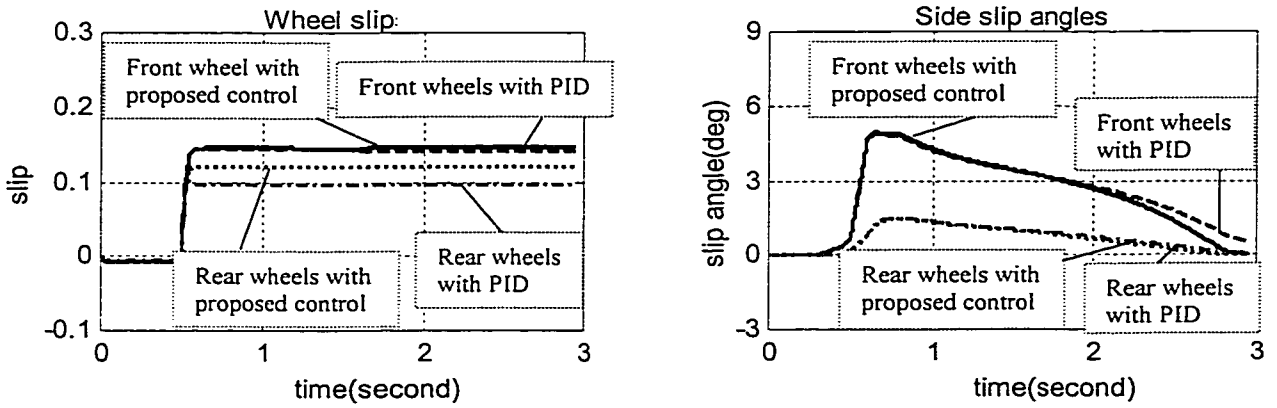

Fig. 4.33 Wheel Slip and Side Slip Angles (V_0=20m/s)

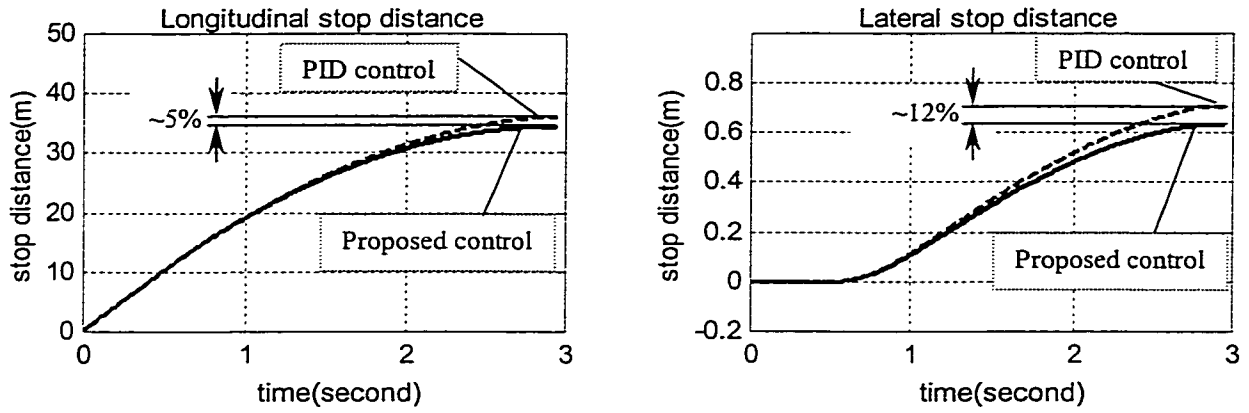

Fig. 4.34 Vehicle Stopping distance (V_0=20m/s)

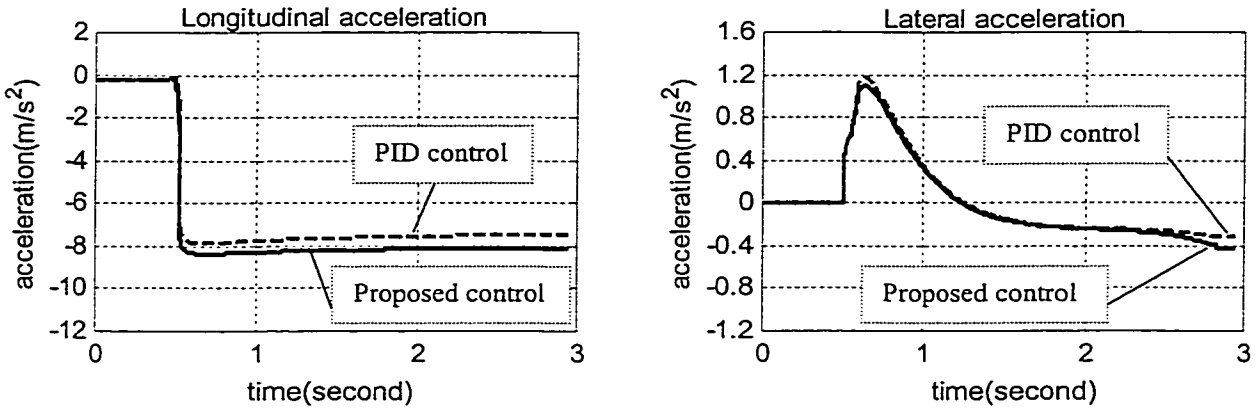

Fig. 4.35 Vehicle Accelerations (V_0=20m/s)

Figures 4.31 and 4.32 show that the proposed system reduces the yaw rate by 4.5deg/s and lateral speed about 0.07m/s from PID system. Figure 4.33 shows that the difference between front wheel slip and rear wheel slip is about 0.025 with proposed control, which is smaller than the one of 0.05 with PID control. The results also show that the slip angles are further reduced when proposed control implemented. From the responses of Figures 4.34, the proposed system shorts the both longitudinal and lateral stopping distances by 5% and 12% because the average decelerations are increased than that with PID control, which can be seen in Figures 4.35.

c). $V_0 = 10$m/s

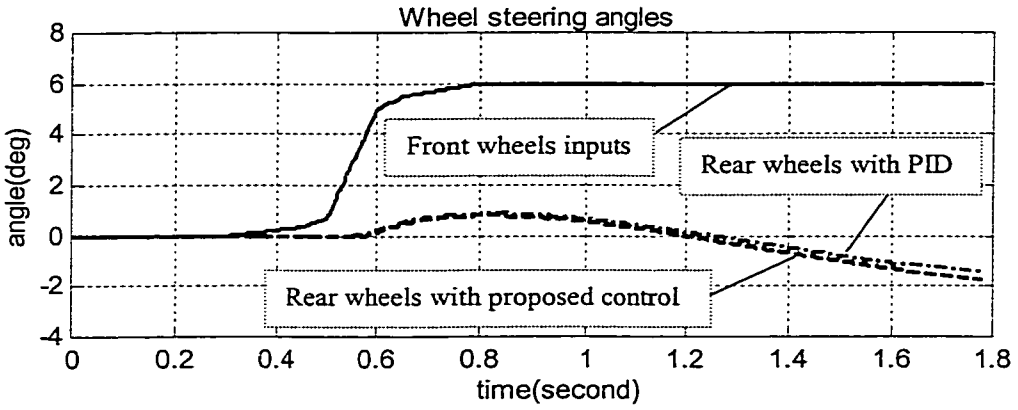

Fig. 4.36 Front and Rear Steering Angles (V_0=10m/s)

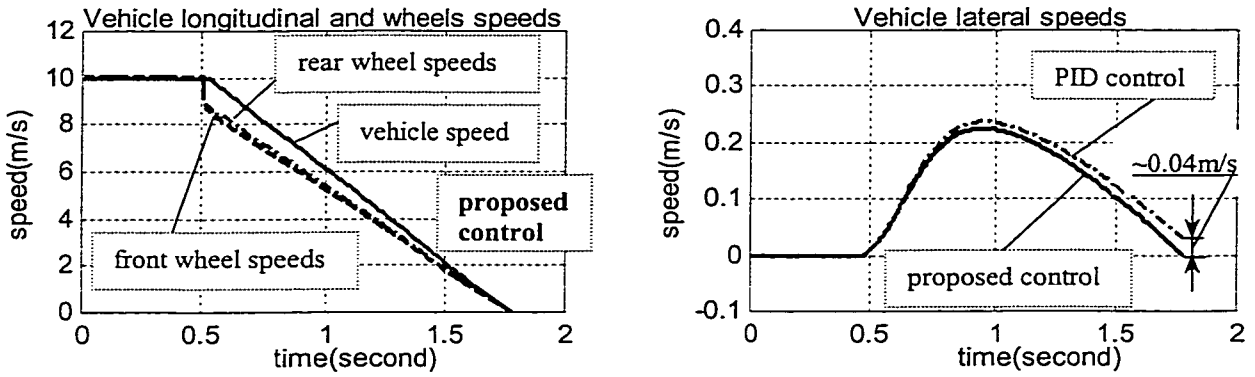

Fig. 4.37 Vehicle and Wheel Speeds (V_0=10m/s)

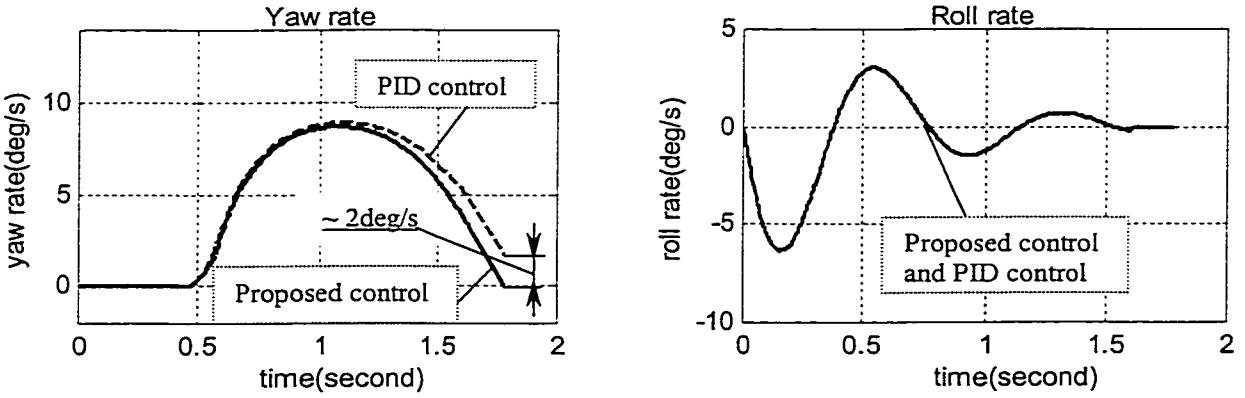

Fig. 4.38 Vehicle Yaw Rate and Roll Rate (V_0=10m/s)

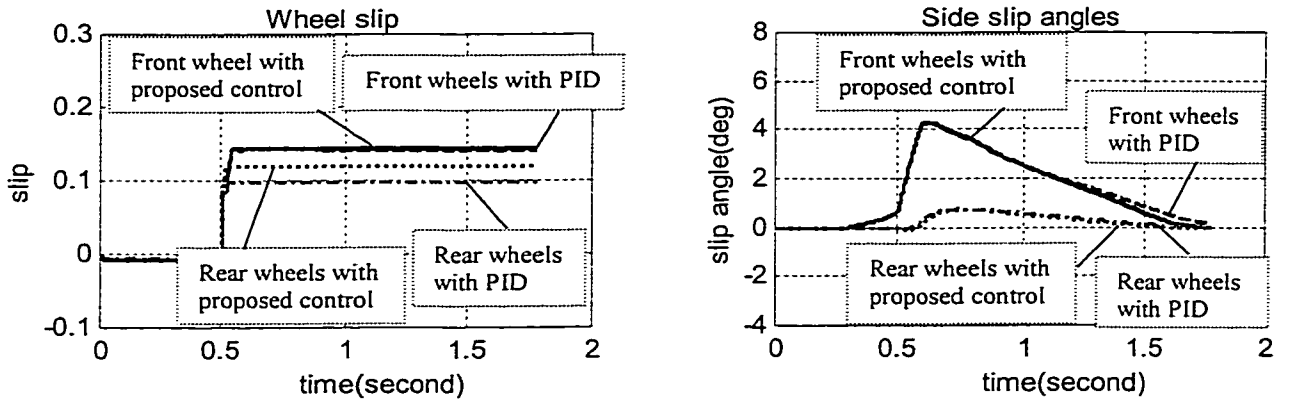

Fig. 4.39 Wheel Slip and Side Slip Angles (V_0=10m/s)

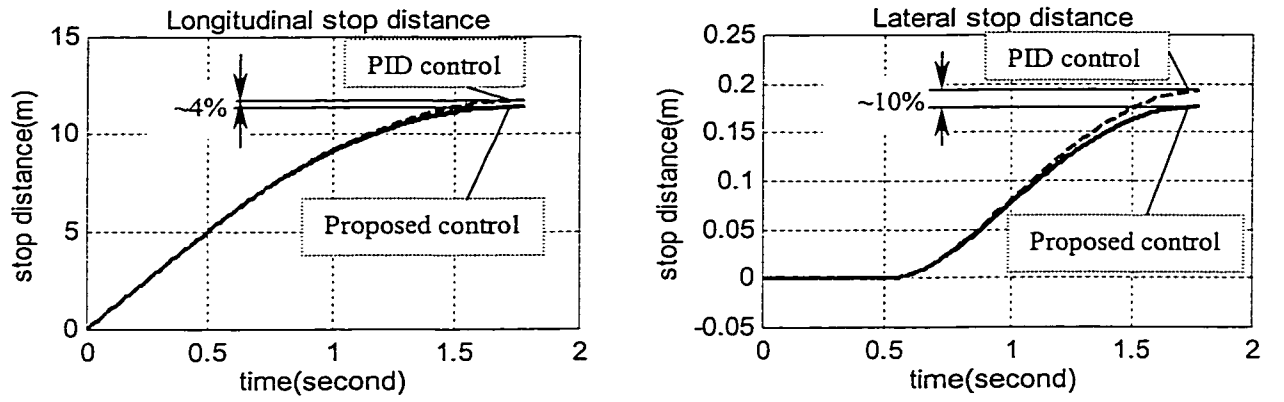

Fig. 4.40 Vehicle Stopping distance (V_0=10m/s)

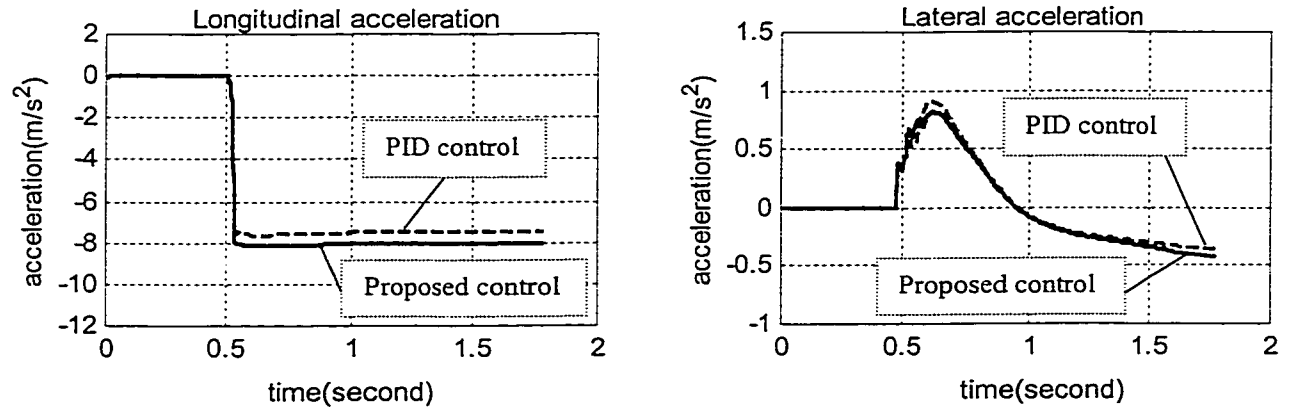

Fig. 4.41 Vehicle Accelerations (V_0=10m/s)

Figures 4.37 and 4.38 show that the proposed system reduces the yaw rate by 2deg/s and lateral speed about 0.04m/s from PID system. Figure 4.39 shows that the difference between front wheel slip and rear wheel slip is about 0.025 with proposed control, which is smaller than the one of 0.05 with PID control. The results also show that the slip angles are further reduced when proposed control is implemented. From the responses of Figures 4.40, the proposed system shorts the both longitudinal and lateral stopping distances by 4% and 10% because the average decelerations are increased than that with PID control, which can be seen in Figures 4.41.

Figures 4.24, 4.30 and 4.36 show the rear wheel steering angles correspond to the front wheel steering angles when Four-wheel Steering control is implemented. As mentioned previously, if the rear steering angle is selected properly, the vehicle will exhibit minimum sideslip angle and will then have low speed maneuverability and high speed stability. The results show that the difference in the rear steer angle is small between the two control systems at high speed. As the velocity of the vehicle is reduced with time, the proposed system only need smaller rear steering angle than PID system. However, when the velocity of the vehicle continues reducing to zero, the rear wheels should be steering a little more in order to reduce the vehicle yaw rate and lateral speed achieve to zero and keep the sideslip angle of the vehicle body at minimum value. Figures 4.25, 4.26, 4.31, 4.32 and 4.37, 4.38 show the yaw rate and lateral speed response to combined braking and steering commands with the proposed and PID controls. The results show that the proposed system has a smaller yaw rate and lateral speed than PID system. The results also show that the yaw rate and lateral speed of the proposed system final achieve a zero value when vehicle total stop, the system could reduce the tendency

to oversteer and undesired handling characteristics and hence exactly more stable than PID control system.

It is well know by the industries, if the rear slip larger than front slip, the vehicle is on a unstable state; when the front slip lager than rear slip, the vehicle can not steering well. The most significant stability specification is expressed by not allowing rear brakes to lock before the front under any loading and nearly all road friction conditions. The ideal braking situation is the front and rear brakes lock in simultaneousness. However, this situation is difficult to be achieved. Figure 4.27, 4.33 and 4.39 show that the difference is becoming smaller between front wheel and rear wheel slips when the proposed control is implemented than the one of implementing with PID control. The results show that the slip angles also smaller with proposed control than the one with PID control. The slip angles of front wheels and rear wheels final become zero value when the vehicle totally stops. Therefore, It is clearly that the proposed control in deed improves the system stability and maneuverability, hence it is an optimal system. From the responses of Figures 4.28, 4.34 and 4.40, the proposed system shorts the both longitudinal and lateral stopping distances because the average decelerations are increased than that with PID control, which can be seen in Figures 4.29, 4.35 and 4.41.

In conclusion, the proposed control presented in this Chapter which is based on NTC, 4WSC and VSC controls incorporates coordinated four wheel braking and steering is shown to enhance the vehicle stability and handling characteristics and short the vehicle stopping distances.

4.4.5 Summary

A Nonlinear Yaw-plane Four-wheel Steering Control Model considers with Limited Roll Motion (YFLR), incorporating nonlinear cornering characteristics of the Magic Formula (MF) tire model, is developed in this Chapter. A new integrated Nonlinear Tracking Control (NTC) Law is used for the hydraulic braking system, and Four-wheel Steering Control (4WSC) Law and Variable Slip-ratio Control (VSC) Law are applied together for the cornering characteristics. The three controllers are independent but are coupled through the states and the longitudinal and lateral tire forces. 4WSC with an additional steering angle of the rear wheels, by steering the rear wheels out-of-phase with the front wheels, thus improving maneuverability and cornering stability, and also yield a quicker response with better damping of the yaw oscillation that occurs with initiation of turn. VSC control is an optimal way to balance the longitudinal and lateral forces. While more longitudinal traction force is desired during driving straight, more lateral force is desired during cornering in order to be able to turn without lateral slippage, and thus to increase the vehicle stability. The desired set points for the slip values are calculated within the control algorithm to aid the controller in maintaining vehicle stability during emergency maneuvers consisting of combined hard braking and severe steering. The response characteristics derived from the proposed model are compared with the available measured data and the results from PID control system to demonstrate its validity. Simulations of the integrated controllers and ABS systems, for each system model, demonstrate a significant increase in performance.

The simulation results show that the vehicle path tracking and its directional stability can be improved while taking into consideration the coupling between the

braking and steering systems using the proposed control system where the NTC, 4WSC and VSC are implemented. The results suggest that if the rear steering angle is properly selected, the vehicle will exhibit minimum sideslip angle and then have low-speed maneuverability and high-speed stability. The vehicle with minimum sideslip controller, however, may still have a tendency to oversteer and to become unstable with PID control. To reduce these tendencies, the NTC system must be implemented. The results indicates that the action of the three controllers implemented in the YFLR model is able to provide the directional control and stability and can reduce the tendencies of oversteer in extreme emergency situations for the specific road conditions. Simulations of the integrated controllers and ABS systems for different conditions demonstrate significant improving in braking and vehicle stability performances.

CHAPTER 5
CONCLUSIONS AND FUTURE WORK

5.1 GENERAL

In this study, the performances of an antilock braking system for straight line braking and braking while turning are investigated through the development of a new integrated Nonlinear Tracking Control (NTC). The vehicle model, tire model and optimized control system are validated and analyzed to enhance an understanding of the complex interaction between braking and steering systems. The NTC combined with Four-wheel Steering Control (4WSC) and Variable Slip-ratio Control (VSC) has significant potential to improve the performances of the vehicle under the assumption that the friction coefficient does not remain constant for operation and different road conditions, and to improve the stability and steering ability of the vehicle during emergency maneuvers.

5.2 MAJOR HIGHLIGHTS OF THE INVESTIGATION

The study presented in this thesis is a systematic investigation on the potential of NTC in application to vehicle braking system and control. The major highlights of the thesis are summarized as follows.

5.2.1 Development of Nonlinear Tracking Control System

A new integrated Nonlinear Tracking Control (NTC) law is investigated for the hydraulic braking system and based on the analysis of hydraulic actuator dynamics, which used Lyapunov's stability theorem for the braking control algorithm with the desired values of

longitudinal slip calculated within the controller based on steering wheel angle. The desired set points for the slip values are calculated within the control algorithm to aid the controller in maintaining vehicle stability during emergency maneuvers consisting of combined hard braking and severe steering. It was concluded that the proposed controller has provided excellent exponential stability for force and position tracking even in the presence of errors in the physical parameters without the complexity of variable structure or adaptive methods. Therefore, the proposed braking control system can maintain desired values of longitudinal slip for both the front and rear wheels at pre-specified values. Compared with those resulting from sliding model PID control system, the proposed system can face changes in the initial conditions for different type of roads and system does not significantly change the pattern of vehicle stopping distance, deceleration and wheel slips for various road conditions, which represents the best performance of stopping distance. Compared with PID control system, the proposed control system is derived from the dynamics analysis of the hydraulic system, which more exactly tracks the desired trajectory. The proposed system can reduce the tendency of oversteer and unstable situations, which enhances the vehicle maneuverability and cornering stability.

5.2.2 Implementation of Comprehensive Vehicle Model

A nonlinear Yaw-plane Four-wheel steering model considers with a Limited Roll motion (YFLR), and incorporate nonlinear cornering characteristics of the Magic Formula (MF) tire model and compliance of the braking column is developed to study the braking response of the vehicle, which account for the effect of weight transfer. A more complex

model of a vehicle does not necessarily yield more accurate result, such as Yaw/Roll and Phase IV models, which require extensive vehicle data and poses unreasonable demands on the analysis. The selected model based upon nonlinear yaw plane, four-wheel steering and limited roll offers a comprehensive compromise between the simplified and complex models. It is validated further for the braking system and demonstrated a good representation of the braking performance.

5.2.3 Tire Model Correlated to the Road Conditions

Magic Formula (MF) is used in the system and developed for the different road types of dry concrete, snow and slippery ice. It is also applied to derive the more comprehensive NTC control and control optimization. MF optimization is strongly dependent on the road conditions because the required shape coefficients differ with road conditions change. The effectiveness for different roads is well accepted to correct with the MF by including two weighting parameters C_1, C_2. From the analysis, it is clear that the MF gives a good representation of measured tire characteristics and certain coefficients of the model retain a physical significance. The more complete version of the MF also accounts for combined cornering and braking maneuvers and is well correlated with the typical experimental test results. The proposed system using NTC combined with MF tire model gives a good control representation for the different road conditions.

5.2.4 Optimized Control System

A new integrated Nonlinear Tracking Control (NTC) Law is applied to the hydraulic braking system, and Four-wheel Steering Control (4WSC) Law and Variable Slip-ratio Control (VSC) Law are performed together to study the cornering characteristics of a

vehicle while braking. Three controllers are independent but are coupled through the states and the longitudinal and lateral tire forces. 4WSC with an additional steering angle of the rear wheels, is accomplished by steering the rear wheels out-of-phase with the front wheels, thus improving maneuverability and cornering stability, and also yield a quicker response with better damping of the yaw oscillation that occurs at the initiation of the turn. VSC is an optimal way to balance the longitudinal and lateral forces. While more longitudinal traction force is desired during driving straight, more lateral force is desired during cornering in order to be able to turn without lateral slippage, and thus to increase the vehicle stability. The desired set of points for the slip values are calculated within the control algorithm to aid the controller in maintaining vehicle stability during emergency maneuvers consisting of combined hard braking and severe steering. The response characteristics derived from the proposed model are compared with the available measured data to demonstrate its validity. Simulations of the integrated controllers and ABS systems, for each system model, demonstrate a significant increase in braking and vehicle stability performances.

5.3 CONCLUSIONS

Base on the investigation and analysis, the major conclusion can be summarized as:

1). The conventional Front-wheel Steering Control system with front steering angle as its only control input cannot simultaneously control the lateral velocity and yaw rate at desired values. The vehicle path tracking and its directional stability can be improved while taking into consideration the coupling between the braking and steering systems when the 4WSC and VSC are implemented.

2). The vehicle will exhibit minimized side-slip angle and improved maneuverability and cornering stability when four-wheel control with an additional steering angle of the rear wheels, by steering the rear wheels out-of-phase with the front wheels is implemented.

3). Variable Slip-ratio control is an optimal way to balance the longitudinal and lateral forces. While more longitudinal traction force is desired during driving straight, more lateral force is desired during cornering in order to be able to turn without lateral slippage, and thus to increase the vehicle stability.

4). The vehicle with 4WSC and VSC controllers, however, may still have a tendency to oversteer and to become unstable when the adaptive PID controller is applied to the actuator system. The NTC has the significant potential to reduce these tendencies, which significantly improves the braking performance of the vehicle.

5). The NTC based on the dynamics analysis of the hydraulic system proves to be more exactly tracked with the desired trajectory and makes the vehicle more stable. Moreover, the system accepts changes in the initial conditions for different type of roads and does not significantly modify the pattern of vehicle stopping distance, deceleration and wheel slips for various road conditions. The NTC proves to yield the best performance of stopping distance under stable condition of the vehicle.

6). The performance of an antilock braking system relies upon a proper identification of the road surface type and strongly nonlinear tire model. The nonlinear characteristics can be effectively characterized using Magic Formula. The Magic Formula and the available experimental results exhibit very similar patterns and in a very good

agreement for the different road conditions, based upon straight line braking and braking during turning.

7). Sliding mode optimizer can be used to determine the optimal slip ratio with maximum friction forces. Both the sliding mode optimizer and the Magic Formula optimization yield very similar optimal tracking to the desired trajectory. However, Magic Formula optimization is strongly dependent on the road conditions because the required shape coefficients differ with the road conditions change. Sliding mode optimizer can be simply controlled by different types of the roads even for very complicated tire and vehicle models.

8). A Nonlinear Yaw-plane Four-wheel steering model with Limited Roll motion (YFLR) can serve as an efficient analysis tool for the braking behavior of the vehicle and yield a good performance in stopping distances under stability of the vehicle.

5.4 RECOMMENDATION FOR FUTURE WORK

In this thesis, the NTC is investigated for the fundamental hydraulic ABS braking system potential in vehicle dynamics application. The following future works to further explore the performance of braking based upon the proposed control methodologies are recommended.

1). To attain superior stability and maneuverability, it is desired that the vehicle system can control lateral velocity and yaw rate at any desired values simultaneously. This requires at least one additional control input, which is independent of the front steering angle. In present Four-wheel Steering system, lateral and yaw motions cannot be independently controlled because the rear steering angle is dependent upon

the front steering angle. In order to solve this problem, it is necessary to introduce an extra independent control input in addition to the front steering angle.

2). The Variable Slip-ratio coefficients set as a function as slip angle need to be validated through site tests under different road conditions.

3). The piston friction coefficients in the master cylinder and braking booster need to be validated through site tests under different operating conditions.

4). The Magic Formula coefficients also need to be validated through site tests under different maneuver and road conditions.

5). The analytical vehicle model consider yaw/roll motion and four-wheel steering needs to be validated through site tests under different operating conditions and steering angle inputs.

6). The evaluation of ABS system on a vehicle with driver who exhibit various driving habits under various driving conditions, various vehicle and hydraulic system configurations will enhance the value of the work.

7). The proposed ABS system of the vehicle offers a significant potential to improve the braking performances of the vehicle and increase the highway safety, which should be further explored and examined.

REFERENCES

1. Birch, S., *'Vehicle sensor'*, Automotive Engineering, vol. 97, no. 6, pp. 91-92, June 1989.

2. Hidetoshi Saito, et al., *'Acceleration sensor for ABS'*, SAE Technical Paper 920477, 1992.

3. Erwin Petersen, *'Anti-lock braking system (ABS) with integrated drive slip control (ASR) for commercial Vehicles'*, SAE Paper 861961, 1986.

4. Tan, H. S., and Tomizuka, M., *'a discrete-time robust vehicle traction controller design'*, 1989 American Control Conference.

5. Tan, H. S., and Chin, Y. K., *'Variable-structure vehicle control'*, ASME 88-WA/DSC-27, November 1988.

6. W. C. Lin, D. J. Dobner, and R. D. Fruechte, *'Design and analysis of an antilock brake control system with electric brake actuator'*, Vehicle Design, vol. 14, no. 1, pp. 13 – 43, 1993.

7. Drakunov, S., Ozguner, U., Dix, P., and Ashrafi, B., *'ABS control using optimum search via sliding modes'*, IEEE Transactions on Control and Systems Technology, vol. 3, pp.79-85, March 1995.

8. Cem Unsal, and Puhskin Kachroo, *'Sliding Mode Measurement Feedback Control for Antilock Braking Systems'*, IEEE Transactions on Control Systems Technology, vol. 7, no. 2, pp. 271-280, March, 1999.

9. A. B. Will, S. Hui, and S. H. Zak, *'Sliding mode wheel slip controller for an antilock braking system'*, Vehicle Design, vol. 19, no. 4, pp. 523-539, 1998.

10. Korovin, S. K., and Utkin, V. I., *'Using sliding modes in static optimization and nonlinear programming"*, Automatica, Vol. 10, pp.525-532, September 1974.

11. Utkin, V. I., *'Sliding modes in control and optimization'*, Heidelberg: Springer-Verlag, Berlin, 1992.

12. G. F. Mauer, G. F. Gissinger, and Y. Chamaillard, *'Fuzzy logic continuous and quantizing control of an ABS braking system'*, SAE Paper 940830, 1994.

13. G. F. Mauer, *'A fuzzy logic controller for an ABS braking system'*, IEEE Transactions on Fuzzy Systems, vol. 3, pp.381-388, November 1995.

14. J. R. Layne, K. M. Passino, and S. Yurkovich, *'Fuzzy learning control for antiskid braking systems'*, IEEE Transactions on Control and Systems of Technology, vol. 1, pp.122-129, June 1993.

15. Ka C. Cheok, et al., *'Fuzzy logic approach to traction control design'*, SAE Paper 960957, 1996.

16. M. C. Wu, L. C. Lee, and M. C. Shih, *'Neuro-Fuzzy Controller Design of the Anti-Lock Braking System'*, JSME International Journal, series C, vol. 41, no. 4, pp. 836-843, 1998.

17. W. K. Lennon, and K. M. Passino, *'Intelligent control for brake systems'*, IEEE Transactions on Control and Systems Technology, vol. 7, pp.188-202, March 1999.

18. M. C. Shih, and Y. R. Sheu, *'The adaptive position control of an electro hydraulic servo cylinder'*, JMNB VSMNE Int. J., vol. 34, no. 3, pp. 370-376, 1991.

19. C. H. Huang, and Y. T. Wang, *'Self-optimization adaptive velocity control of asymmetric actuator'*, Int. J. Adaptive Contr. Signal Processing, vol. 9, no. 3, pp. 271-283, May-June 1995.

20. Landau, I. D., and L. Dugard, *'Commande adaptative. Aspects pratiques et theoretiques'*, Masson, Paris, France, 1986.

21. Guntur, R. R., and Ouwerkerk, H., *'Adaptive brake control system'*, Proceedings of the Institution of Mechanical Engineers, vol. 186, 1972.

22. H. S. Tan, and M. Tomizuka, *'An adaptive sliding mode vehicle traction controller design'*, Proceedings of 1990 American Control Conference, vol. 2, pp.1856-1861, 1990.

23. Masugi, K., and J. Karl, H., *'Adaptive sliding mode control in the presence of saturating tire forces'*, JSME International Journal, series C, vol. 42, no.2, pp. 281-386, 1999.

24. L. X. Wang, *'Stable adaptive fuzzy control of nonlinear systems'*, IEEE Transactions on Control Systems Technology, vol. 1, no. 2, pp. 146-155, May, 1993.

25. K. S. Narendra and A. M. Annaswamy, *Stable Adaptive Sysytems*, Prentice-Hall, 1989.

26. Y. Shibahata, et al., *'Improvement of vehicle maneuverability by direct yaw moment control'*, Vehicle System Dynamics, vol. 22, pp. 465-481, 1993.

27. Taheri, S., and Law, E. H., *'Investigation of a combined slip control braking and closed loop four wheel steering system for an automobile during combined hard*

braking and severe steering', Proceedings of 1990 American Control Conference, vol. 2, pp.1862-1867, 1990.

28. Kazunori, M., *'Vehicle cornering characteristics in acceleration and braking through attitude control of front and rear tires'*, JSME International Journal, series C, vol. 39, no. 1, 1996.

29. Masao, N., Sachiko, Y., and Yutaka, H., *'Integrated control of active rear wheel steering and yaw moment control using braking forces'*, JSME International Journal, series C, vol. 42, no. 2, pp. 301-308, 1999.

30. D. E. Williams, and W. M. Haddad, *'Nonlinear control of roll moment distribution to influence vehicle yaw characteristics'*, IEEE Transactions on Control Systems Technology, vol. 3, no. 1, pp. 110-116, March, 1995.

31. Jong, H. P., and Chan, Y. K., *'Wheel slip control in traction control system for vehicle stability'*, Vehicle System Dynamics, vol. 31, pp. 263-278, 1999

32. Bakker, E., Pacejka, H. B., and Lidner, L., *'A new tire model with an application in vehicle dynamnics studies'*, SAE paper 890087, 1989.

33. H. B. Pacejka, *Tire Models for Vehicle Dynamics Analysis: proceedings of the 1st International Colloquium on Tire Models for Vehicles Dynamics Analysis.* Amsterdam, Swets & Zeitlinger B. V., Amterdam/Lisse, 1993.

34. Schuring, D. J. et al, *'The BNPS model-an automated implementation of the "Magic Formula" concept'*, SAE paper 931909, 1993.

35. Pacejka, H. B., and Sharp, R. S., *'Shear force development by pneumatic tire in steady state conditions: a review of modeling aspects'*, Vehicle System Dynamics, Vol. 20, 1991.

36. Furukawa, Y., Yuhara, N., et al., *'A review of four-wheel steering studies from the viewpoint of vehicle dynamics and control'*, Vehicle System Dynamics, vol. 18, pp. 151-186, 1989.

37. R. Limpert, *Brake Design and Safety.* Warrendale, Society of Automotive Engineers Inc., 1992.

38. Oakley, W. J., Roller, A. E., and Cattin, W. J., *'Development of the brake system for General Motors experimental safety vehicle'*, SAE Technical Paper 730081, 1973.

39. Klein, H.C. and Fink, W., *'Introduction of antilock braking systems for cars'*, SAE Technical Paper 741084, 1974.

40. O'keefe, P. J., *'Tande antilock system for air braked vehicles'*, SAE Technical Paper 770662, 1977.

41. Satoh, M., and Shiraishi, S., *'Performace of a simplified control technique for antilock brakes'*, SAE Technical Paper 826097, 1982.

42. Leiber, H.C., and Czinczel, A., *'Four years of experience with 4-wheel antiskid brake systems (ABS)'*, SAE Technical Paper 830481, 1983.

43. Bleckmann, H. W., and Weise, L., *'The new four-wheel antilock generation - a compact antilock and booster aggregate and an advanced electronic safety concept'*, SAE Technical Paper 865981, 1986.

44. W. D. Jonner, *'Upgrade levels of the Bosch ABS'*, SAE Technical Paper 860508, 1986.

45. *Automotive Handbook*, Robert Bosch GmbH, VDI Verlag, Dusseldorf, Germany, ISBN 3-18-418004-2.

46. J. Gerstenmeier, *'Traction control (ASR) – an extension of the antilock braking system (ABS)'*, SAE Technical Paper 861033, 1986.

47. W. Maisch, W. D. Jonner, and A. Sigl, *'ASR – Traction control – a logical extension of ABS'*, SAE Technical Paper 870337, 1987.

48. E. Petersen, et al. *'A new ABS with integral automatic traction control for air–braked trucks and buses'*, SAE Technical Paper 902210, 1990.

49. W. Maisch, et al., *'ABS5 and ASR5: the new ABS/ASR family to optimize directional stability and traction'*, SAE Technical Paper 930505, 1993.

50. Igata, H., et al., *'Development of new control method to improve response of throttle type traction control system'*, SAE paper, 920608, 1992.

51. Hffman, D. D., *'The corvette acceleration slip regulation (ASR) application with preloaded limited slip differential'*, SAE paper, 920652, 1992.

52. Heinz, L., *'The brake system of the new 7 series BMW with electronic brake and wheel slip control'*, SAE paper, 950792, 1995.

53. Van Zanten, A. T., et al., *'The vehicle dynamics control system of Bosch'*, SAE paper, 950759, 1995.

54. Heinz Leffer, *'Electronic brake management EBM – prospects of an integration of brake system and driving stability control'*, SAE Paper 960954, 1996.

55. *Electronic Stability Program,* www.contitevesna.com/esp.htm, Continental TEVES.

56. Guntur, R. R., and Ouwerkerk, H., *'Anti-lock reselection'*, Automotive Design Engineering, pp.13-15, 1973.

57. Fling, R. T., and Fenton R. E., *'A describing-function approach to antiskid design'*, IEEE Transactions on Vehicular Technology, vol. VT_30, no.3, pp.134-144, 1981.

58. Zellner, J. W., *'An analytical approach to antilock brake system design'*, SAE Paper 840249,1984.

59. J. J. Eubanks, et al., *'A comparison of devices used to measure vehicle braking deceleration'*, SAE Technical Paper, 930665, 1993.

60. MacAdam, C. C., Fancher, P. S., Hu, G. T., and Gillespie, T. D., *'A computerized model for simulating the braking and steering dynamics of trucks, tractor-semitrailers, doubles and triples combinations. User's Manual – PHASE 4'*, Highway Safety Research Institute, University of Michigan, Report No. UM-HSRI-80-58, 1980.

61. Dugoff, H., Segel, L., and Ervin, R. D., *'Measurement of vehicle response in severe barking and steering maneuvers'*, SAE Technical Paper 710080, 1971.

62. El-Gindy, M., and Ilosvai, L., *'An experimental investigation into vehicle response during steering and braking maneuvers'*, International Journal of Vehicle design, vol.2, no. 4, pp. 463-469, 1981.

63. Uffelmann, F., *'Automotive stability and handling dynamics in cornering and braking maneuvers'*, Vehicle System Dynamics, vol. 12, pp. 203-223, 1983.

64. Abe, M., *' A study on vehicle turning behavior in acceleration and in braking'*, SAE Technical Paper 852184, 1985.

65. Bernad, J. E. et al, *'Linear analysis of a vehicle with four wheel steering'*, SAE Technical Paper 880653, 1988.

66. X. Xia, and E. H. Law, *'Linearized analysis of front and four wheel steering automobiles: understeer, oversteer, and handling* qualities', The Winter Annual Meeting Engineers Dallas, Texas, November 25-30, AMD-vol.108, pp.9-18, 1990.

67. Kazunori, M., *'Vehicle cornering characteristics in acceleration and braking through attitude control of front and rear tires'*, JSME International Journal, series C, vol. 39, no.1, pp. 58-66, 1996.

68. Huei, P. and Masayoshi, T., *'Vehicle lateral for highway automation'*, Proceedings of the 1990 ACC Conference, vol. 2, pp788-792, 1990.

69. His-Fu, L. and Ali, A. S., *'Vehicle dynamics and stabilisation using a nonlinear tyre model with four-wheel steering and braking'*, International Journal of Computer Applications in Technology, vol. 11, Nos ½ pp. 53-65, 1998.

70. J. Eric Bowman, and E. H. Law, *'A feasibility study of an automotive slip control braking system'*, SAE Technical Paper, 930762, 1993.

71. Pacejka, H. B., *'Analysis of the dynamic response of a rolling string-type tire model to lateral wheel-plane vibrations'*, Vehicle Dynamics, vol. 1, pp.37-66, 1972.

72. Loeb, J. S. et al., *'Lateral stiffness, cornering stiffness of relaxation length of the pneumatic tire'*, SAE Technical Paper, 900129, 1990.

73. Lee, S., Chrstos, J. P., and Guenther, D. A., *'Modeling of dynamic characteristics of tire lateral and longitudinal force responses to dynamic inputs'*, SAE Technical Paper, 950315, 1995.

74. Van Zanten, A., Ruf, W. D., and Lutz, A., *'Measurement and simulation of transient tire forces'*, SEA Technical Paper, 890650, 1989.

75. Segel, L., *'An overview of development in road-vehicle dynamics: past, present, and future'*, Proceedings of The Institution of Mechanical Engineers, Automobile Division, 1993.

76. Ray, L. R., *'Nonlinear tire force estimation and road friction identification: field results'*, SAE Technical Paper, 960181, 1996.

77. Eichhorn, U., and Roth, J., *'Prediction and monitoring of tire/road friction'*, XXIV. FISITA Congress, London, Great Brittain, 1992.

78. Bakker, E., Nyborg, L., and Pacejka, H. B., *'Tire modeling for use in vehicle dynamics studies'*, SAE paper 870421, 1987.

79. P. Van Der Jagt, and A. W. Parsons, *'Road surface correction of tire test data'*, Vehicle System Dynamics, vol. 25, pp.147-165, 1996.

80. Ohyama, Y., *'A totally integrated vehicle electronic control system'*, SAE Technical Paper, 881772, 1988.

81. Nakazato, H., et al., *'A new system for independently controlling braking force between inner and outer rear wheels'*, SAE Technical Paper, 890835, 1989.

82. Matsumoto, N., and Tomizuka, M., *'Vehicle lateral velocity and yaw rate control with two independent control inputs'*, Proceedings of 1990 American Control Conference, vol. 2. Pp. 1868-1875, 1990.

83. Davison, E. J., and Ferguson, I. J., *'The design of controllers for multivariable robust servomechnism problem using parameter optimization methods'*, IEEE Transactions on Automatic Control, vol. AC-26, no. 1, pp. 93-110, 1981.

84. Salman, M., *'Coordinated control of braking and steering'*, ASME Symposium on Advanced Automotive Technologies, 1990 Winter Annual Meeting, AMD-vol. 108, pp.69-76, 1990.

85. Salman, M., et al., *'Coordinated control of four wheel braking and rear steering'*, Proceedings of 1992 American Control Conference, vol. 1, pp.6-10, 1992.

86. Taheri, S., and Law, E. H., *'Slip control braking of an automobile during combined braking and steering maneuvers'*, ASME Symposium on Advanced Automotive Technologies, 1991 Winter Annual Meeting, DE - vol. 40, pp.209-227, 1991.

87. Margolis, D. L., et al., *'Integrated torque and steering control for improved vehicle handling'*, ASME Symposium on Advanced Automotive Technologies, 1991 Winter Annual Meeting, DE - vol. 40, pp.267-290, 1991.

88. Yu, s., and Moskwa, J. J., *'A global approach to vehicle control: coordination of four wheel steering and wheel torque'*, ASME Symposium on Advanced Automotive Technologies, 1991 Winter Annual Meeting, DE - vol. 40, pp. 259-266, 1991.

89. Ackermann, J., and Sienel, W., *'Robust yaw damping of cars with front and rear wheel steering'*, IEEE Trans. on Control Systems Technology, vol. 1, no. 1, pp.15-20, 1993.

90. Sato, H., et al., *'Dynamic characteristics of whole wheel steering vehicle with yaw velocity feedback rear wheel steering'*, I. Mech. E. (C124/83), Road Vehicle Handling, pp. 147-156, 1983.

91. Sano, S., et al., *'Four wheel steering system with rear wheel steer angle controlled as a function of steering wheel angle'*, SAE Transactions Paper, 860625, 1986.

92. Shibahata, Y., et. al., *'The development of an experimental four-wheel-steering vehicle'*, SAE Transactions paper, 860623, 1986.

93. Takiguchi, T., et al., *'Improvement of vehicle dynamics by vehicle-speed-sensing four-wheel steering system'*, SAE Paper, 860624, 1986.

94. Whitehead, J. C., *'Four wheel steering: Maneuverability and high speed stabilization'*, SAE paper 880652, 1988.

95. X. Xia, and E. H. Law, *'Nonlinear dynamic response of front and four wheel steering automobiles to combined braking and steering commands in collision avoidance maneuvers'*, SAE Paper, 901731, 1990.

96. Lee, A. Y., *'Design of stability augmentation systems for automotive vehicles'*, ASME Jounal of Dynamic Systems, Measurement and Control, vol. 112, pp. 489-495, 1990.

97. Hirano, Y., and Fukatani, K., *'Advanced chassis control technology for vehicle handling and active stability'*, Proc. AVEC' 96, Aachen, pp.1-12, 1996.

98. R. Srinivasa, R. R. Guntur, and J. Y. Wong, *'Evaluation of the anti-lock brake systems using laboratory simulation techniques'*, Vehicle Design, vol. 1, no.5, 467-485,1980.

99. Paul, Oppenheimer, *'Comparing stopping capability of cars with and without antilock braking systems (ABS)'*, SAE Paper 880324, 1988.

100. U. Essers, and E. C. Von Glasner, *'The braking Performance of commercial vehicles while cornering with and without an antilock system'*, SAE Paper 881823, 1988.

101. Y. Shibahata, et al., *'The development of an experimental Four-wheel-steering vehicle'*, SAE Paper 860623, 1986.

102. T. Takiguchi, et al., *'Improvement of vehicle dynamics by vehicle-speed-sensing Four-wheel steering system'*, SAE Paper 860624, 1986.

103. S. Sano, et al., *'Four wheel steering system with rear wheel steer angle control as a function of steering wheel angle'*, SAE Paper 860625, 1986.

104. E. Petersen, et al., *'A new ABS with integral automatic traction control for air-braked trucks and buses'*, SAE Paper 902210, 1990.

105. J. J. Eubanks, et al., *'A comparison of devices used to measure vehicle braking deceleration'*, SAE Paper 930665, 1993.

106. A. Strickland and K. Dagg, *'ABS braking performance and steering input'*, SAE Paper 980240, 1998

107. W. W. Olson, and D. Milacic, *'Development of anti-lock braking traction and control systems of the advanced technology demonstrator II using DADS simulation code'*, Vehicle Design, vol. 17, no. 3, pp.295-317, 1996.

108. J. E. Bowman and E. H. Law, *'A feasibility study of an automotive slip control braking system'*, SAE 930762, 1993.

109. Larry Michaels, *'The use of a graphical modeling environment for real-time hardware-in-the-loop simulation of automotive ABS systems'*, SAE Technical Paper 930907, 1993.

110. M. W. Suh, et al., *'Hardware-in-the-loop simulation for ABS'*, SAE Paper 980244, 1998.

111. F. Svaricek, *'Automatic valuation and verification of ABS controllers by using a hardware-in-the-loop simulation'*, SAE Paper 980241, 1998.

112. M. J. Schneider, *'Use of a Hazard and Operability study for evaluation of ABS control logic'*, SAE Paper 970815, 1997.

113. C. Maron, *'Electromechanical brake system: actuator control development system'*, SAE Paper 970814, 1997.

114. M. W. Sayers, *'Vehicle models for RTS applications'*, Vehicle System Dynamics, 32, pp.421-438, 1999.

115. Xiaobo, Y., *'A closed-loop driver/vehicle directional dynamics predictor'*, Ph.D. Thesis, Concordia University, Canada, 1999.

116. Y. Konishi, et. al, *'Development of Hydraulic Booster Unit for Active Brake Control'*, SAE Paper 980602, 1998.

117. J. Erjavec, *Automotive Technology: a system approach.* Delmar, Thomson Leaning, New York, 1999.

118. J. Y. Wong, *Theory of Ground Vehicles*. New York, John Wiley & Sons Inc., 1993.

119. Gillespie, T. D., *Fundamentals of Vehicle Dynamics*, Warrendale, Society of Automotive Engineers, Inc., 1992.

120. A. Alleyne, *'Improved vehicle performance using combined suspension and braking forces'*, Vehicle System Dynamics, vol. 27, pp. 235-265, 1997.

121. H. E. Merrit, *Hydraulic Control Systems*. New York, John Wiley & Sons Inc., 1976.

122. Garett, A. Sohl, and James, E. Bobrow, *'Experiments and simulations on the nonlinear control of a hydraulic servosystem'*, IEEE Transactions on Control Systems Technology, vol. 7, no.2, pp.238-247, March 1999.

123. Halseth, M., *'Simulation of a vacuum booster for traction control'*, Inter office Memorandum, Delco Systems Operations, July 25, 1990.

124. Khan, Y., et al., *'Modeling, experimentation and simulation of a brake apply system'*, ASME Journal of Dynamic Systems, Measurement, and Control, vol. 116(1), pp. 111-122, 1994.

125. Raza, H., et al., *'Modeling and control design for computer-controlled brake system'*, IEEE Transactions on Control System technology, vol. 5(3), pp. 279-296, 1997.

126. J. C. Gerdes and J. K. Hedrick, *'Brake system modeling for simulation and control'*, ASME Journal of Dynamic Systems, Measurement, and Control, vol. 121, pp. 496-503, 1999.

127. P. Kokotovic, *'The joy of feedback: Nonlinear and adaptive'*, IEEE Control System, vol. 12, no. 3, pp.7-17, 1992.

128. A. Alleyne, *'Nonlinear force control of an electro-hydraulic actuator'*, in Proc. 1996 Japan/USA Symp. Flexible Automat., Boaston, MA, 1996.

129. J. J. Slotine and W. Li, *Applied Nonlinear Control.* Englewood Cliffs, NJ: Prentice-Hall, 1991.

130. C. T. Johnson and R. D. Lorenz, *'Experimental identification of friction and its compensation in precise, position controlled mechanisms,'* IEEE trans. Ind. Applicat., vol. 28, pp. 1392-1398, Nov.-Dec. 1992.

131. C. Canudas de Wit, et. al, *'Adaptive friction compensation in robot manipulators: Low-velocities,'* Int. J. Robot. Res., no.3, pp.189-199, June 1991.

132. *Automotive Brake Systems,* BOSCH 1st Edition, Robert Bosch GmbH, 1995.

133. Kaminaga, M. and Hedrick, J. K., *'Vehicle Control Using Intelligent Sliding Surfaces'*, Proc. AVEC '96, 1996.

134. H. L. Stalford, *'High-alpha aerodynamic model identification of T-2C aircraft using the EBM method'*, J. Aircraft, vol.18, no.10, pp. 801-809, October 1981.

135. M. Sri-Jayantha and R. F. Stengel, *'Determination of nonlinear aerodynamics coefficients using the estimation-before-modeling method'*, J. Aircraft, vol.25, no.9, pp.796-804, September 1988.

136. Cole, D., *'Elementary vehicle dynamics'*, course notes in Mechanical Engineering, The University of Michigan, Ann Arbor, MI, 1972.

137. Hogue, J. R., *'Aerodynamics of six passenger vehicles obtained from full scale wind tunnel tests'*, SAE Paper 800142, 1980.

138. Sharp, R. S., and Crolla, D. A., *'Controlled rear steering for cars – a review'*, Proceedings of the Institution of Mechanical Engineers, International Conference on Advanced Suspensions, pp. 149-163, 1988.

139. X. Xia, and E. H. Law, *'Response of four wheel steering vehicles to combined steering and braking inputs'*, ASME Winter Annual Meeting DSC-vol.13, 1989.

140. Laura, R. Ray, *'Nonlinear state and tire force estimation for advanced vehicle control'*, IEEE Transactions on Control Systems Technology, vol. 3, no.1, pp.117-124, March 1995.

141. Gunther Buschmann, and Wieland Kuhn, *'Electronic brake force distribution control – a sophisticated addition to ABS'*, SAE Paper 920656, 1992.

142. Cauer, G. F. Gissinger, and Y. Chamaillard, *'Fuzzy logic continuous and Quantizing control of an ABS braking system'*, SAE Paper 940830, 1994.

143. Masao Watanabe, and Noboru Noguchi, *"A new algorithm for ABS to compensate for road-disturbance"*, SAE Paper 900205, 1990.

144. Paul Oppenhei, *'Comparing stopping capability of cars with and withcut antilock braking systems (ABS)'*, SAE Paper 880324, 1988.

145. E. Gohring, *'Reliablity of daimler – benz / wabco anti – lock systems – five years of experience after production began'*, SAE Paper 880986, 1988.

146. Steven M. McIntire, *'Two functions, one microcontroller four – wheel ABS and ride control using 80c196kb'*, SAE Paper 881138, 1988.

147. U. Essers, *'The breaking performance of commercial vehicles while cornering with and withcut an anti-lock system'*, SAE Paper 881823, 1988.

148. Erwin Petersen and Klaus Lindemann, *'A new ABS with integral automatic traction control for air – braked trucks and buses'*, SAE Paper 902210,1990.

149. M. Watanaba, and N. Noguchi, *'A new algorithm for ABS to compensate for road – disturbance'*, SAE Technical Paper, 900205, 1990.

150. *Braking Systems for Passenger Cars*, BOSCH Technical Instruction, Stuttgart, Germany.